PHASE CONTROL BY INJECTION LOCKING

A THESIS SUBMITTED TO

THE GRADUATE SCHOOL OF NATURAL AND APPLIED SCIENCES

OF

THE MIDDLE EAST TECHNICAL UNIVERSITY

BY

GÖKER ŞENER

IN PARTIAL FULFILLMENT OF THE REQUIREMENTS

FOR

THE DEGREE OF MASTER OF SCIENCE

IN

ELECTRICAL AND ELECTRONICS ENGINEERING

JULY 2004

Approval of the Graduate School of Natural and Applied Sciences

Prof. Dr. Canan Özgen
Director

I certify that this thesis satisfies all the requirements as a thesis for the degree of Master of Science.

Prof. Dr. Mübeccel Demirekler
Head of Department

This is to certify that we have read this thesis and that in our opinion it is fully adequate, in scope and quality, as a thesis for the degree of Master of Science.

Prof. Dr. Canan Toker
Supervisor

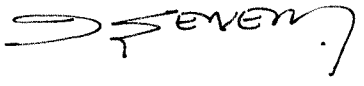
Co-Supervisor

Examining Committee Members

Prof. Dr. Altunkan HIZAL	METU-EE	
Prof. Dr. Canan TOKER	METU-EE	
Prof. Dr. Gönül Turhan SAYAN	METU-EE	
Doç. Dr. Yahya BAYKAL	ÇANKAYA U.-ECE	
Yrd. Doç. Dr. Şimşek DEMİR	METU-EE	

I hereby declare that all information in this document has been obtained and presented in accordance with academic rules and ethical conduct. I also declare that, as required by these rules and conduct, I have fully cited and referenced all material and results that are not original to this work.

Name, Surname: Göker Şener

Signature: 

ABSTRACT

PHASE CONTROL BY INJECTION LOCKING

Şener, Göker

Ms.D., Department of Electrical and Electronics Engineering

Supervisor: Prof. Dr. Canan Toker

July 2004, 102 pages

Phase control in microwave circuits is an important process. Especially, in certain applications such as phase array antennas, it is the main principle of operation.

In antenna arrays, each array element is fed by an individual oscillator. By controlling the phase of each oscillator, the radiation pattern and the rf power can be combined in space in certain directions. For such applications, phase shifters have been utilized extensively. However, their high costs, difficulties in design and efficiency are important disadvantages.

More recently, another technique, "Injection Locking" or "Phase Locking", suggests to use a single reference signal injected into each oscillator element. Through this signal, the phase of the individual oscillators can be controlled and set to a desired value.

Therefore, power combining in space or known as "Spatial Power Combining" is possible by using "Phase Locking" of individual oscillator elements.

In this thesis, this new phase control technique is examined in theory and in application of a 1GHz oscillator system. A reference signal is injected into a voltage controled oscillator, and the phase progression is obtained by tuning the oscillator's free running frequency.

ÖZ

ENJEKTE KİTLEME İLE FAZ KONTROLÜ

Şener, Göker

Ms.D., Elektrik ve Elektronik Mühendisliği Bölümü

Tez Yöneticisi: Prof. Dr. Canan Toker

Temmuz 2004, 102 sayfa

Mikrodalga devrelerde faz kontrolü önemli bir işlemdir. Bu işlem özellikle faz kontrollü anten dizileri gibi uygulamalarda temel çalışma prensibidir.

Anten dizilerinde her dizi elemanı tek bir oscillatör ile beslenir. Osilatörlerin fazları control edilerek radyasyon şekli ve rf güç belirli yönlerde uzayda birleştirilir. Bu tür uygulamalarda, faz kaydırıcılar sıkça kullanılmaktadır. Bununla birlikte, faz kaydırıcıların yüksek fiyatı, verimlilik ve tasarım güçlükleri önemli kayıplarıdır.

Son zamanlarda, "Enjekte Kitlemesi" veya "Faz Kitlemesi" adında başka bir teknik, tek bir referans sinyalinin herbir osilatöre enjekte edilmesini öngörmektedir. Bu sinyal ile herbir osilatörün fazı kontröl edilerek istenilen değere ayarlanması mümkündür.

Bu nedenle, uzayda güç birleştirme veya başka bir adla "Uzaysal Güç Birleşimi", herbir osilatörün "Faz Kitlemesi" kullanması ile mümkündür.

Bu tezde, bu yeni faz kontröl tekniği hem teoride hemde 1GHz osilatör sistemi uygulamasında incelenmiştir. Referans sinyali osilatöre uygulanmış ve osilatörün serbest çalışma frekansı değiştirilerek faz farkları elde edilmiştir.

To My Wife, Ebru Şener

ACKNOWLEDGMENTS

I would like to thank to my advisor, Prof. Dr. Canan Toker for all of his guidance and support throughout the work of this project. His insights, wealth of knowledge, and helpful personality have been an inspiration and a guidance through this thesis.

In addition, I would like to extend sincere appreciation to all the instructors in the Middle East Technical University Electrical Engineering department for their assistances and teaching efforts.

To my wife, Ebru Şener, I offer sincere thanks for her dedication and motivation at all times. To my mother and father, I thank them for their understanding and self-sacrifices throughout my life.

TABLE OF CONTENTS

PLAGIARISM iii

ABSTRACT iv

ÖZ vi

DEDICATION viii

ACKNOWLEDGMENTS ix

TABLE OF CONTENTS x

LIST OF TABLES xii

LIST OF FIGURES xiii

CHAPTER

1. **INRODUCTION** 1
2. **THEORY OF OSCILLATOR PHASE CONTROL BY INJECTION LOCKING** 5
   - 2.1 Feedback Oscillator Modeling 5
   - 2.2 Microwave Oscillators 8
   - 2.3 Phased Locked Oscillator Modeling 10
   - 2.4 Adler's Equation 21
3. **DESIGN AND SIMULATIONS** 28
   - 3.1 VCO Design and Simulations..... 28
     - 3.1.1 Design Theory 28
     - 3.1.2 Design Topology 31
     - 3.1.3 Feedback 33
     - 3.1.4 DC Biasing 33
     - 3.1.5 S-Parameter Analysis 35
     - 3.1.6 Harmonic Balance Analysis 41

3.1.7 Time Domain Analysis 44
3.1.8 Frequency Control via Varactor Diodes 47
3.2 Phase Locking Circuit Design and Simulations 50
4. EXPERIMENTAL IMPLEMENTATION 57
4.1 VCO Layout and Simulations 57
4.2 Phase Locking Circuit Layout 68
4.3 Phase Locking Circuit Simulations 70
4.4 Permittivity Calculations 73
5. MEASUREMENT RESULTS 75
5.1 Realization of the VCO 75
5.2 Realization of the Phase Locking Circuit 77
5.2 Measurement Results 77
5.3 Comparison of Simulations and Measurements
Under Optimum Conditions 95
6. CONCLUSION 99
REFERENCES 101

LIST OF TABLES

TABLE

3.1.4 DC bias conditions 35

3.1.5 S-parameters 38

3.1.6 Resonator impedance simulation 44

4.1.1 Voltage versus frequency values 68

5.2.3 1st Set of Measurements I 82

5.2.4 1st Set of Measurements ii 83

5.2.5 1st Set of Measurements iii 84

5.2.6 1st Set of Measurements iv 85

5.2.7 1st Set of Measurements v 86

5.2.8 1st Set of Measurements vi 87

5.2.9 2nd Set of Measurements i (V_{mt} is constant, V_{it} is variable) 88

5.2.10 2nd Set of Measurements ii 89

5.2.11 2nd Set of Measurements iii 90

5.2.12 2nd Set of Measurements iv 91

5.2.13 2nd Set of Measurements v 92

5.2.14 3rd Set of Measurements i(Optimum range) 93

5.2.15 3rd Set of Measurements ii 94

LIST OF FIGURES

FIGURES

1.1 Conventional array system 1

1.2 Phase locking system 2

1.3 Phase Locking diagram 3

2.1.1 Feedback block diagram 5

2.2.1 Current series feedback diagram 8

2.3.1 Microwave oscillator model 10

2.4.1 Phase Difference in injection locking 27

3.1.1 Microwave oscillator network diagram 28

3.1.2 Oscillator design topology 31

3.1.3 Feedback circuit 33

3.1.4 DC bias circuit 34

3.1.5.1 S-parameter analysis circuit 36

3.1.5.2 Stability circles 37

3.1.5.3 Resonator and load impedances 40

3.1.6.1 Harmonic balance analysis circuit 42

3.1.6.2 Harmonic balance simulations 43

3.1.7.1 Time domain analysis circuit 45

3.1.7.2 Time domain simulations 46

3.1.7.3 Frequency response of V_{out} 46

3.1.8.1 VCO circuit 48

3.1.8.2 VCO outputs for V_r(V_DC SRC2)=0V,-6V,-12V 49

3.2.1 Phase locking test diagram 50

3.2.2 Phase locking test circuit 51

3.2.3 Phase Locking Simulation for V_r = 0,-10V,-14V 52

3.2.4 Current series feedback topology 53
3.2.5 Feedback oscillator model 53
3.2.6 Phase locking circuit 55
3.2.7 Phase Locking Simulations for V_r = 0,-6V,-10V,-14V 56
4.1.1 S-domain analysis 57
4.1.2 Collector inductance length 58
4.1.3 Base inductance length 59
4.1.4 Emitter inductance length 60
4.1.5 VCO Layout 63
4.1.6 VCO Schematics 64
4.1.7 VCO Layout simulations for V_r (SRC_2)= 0,-6V,-12V,-14V ... 65
4.1.8 Modified VCO layout 67
4.2.1 Phase locking circuit layout 69
4.2.2 Phase locking schematics 71
4.3.1 LCR meter measurement 72
4.4.1 Phase locking simulations 74
5.1.1 VCO Implementation 75
5.1.2 VCO Measurements for Vr=0V,-6V,-12V 76
5.2.1 Phase locking test circuit 78
5.2.2.1 Resonator circuit 79
5.2.2.2 Resonator circuit response 80
5.2.3 Phase and Amplitude plots i 82
5.2.4 Phase and Amplitude plots ii 83
5.2.5 Phase and Amplitude plots iii 84
5.2.6 Phase and Amplitude plots iv 85
5.2.7 Phase and Amplitude plots v 86
5.2.8 Phase and Amplitude plots vi 87
5.2.9 Phase and Amplitude plots 2-i 88
5.2.10 Phase and Amplitude plots 2-ii 89
5.2.11 Phase and Amplitude plots 2-iii 90
5.2.12 Phase and Amplitude plots 2-iv 91

5.2.13 Phase and Amplitude plots 2-v 92
5.2.14 Phase and Amplitude plots 3-ii 93
5.2.15 Phase and Amplitude plots 3-iii 94
5.3.1 Simulations for the optimum case 96
5.3.2.1 Oscilloscope measurements for the optimum case i 97
5.3.2.2 Oscilloscope measurements for the optimum case ii 98

CHAPTER 1

INTRODUCTION

Phase control in microwave circuits can be used to achieve synchronous operation of a number of antenna array elements for beam-scanning systems. Array antennas are made by multiple antennas located separately in the antenna structure. They are used to obtain high directivities making use of the phenomena that fields of every antenna element are additive in space. By changing the spacing between the elements and also by changing the excitation currents driven to each element, it's possible to obtain high directivities and hence high powers at certain directions. [1]

Array antennas find a gear in many applications such as microwave radars, imaging and communication technology. Therefore, simple and cost effective implementations are very important factors in designing such systems. In the conventional array theory, the spacing between antenna elements are kept constant and the phase of each element is progressively changed to obtain beam shifting and power control in space. A diagram of such system is given in Figure 1.1.[2]-[9]

One of the main difficulties in designing such systems is to build the phase shifters. They are usually hard to manufacture in terms their precision and they can be quite costly especially in certain applications.

Another difficulty comes from the design of high power sources themselves. As in the case of many applications, to obtain high powers, many transistor amplifiers and other microwave networks are cascaded.[2]-[9]

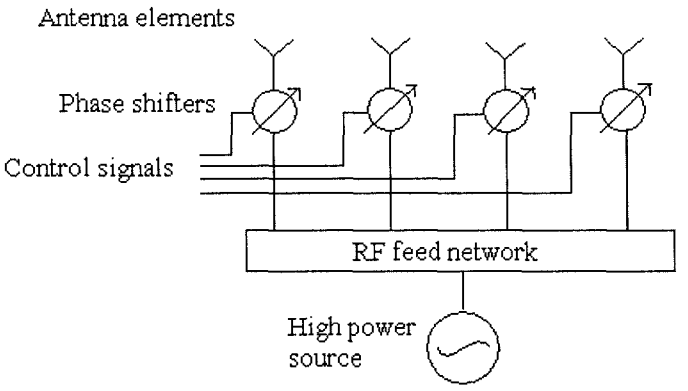


Figure 1.1 Conventional array system.

In this cascaded network structures, losses may be unavoidable due to matching difficulties among the sub-networks. Instead of power amplification by cascaded networks, it is also possible to drive each array element by a single oscillator-amplifier system. However, due to phase synchronization problems, the shifters may not be the solution over again.

An alternative approach to these difficulties is to use "Spatial Power Combining" technique where each antenna element is connected to a single oscillator-amplifier system [2]-[9]. Then, the phases of the oscillators can be coherently adjusted by the injection of a single reference signal into each oscillator. In the terminology, this phase control system is called the "Injection Locking" or "Phase Locking". A diagram of such system is given in Figure 1.2.

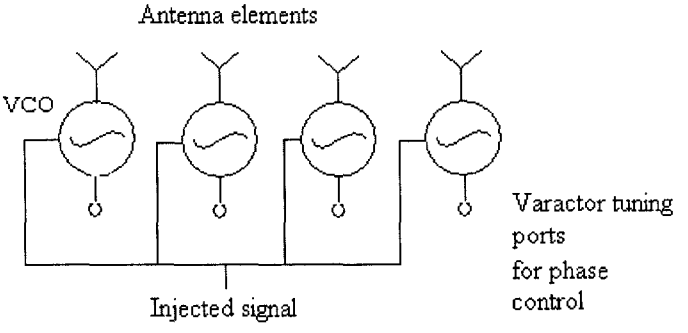


Figure 1.2 Phase locking system.

Here, the injected signal synchronizes each oscillator to a single frequency. Then, phases can be controlled by several parameters. Of those, varactor diodes can be used to change the oscillator's free running frequencies thereby changing their phases.

Using a simple single-tuned oscillator model, it will be shown that the output phase of the oscillator under phase locking is given by Adler's equation [2] [3]

$$\frac{d\phi}{dt} = w_0 - w_{inj} + \frac{\rho}{\alpha}\frac{w_0}{2Q}\sin(\psi - \phi)$$

where w_0 is the free-running frequency, α is the amplitude of the free-running oscillator, ρ is the amplitude of the injected oscillator, Q is the quality factor of the resonator circuit, and the other variables are shown in Figure 1.3.

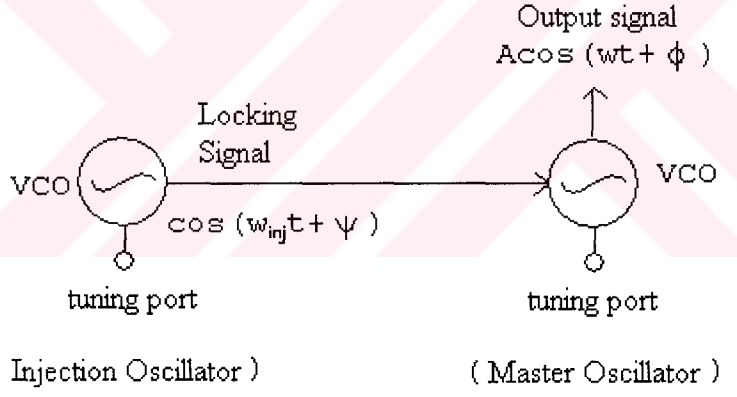


Figure 1.3 Phase Locking diagram.

Adler's equation defines the phase relation completely. Its solution for $\frac{d\phi}{dt} = 0$ gives the values of the phases, ϕ, for which the oscillator is synchronized to the injected signal. In other words, it's the solution when the output signal has a constant phase and frequency.

Therefore, solving the Adler's equation for ϕ, one obtains the phase relation for injection locked oscillator. It will be shown that the phase difference takes values from -90^0 to $+90^0$ depending on the variables w_0, w_{inj}, α, ρ and Q for the range in which the injected signal is locked to the oscillator. This range is called "Adler's Locking Range" and it's defined as the frequency range of the injection signal for which the system remains locked. Later, it will also be shown that this range is dependent to a variable, $\Delta w_m=(\rho/\alpha)(w_0/2Q)$.

Various tunings are possible to increase the Adler's locking range in bandwidth. One way is to increase the injected signal amplitude, another is to decrease the Q factor of the resonator. If high Q resonators must be used, then practically, the same oscillator with a slightly different frequency can be used as the injected signal. This tuning is possible by small impedance changes at the oscillator's resonator circuit. After the locking, the phase control can be achieved by varying w_0, oscillator's free-running frequency.

In this thesis, injection locking phenomena is analyzed in theory and it is examined in an application of a 1GHz oscillator system. In the first part, the theory is given and related equations are derived. In the next chapter, a single voltage controlled oscillator (VCO) is designed and simulated by a computer program. Oscillations are obtained in the frequency range of 800MHz to 1GHz. Then, by using two of these oscillators, a circuit for phase control is designed and simulated. In chapter 4, these pre-designed circuits (VCO and Phase Locking Circuit) are implemented in reality and several phase measurements are taken. Finally, the measurements are compared with the theory and simulations and it is concluded that phase control by injection locking is possible within certain limits that are defined in theory.

CHAPTER 2

THEORY OF OSCILLATOR PHASE CONTROL BY INJECTION LOCKING

2.1 Feedback Oscillator Modeling:

Oscillator theory, in general, is based on the feedback theory where an active device such as a transistor amplifier is fed-back by a passive feedback circuit. This is shown in Figure 2.1.1.

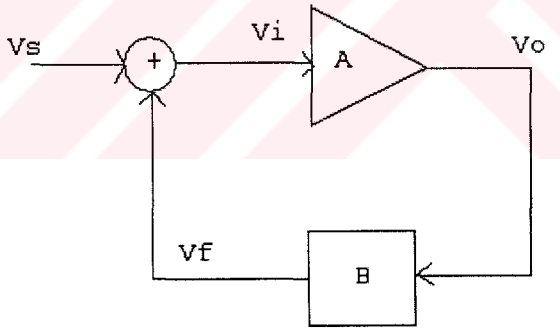


Figure 2.1.1 Feedback block diagram.

In this figure, A is the gain of the active device and B is for the passive feedback network.

From the diagram,

$$V_i = V_s - V_f$$

$$\frac{v_0}{v_i} = A \Rightarrow v_i = \frac{v_0}{A}$$

Similarly,

$$\frac{v_f}{v_0} = B \Rightarrow v_f = Bv_0$$

It follows that

$$v_i = \frac{v_0}{A} = v_s - Bv_0$$

or

$$\frac{v_0}{A} - v_s = -Bv_0$$

$$\frac{v_0 - Av_s}{A} = -Bv_0$$

$$v_0 - Av_s = -ABv_0$$

Divide both sides by V_0,

$$1 - A\frac{v_s}{v_0} = -AB$$

or

$$A\frac{v_s}{v_0} = 1 + AB$$

After manupilating the last equation, we end up with the following gain relation

$$\frac{v_0}{v_s} = \frac{A}{1+AB}$$

which defines the general feedback transfer function. In the case of a positive feedback circuit

$$v_i = v_s + v_f$$

Also, gain relations are

$$\frac{v_f}{v_0} = B \text{ and } \frac{v_0}{v_i} = A$$

Substitute these equations in the first equation

$$\frac{v_0}{A} = v_s + v_0 B$$

$$v_0\left(\frac{1}{A} - B\right) = v_s$$

or

$$\frac{v_0}{v_s} = \frac{1}{\frac{1}{A} - B} = \frac{A}{1-AB}$$

which defines the equation for positive feedback circuits.

It's seen that for the open loop gain, AB, gets closer to 1, the closed-loop gain starts to peak up.

Consider the following gain relations

$$\frac{v_f}{v_0} = B \text{ and } \frac{v_0}{v_i} = A$$

or

$$v_f = Bv_0 \text{ and } v_0 = Av_i$$

Substitute V_0 from the second relation into the first one,

$$\frac{v_f}{v_i} = AB$$

Therefore, for AB>1, $v_f > v_i$, the input to the amplifier grows steadly each time. When AB=1, $v_f = v_i$, steady state oscillation is reached.

2.2 Microwave Oscillators:

Feedback oscillator theory can be further examined in terms of microwave theory.

Consider a current series feedback circuit [10] in the following figure

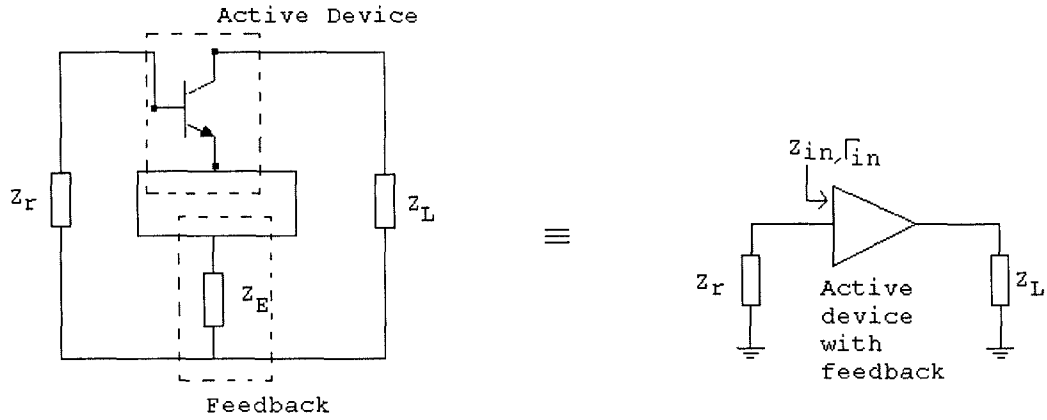


Figure 2.2.1 Current series feedback diagram.

In this figure, Z_r is the source impedance (resonator impedance) and Z_L is the load impedance.

Starting condition for oscillations requires that input signal grows from noise levels. In other words, $v_f > v_i$ must hold as it was mentioned in the previous section. In microwave theory, this means that $\Gamma_{in}>1$ or $R_{in}<0$.

In terms of traveling waves, explanation of this theory follows that

$$|\Gamma_{in}| = \frac{|V_{reflected}|}{|V_{in}|}$$

or

$$V_{reflected} = |\Gamma_{in}|V_{in}$$

This voltage wave is re-reflected from the resonator as

$$V_{re-reflected} = |\Gamma_r \Gamma_{in}|V_{in}$$

For growing input signals, $V_{re\text{-}reflected} > V_{in}$. This is analogous to $v_f > v_i$. Hence, $|\Gamma_{in}\Gamma_r| > 1$ is the starting condition for oscillations.

Since the resonator is a passive device ($|\Gamma_r| < 1$), $|\Gamma_{in}\Gamma_r| > 1$ requires that $|\Gamma_{in}| > 1$. To obtain this,

$$|\Gamma_{in}| = \left|\frac{Z_{in} - Z_0}{Z_{in} + Z_0}\right| > 1$$

where $Z_{in} = R_{in} + jX_{in}$. Then, the relation becomes

$$\left|\frac{(R_{in} - Z_0) + jX_{in}}{(R_{in} + Z_0) + jX_{in}}\right| > 1$$

Then, one should have $R_{in} < 0$, the negative resistance.

2.3 Injection Locked Oscillator Modeling:

A typical microwave oscillator design is analogues to positive feedback oscillators. For current series feedback topology, the phase locking circuit can be modeled as in the Figure 2.3.1. [3]

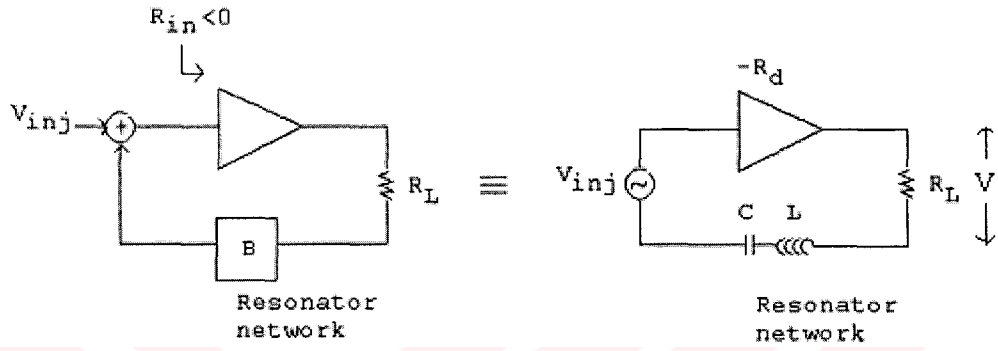


Figure 2.3.1 Microwave oscillator model.

In this figure, $V = A(t)e^{j(w_0 t+\phi(t))} = A(t)e^{j\theta(t)}$ is the output voltage phasor where w_0 is the resonant frequency of the circuit under the assumption that Q of the resonator is sufficiently large and the oscillations will remain very near to w_0. Also, $V_{inj} = A_{inj}(t)e^{j(w_{inj}t+\psi(t))}$ represents any externally injected signal.

Mesh equation for this circuit is (in terms of the current)

$$V_{inj} = i(t)(-R_d) + V + V_L + V_C$$

where V_L and V_C are the voltages across the inductor and capacitor respectively.

Substitute the relevant terms in the mesh equation, one obtains

$$V_{inj} = i(t)(-R_d) + i(t)R_L + L\frac{di(t)}{dt} + \frac{1}{C}\int i(t)dt$$

Differentiating both sides with respect to t, the following equation is obtained

$$\frac{dV_{inj}}{dt} = \frac{di(t)}{dt}(-R_d) + \frac{di(t)}{dt}R_L + L\frac{d^2i(t)}{dt^2} + \frac{1}{C}i(t)$$

Substitute $i(t) = \frac{V}{R_L}$ in the previous equation

$$\frac{dV_{inj}}{dt} = \frac{dV}{dt}(\frac{-R_d}{R_L}) + \frac{dV}{dt} + \frac{L}{R_L}\frac{d^2V}{dt^2} + \frac{1}{C}\frac{V}{R_L}$$

The Q of the circuit is large and the oscillations stay close to w_0. Therefore the voltage amplitude and phase terms will be slowly varying functions of time comparing with the period of oscillation. Then, it can be defined that

$$\frac{d}{dt} = jw_0$$

and

$$\frac{d^2V}{dt^2} = -w_0^2V .$$

Substitute them in the mesh equation, one obtains

$$jw_0V_{inj} = jw_0V(\frac{-R_d}{R_L}) + jw_0V - \frac{L}{R_L}w_0^2V + \frac{1}{C}\frac{V}{R_L}$$

After dividing both sides by 1/Q

$$\frac{jw_0}{Q}V_{inj} = \frac{jw_0}{Q}V(\frac{-R_d}{R_L}) + \frac{jw_0}{Q}V - \frac{L}{R_L}\frac{w_0^2}{Q}V + \frac{1}{QC}\frac{V}{R_L} \qquad (1)$$

Emphasizing the last two terms of equation (1) , first consider the following term

$$\frac{L}{R_L}\frac{w_0^2}{Q}V = \frac{L}{R_L}\frac{w_0}{Q}(w_0 V)$$

Using the relation

$$(w_0 V) = (-j)\frac{dV}{dt}$$

the last equality becomes

$$\frac{L}{R_L}\frac{w_0^2}{Q}V = \frac{L}{R_L}\frac{w_0}{Q}(w_0 V) = \frac{L}{R_L}\frac{w_0}{Q}(-j)\frac{dV}{dt}$$

where Q = Quality factor of the series resonant circuit.

Since Q= X/R, where X is the reactance.

$$Q = \frac{w_0 L}{R_L}$$

Substitute it in the final expression

$$\frac{L}{R_L}\frac{w_0^2}{Q}V = -j\frac{dV}{dt} \qquad (2)$$

Considering the 2nd term in equation (1),

$$\frac{1}{QC}\frac{V}{R_L}$$

where $Q = \frac{1}{w_0 C R_L}$. Therefore, after the substitution into the last expression, it gives

$$\frac{1}{QC}\frac{V}{R_L} = w_0 V$$

Using the relation

$$\int V dt = \frac{1}{jw_0} V(t)$$

It can be shown that

$$\frac{1}{QC}\frac{V}{R_L} = w_0 V = jw_0^2 \int V dt \qquad (3)$$

Now, substitute (2) and (3) into (1), one obtains the following equation

$$\frac{jw_0}{Q} V_{inj} = \frac{jw_0}{Q} V(\frac{-R_d}{R_L}) + \frac{jw_0}{Q} V + j\frac{dV}{dt} + jw_0^2 \int V dt$$

Divide both sides by j,

$$\frac{w_0}{Q} V_{inj} = \frac{w_0}{Q} V(\frac{-R_d}{R_L}) + \frac{w_0}{Q} V + \frac{dV}{dt} + w_0^2 \int V dt \qquad (4)$$

Thus, equation (4) is the mesh equation that describes the rate of change in the amplitude and phase of the oscillator voltage V.

Consider the integral term in equation (4),

$$\int V dt = \int A(t) e^{j(w_0 t + \phi(t))} dt,$$

it can be approximated after the following steps:

Let

$$V(t) = A(t) e^{j(w_0 t + \phi_0)}$$

where, ϕ_0 constant phase is taken from the assumption of slowly varying phase term. The amplitude A(t) can be taken as a function of time.

Using integration by parts, let $u = A(t)$, then $du = A'(t)dt$, and $dv = e^{j(w_0 t + \phi_0)} dt$, then $v = \frac{1}{jw_0} e^{j(w_0 t + \phi_0)}$.

The integral becomes

$$\int V dt = \int A(t) e^{j(w_0 t + \phi_0)} dt = uv - \int v du$$

$$\int V dt = \frac{A(t) e^{j(w_0 t + \phi_0)}}{jw_0} - \frac{1}{jw_0} \int A'(t) e^{j(w_0 t + \phi_0)} dt$$

or

$$\int V dt = \frac{V}{jw_0} - \frac{1}{jw_0} \int A'(t) e^{j(w_0 t + \phi_0)} dt \qquad (5)$$

Consider the integral

$$\int A'(t) e^{j(w_0 t + \phi_0)} dt$$

and apply integration by parts, let $u = A'(t)$, then $du = A''(t)dt$, and $dv = e^{j(w_0 t + \phi_0)} dt$ then $v = \frac{1}{jw_0} e^{j(w_0 t + \phi_0)}$.

After the substitutions, the integral $\int A'(t)e^{j(w_0t+\phi_0)}dt$ takes the following form

$$\int A'(t)e^{j(w_0t+\phi_0)}dt = uv - \int vdu = \frac{A'(t)}{jw_0}e^{j(w_0t+\phi_0)} - \frac{1}{jw_0}\int A''(t)e^{j(w_0t+\phi_0)}dt$$

Substitute this integral expression into equation (5), it gives

$$\int Vdt = \frac{V}{jw_0} - \frac{1}{jw_0}\left(\frac{A'(t)}{jw_0}e^{j(w_0t+\phi_0)} - \frac{1}{jw_0}\int A''(t)e^{j(w_0t+\phi_0)}dt\right)$$

Carrying out the computations will yield

$$\int Vdt = \frac{V}{jw_0} + \frac{A'(t)}{w_0^2}e^{j(w_0t+\phi_0)} - \frac{1}{w_0^2}\int A''(t)e^{j(w_0t+\phi_0)}dt \qquad (6)$$

Now, for further analysis, consider the following expression

$$\frac{dV}{dt} = \frac{d(A(t)e^{j(w_0t+\phi_0)})}{dt} = A'(t)e^{j(w_0t+\phi_0)} + A(t)jw_0e^{j(w_0t+\phi_0)}$$

that is obtained from the chain rule. Solving for the second term

$$A'(t)e^{j(w_0t+\phi_0)} = \frac{dV}{dt} - jw_0V$$

Substitute this last term into equation (6), it gives the following integral equation.

$$\int Vdt = \frac{V}{jw_0} + \frac{1}{w_0^2}\left(\frac{dV}{dt} - jw_0V\right) - \frac{1}{w_0^2}\int A''(t)e^{j(w_0t+\phi_0)}dt$$

or $$\int V dt = -\frac{jV}{w_0} + \frac{1}{w_0^2}\frac{dV}{dt} - \frac{1}{w_0} jV - \frac{1}{w_0^2}\int A''(t) e^{j(w_0 t+\phi_0)} dt$$

After re-arranging the terms

$$\int V dt = -\frac{2jV}{w_0} + \frac{1}{w_0^2}\frac{dV}{dt} + \text{High Order Terms.} \qquad (7)$$

where high order terms come from the part

$$-\frac{1}{w_0^2}\int A''(t) e^{j(w_0 t+\phi_0)} dt$$

which yields second and higher order derivatives of V when it's exposed to integration by parts as was performed previously.

Once again, under the assumption of slowly varying amplitude parameters, high order terms in equation (7) can be neglected. Following Van der Pol [11], the device saturation is modeled by a quadratic such that

$$1 - \frac{R_d}{R_L} \approx \mu(\alpha_0^2 - |V|^2) \qquad (8)$$

where α_0 is the free running amplitude of oscillation, and μ is an empirical nonlinearity parameter describing the oscillation.

Substituting (7) into the mesh equation (4), the differential equation becomes

$$\frac{w_0}{Q} V_{inj} = \frac{w_0}{Q} V\left(1 - \left(\frac{R_d}{R_L}\right)\right) + \frac{dV}{dt} + w_0^2\left[-\frac{2jV}{w_0} + \frac{1}{w_0^2}\frac{dV}{dt}\right]$$

After the substitution of expression (8), it gives the following mesh equation.

$$\frac{w_0}{Q}V_{inj} = \frac{w_0}{Q}V\left[\mu(\alpha_0^2 - |V|^2)\right] + \frac{dV}{dt} + w_0^2\left[-\frac{2jV}{w_0} + \frac{1}{w_0^2}\frac{dV}{dt}\right]$$

Rearranging the terms

$$\frac{w_0}{Q}V_{inj} = \frac{w_0}{Q}V\left[\mu(\alpha_0^2 - |V|^2)\right] + \frac{dV}{dt} - 2jw_0V + \frac{dV}{dt}$$

or

$$\frac{2dV}{dt} = 2jw_0V - \frac{Vw_0\mu}{Q}(\alpha_0^2 - |V|^2) + \frac{w_0}{Q}V_{inj}$$

Solving for dV/dt and make a common factor V, it gives

$$\frac{dV}{dt} = V\left[\frac{w_0\mu}{2Q}(\alpha_0^2 - |V|^2) + jw_0\right] + \frac{w_0}{2Q}V_{inj} \qquad (9)$$

Since $V(t) = A(t)e^{j\theta(t)} = A(t)e^{j(w_0t+\phi(t))}$, the equation (9) can be separated into two parts, rate of change of amplitude and rate of change of angle terms

$$\frac{dA}{dt} \text{ and } \frac{d\theta}{dt}$$

Once again, using the chain rule

$$\frac{dV}{dt} = \frac{d(A(t)e^{j\theta(t)})}{dt} = e^{j\theta(t)}\frac{dA(t)}{dt} + A(t)\frac{de^{j\theta(t)}}{dt} \qquad (10)$$

Equation (9) can be rearranged in the form of (10). Then, the following equation is obtained.

$$\frac{dV}{dt} = A(t)e^{j\theta(t)}\left[\frac{w_0\mu}{2Q}(\alpha_0^2 - \left|A(t)e^{j\theta(t)}\right|^2) + jw_0\right] + \frac{w_0}{2Q}V_{inj}$$

or

$$\frac{dV}{dt} = Ae^{j\theta}\left[\frac{w_0\mu}{2Q}(\alpha_0^2 - A^2\left|e^{2j\theta}\right|) + jw_0\right] + \frac{w_0}{2Q}V_{inj}$$

where $Ae^{j\theta} = A(t)e^{j\theta(t)}$ is taken for simplicity. Since $\left|e^{2j\theta}\right| = 1$, the equation becomes

$$\frac{dV}{dt} = Ae^{j\theta}\left[\frac{w_0\mu}{2Q}(\alpha_0^2 - A^2) + jw_0\right] + \frac{w_0}{2Q}V_{inj}$$

Carrying out with multiplication of the terms, the following equation is obtained.

$$\frac{dV}{dt} = Ae^{j\theta}\frac{w_0\mu}{2Q}(\alpha_0^2 - A^2) + Ae^{j\theta}jw_0 + \frac{w_0}{2Q}V_{inj} \qquad (11)$$

In (11), consider the term

$$Ae^{j\theta}jw_0 + \frac{w_0}{2Q}V_{inj}$$

Common factor the expression for $Ae^{j\theta}$

$$Ae^{j\theta}jw_0 + \frac{w_0}{Q}V_{inj} = Ae^{j\theta}\left(jw_0 + \frac{w_0}{Ae^{j\theta}2Q}V_{inj}\right)$$

$$= Ae^{j\theta}\left(jw_0 + \frac{w_0}{2VQ} V_{inj} \right)$$

$$= Ae^{j\theta} j\left(w_0 + \frac{w_0}{j2VQ} V_{inj} \right) \tag{12}$$

Equation (12) resembles the second term in (10) which is

$$A(t)\frac{de^{j\theta(t)}}{dt} = A(t)e^{j\theta(t)} j\frac{d(\theta(t))}{dt} \tag{13}$$

where $\theta(t) = w_0 t + \phi(t)$.

Therefore, looking at (12), the following angle differential equation can be obtained

$$\frac{d\theta(t)}{dt} = w_0 + \frac{w_0}{2Q} \mathrm{Im}\left(\frac{V_{inj}}{V}\right) \tag{14}$$

and the imaginary part is taken to cancel the j term in the resulting expression so that $\phi(t)$ should be a real phase function.

Similarly, the rest of the expression in (11) will lead us to the amplitude differential term, $\frac{dA(t)}{dt}$.

Writing (11) once more,

$$\frac{dV(t)}{dt} = Ae^{j\theta}\left[\frac{w_0 \mu}{2Q}(\alpha_0^2 - A^2) + jw_0 \right] + \frac{w_0}{2Q} V_{inj}$$

or

$$\frac{dV(t)}{dt} = e^{j\theta}\left(\frac{w_0 \mu}{2Q} A(\alpha_0^2 - A^2) + Ajw_0 \right) + \frac{w_0}{Q} V_{inj}$$

or $$\frac{dV(t)}{dt} = Ae^{j\theta}\frac{w_0\mu}{2Q}(\alpha_0^2 - A^2) + Ae^{j\theta}jw_0 + \frac{w_0}{2Q}V_{inj}$$

This time, we consider the remaining term

$$Ae^{j\theta}\frac{w_0\mu}{2Q}(\alpha_0^2 - A^2) \tag{15}$$

The equation resembles the first term in (10) which is

$$e^{j\theta(t)}\frac{dA(t)}{dt}$$

After comparing with (15),

$$\frac{dA(t)}{dt} = \mu\frac{w_0}{2Q}A(\alpha_0^2 - A^2) \tag{16}$$

However, in the angle derivative expression (14), only the imaginary part of $\frac{V_{inj}}{V}$ was considered. Here, to complete (11), we need to modify (16) as

$$\frac{dA(t)}{dt} = \mu\frac{w_0}{2Q}A(\alpha_0^2 - A^2) + \frac{w_0}{2Q}Re(\frac{V_{inj}}{V}) \tag{17}$$

Hence, we end up with two transient equations, (14) and (17), describing the angle and amplitude behavior of the oscillator voltage waveform. They are summarized below for convenience.

$$\frac{dA(t)}{dt} = \mu\frac{w_0}{2Q}A(\alpha_0^2 - A^2) + \frac{w_0}{2Q}Re(\frac{V_{inj}}{V}) \tag{18}$$

$$\frac{d\theta(t)}{dt} = w_0 + \frac{w_0}{2Q}Im(\frac{V_{inj}}{V}) \tag{19}$$

for both which $\frac{dV}{dt} = Ae^{j\theta}\frac{w_0\mu}{2Q}(\alpha_0^2 - A^2) + Ae^{j\theta}jw_0 + \frac{w_0}{2Q}V_{inj}$ where $V = A(t)e^{j(w_0t+\phi(t))}$ is the oscillator voltage.

2.4 Adler's Equation:

For low level injected signals, in other words, for $|V_{inj}| << |V|$, the amplitude of the oscillator will stay close to its free-running value. Therefore, at the steady state, the contribution of the amplitude term (18) can be ignored and the system behavior is predominantly governed by the angle derivative (19)

$$\frac{d\theta(t)}{dt} = w_0 + \frac{w_0}{2Q}\mathrm{Im}(\frac{V_{inj}}{V})$$

Writing that

$$V_{inj} = A_{inj}e^{j(w_{inj}t+\psi_{inj})} = A_{inj}e^{j\theta_{inj}}$$

and substituting in (19) gives

$$\frac{d\theta(t)}{dt} = w_0 + \frac{w_0}{2Q}\frac{A_{inj}}{A}\sin(\theta_{inj} - \theta) \qquad (20)$$

which is the Adler's equation for injection locking.

When the oscillator locks onto the injected signal, the oscillation frequency must follow the injected signal frequency w_{inj}, such that

$$\theta(t) = w_{inj}t + \phi(t) \qquad (21)$$

is the injection-locked oscillation angle at steady state.

Substitute (21) in (20), following equation is obtained.

$$\frac{d\theta(t)}{dt} = w_0 + \frac{w_0}{2Q}\frac{A_{inj}}{A}\sin(w_{inj}t + \psi - w_{inj}t - \phi_0)$$

or

$$\frac{d\theta(t)}{dt} = w_0 + \frac{w_0}{2Q}\frac{A_{inj}}{A}\sin(\psi - \phi_0) \tag{22}$$

where ψ is the injection signal phase and ϕ_0 is the steady state output oscillator phase.

Taking the derivative of (21)

$$\frac{d\theta(t)}{dt} = w_{inj} + \frac{d\phi(t)}{dt}$$

and substituting in (22) gives

$$\frac{d\phi(t)}{dt} = w_0 - w_{inj} + \frac{w_0}{2Q}\frac{A_{inj}}{A}\sin(\psi - \phi_0) \tag{23}$$

In steady state, when the oscillator is synchronized with the injected signal, there must be no phase variation in order for stable oscillation.

Therefore, it must be that

$$\frac{d\phi(t)}{dt} = 0$$

Under this condition, equation (23) can be re-written as

$$0 = w_0 - w_{inj} + \frac{w_0}{2Q}\frac{A_{inj}}{A}\sin(\theta_{inj} - \theta)$$

or $$w_{inj} = w_0 + \frac{w_0}{2Q}\frac{A_{inj}}{A}\sin(\theta_{inj} - \theta)$$

Define the following abbreviations,

$$\Delta\phi = \psi - \phi_0 \tag{24}$$

and

$$\Delta w_m = \frac{w_0}{2Q}\frac{A_{inj}}{A} \tag{25}$$

where ψ is the injected signal phase and ϕ_0 is the steady state oscillator phase.

After the substitution of the abbreviations, the steady state Adler's equation becomes

$$w_{inj} = w_0 + \Delta w_m \sin(\Delta\phi) \tag{26}$$

which is another form of Adler's equation. Solving it for $\Delta\phi$

$$\Delta\phi = \sin^{-1}\left(\frac{w_{inj} - w_0}{\Delta w_m}\right) \tag{27}$$

whose solution domain for w_{inj} can be evaluated from

$$-1 < \frac{w_{inj} - w_0}{\Delta w_m} < 1$$

where the solution lies in the range

$$w_{inj} = w_0 \pm \Delta w_m \tag{28}$$

From this range equation, the most important observation is that the injected signal frequency is highly dependent on the parameter Δw_m, which is often referred as the "Adler's locking range".

Therefore, for a given free-running oscillator frequency, injected signal frequency must lie within the bandwidth of $2\Delta w_m$. As an example, considering a 1GHz oscillator is to be locked by an injection signal, and assuming Δw_m to be 100MHz, it's therefore necessary to apply the injection signal between 0.9 to 1.1GHz.

Certainly, it may be desirable to have large locking ranges, however, the difficulty is that large signal strengths and low Q resonators are required.

In order to examine phase variations of the oscillator when being inside the locking range, we utilize the stability analysis as follows:

At the steady state, the Adler's equation is given by the equation

$$\left.\frac{d\phi(t)}{dt}\right|_0 = w_0 - w_{inj} + \frac{w_0}{2Q}\frac{A_{inj}}{A}\sin(\psi - \phi_0)$$

Since $\left.\frac{d\phi(t)}{dt}\right|_0 = 0$ at the steady state, the equation becomes

$$0 = w_0 - w_{inj} + \Delta w_m \sin(\Delta\phi)$$

where

$$\Delta w_m = \frac{w_0}{2Q}\frac{A_{inj}}{A}$$

and

$$\Delta\phi = \psi - \phi_0 = \text{constant.}$$

When the phase is to be changed, it will be perturbed from its steady state value (ϕ_0) by

$$\phi = \phi_0 + \delta\phi$$

where $\delta\phi$ is the phase perturbation in a small unit of time. Therefore, it can be written that

$$\delta\phi = \frac{d\phi}{dt}$$

and the Adler's equation becomes

$$\delta\phi = w_0 - w_{inj} + \Delta w_m \sin[\psi - (\phi_0 + \delta\phi)]$$

or

$$\delta\phi = w_0 - w_{inj} + \Delta w_m \sin[\psi - \phi_0 - \delta\phi] \quad (29)$$

Equation (29) is the new phase equation after the perturbation.

Taking the time derivative of (29) gives the information about how the perturbation will progress in time.

Therefore,

$$\frac{d\delta\phi}{dt} = \frac{d}{dt}\{w_0 - w_{inj} + \Delta w_m \sin[\psi - \phi_0 - \delta\phi]\}$$

$$\frac{d\delta\phi}{dt} = -\delta\phi\Delta w_m \cos[\psi - \phi_0 - \delta\phi]$$

$$\frac{d\delta\phi}{dt} = -\delta\phi\Delta w_m \cos(\Delta\phi) \quad (30)$$

where $\Delta\phi = \psi - (\phi_0 + \delta\phi)$ is the phase difference after the perturbation.

In order perturbation to decay in time so that the phase stabilizes back to steady state (otherwise grows to infinity) , the right hand side of (30) should be kept negative. (negative slope)

This occurs for $\cos(\Delta\phi) > 0$, which restricts the phase difference to the range

$$-\frac{\pi}{2} \leq \Delta\phi \leq \frac{\pi}{2} \tag{31}$$

that is called the "Locking Range". According to this relation, the phase can be changed from $-\pi/2$ to $\pi/2$, depending on the variables w_{inj}, w_0 and Δw_m in accordance with (27).

In addition, consider the term

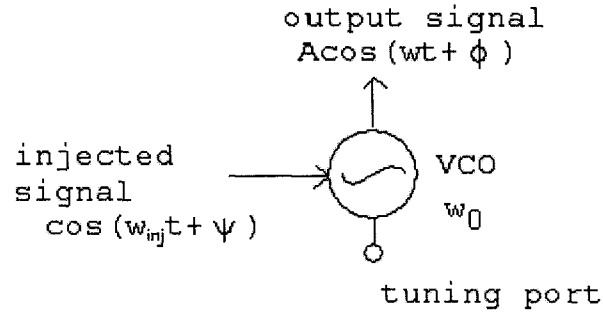
$$\Delta w_m = \frac{w_0}{2Q}\frac{A_{inj}}{A}$$

It's concluded that, the locking range is proportional to the injected signal strength, and inversely related to the Q-factor. In microwave feedback oscillators, Q-factor is usually above 10. Therefore, larger amplitude injections are required for larger ranges.

Rewriting (27),

$$\Delta\phi = \sin^{-1}\left(\frac{w_{inj} - w_0}{\Delta w_m}\right)$$

A plot that shows the behavior of the oscillator phase difference with respect to $\frac{w_{inj} - w_0}{\Delta w_m}$, is given in Figure 2.4.1. [16]-[18]



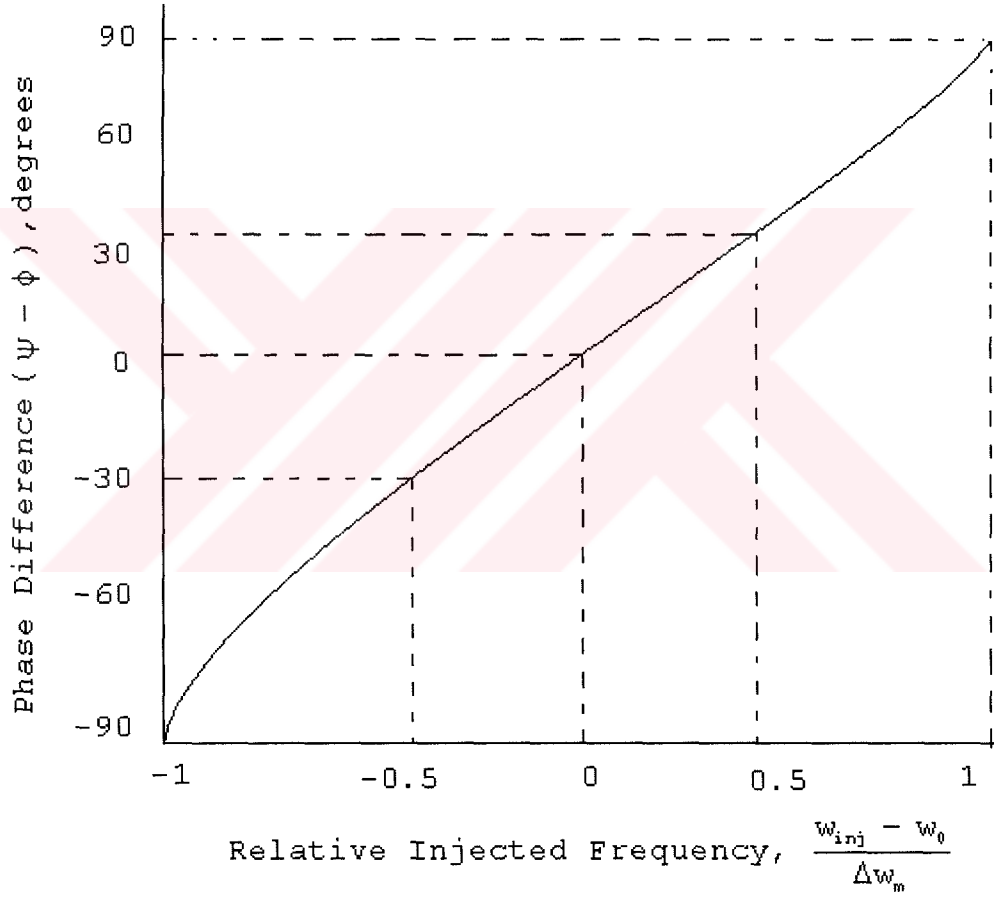


Figure 2.4.1 Phase Difference in injection locking.

CHAPTER 3

DESIGN AND SIMULATIONS

3.1 VCO (Voltage Controlled Oscillator) Design and Simulations:

3.1.1 Design Theory:

In general, the circuit diagram of a microwave oscillator contains a resonator circuit, a load circuit and the active network being a transistor amplifier. This scheme is given in the following diagram. [12]

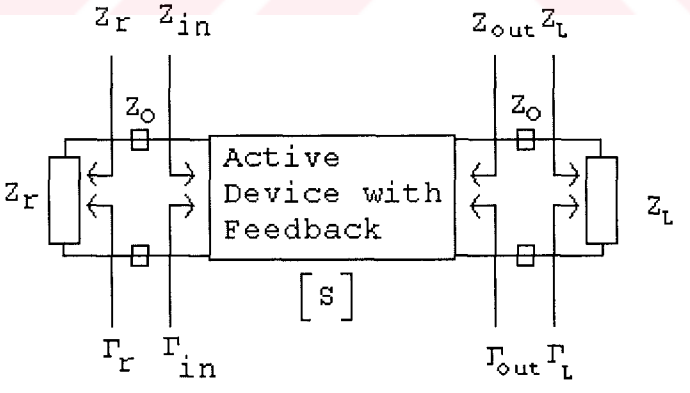


Figure 3.1.1 Microwave oscillator network diagram.

where

$$\Gamma_r = \frac{Z_r - Z_0}{Z_r + Z_0}, \qquad \Gamma_{in} = \frac{Z_{in} - Z_0}{Z_{in} + Z_0},$$

$$\Gamma_{out} = \frac{Z_{out} - Z_0}{Z_{out} + Z_0}, \qquad \Gamma_L = \frac{Z_L - Z_0}{Z_L + Z_0}.$$

In a transmission line, incident and reflected powers can be defined as

$$P_i = \frac{\left|V^+\right|^2}{Z_0}$$

$$P_r = \frac{\left|V^-\right|^2}{Z_0}$$

respectively.

Here, $\left|V^+\right|$ and $\left|V^-\right|$ are incident and reflected voltage waves inside the transmission line with characteristic impedance Z_0.

Writing that

$$\frac{P_r}{P_i} = \frac{\left|V^-\right|^2}{\left|V^+\right|^2} = \left|\Gamma\right|^2$$

Then,

$$P_r = P_i\left|\Gamma\right|^2$$

Now, let k watts be the incident power at one moment inside the line with Z_0. Then, according to the previous equation, the reflected power from the active device is $k|\Gamma_{in}|^2$. This power is re-reflected from the resonator as $k|\Gamma_{in}|^2|\Gamma_r|^2$.

Hence, if $|\Gamma_{in}|^2|\Gamma_r|^2 > 1$ the oscillations build up.

Similarly for $|\Gamma_{in}|^2|\Gamma_r|^2 < 1$ waves will decay rapidly and no oscillations take place.

Finally for $|\Gamma_{in}|^2|\Gamma_r|^2 = 1$ the equation is

$$\left|\frac{V_{r1}}{V_{in1}}\right|^2 \left|\frac{V_{in1}}{V_{r2}}\right|^2 = 1$$

or

$$\left|\frac{V_{r1}}{V_{r2}}\right|^2 = 1$$

or

$$V_{r1} = V_{r2}$$

where V_{r2} represents the incident wave V_{inc2}.

Hence, for $|\Gamma_{in}|^2|\Gamma_r|^2 = 1$, incident and reflected powers are equal and the oscillation is at the steady state.

For all networks whose input impedance $Z_{in} = R_{in} + jX_{in}$, if $R_{in} \geq 0$ then $\Gamma_{in} \leq 1$. On the other hand, if $R_{in} < 0$ then $\Gamma_{in} \geq 1$ and if $R_{in} = 0$ then $\Gamma_{in} = 1$.

Since the resonator is a passive device, $\Gamma_r \leq 1$. Hence, $|\Gamma_{in}\Gamma_r| > 1$ requires that $|\Gamma_{in}| > 1$. To obtain this, $R_{in} < 0$, negative resistance must retained.

3.1.2 Design Topology:

A typical oscillator design topology is given in the following scheme [12].

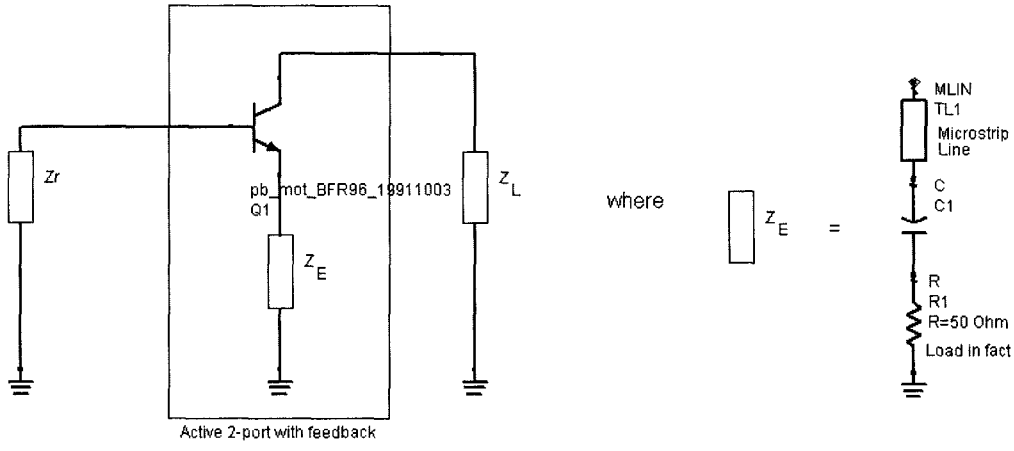


Figure 3.1.2 Oscillator design topology.

In the design process, $|\Gamma_{in}| = 1$ circle is drawn on the Smith Chart. Then, by using the transformation equation [13]

$$\Gamma_{in} = s_{11} + \frac{s_{12}s_{21}\Gamma_L}{1-\Gamma_L s_{22}} \tag{32}$$

it's mapped onto Γ_L (or Z_L) plane. Regions on the load plane (Γ_L-plane) in which $|\Gamma_{in}| > 1$ is unstable and the load impedance Z_L is chosen from this region.

Once Z_L is determined, Γ_{in} can be evaluated by using the equation (32). S-parameters can be obtained from the transistor's datasheet.

Then, by using the equality

$$\Gamma_{in} = \frac{Z_{in} - Z_0}{Z_{in} + Z_0} \quad \text{or} \quad Z_{in} = Z_0 \frac{1 + \Gamma_{in}}{1 - \Gamma_{in}}$$

Z_{in} can be determined.

At the steady state, $|\Gamma_{in}\Gamma_r| = 1$. Substitute, $\Gamma_{in} = \frac{Z_{in} - Z_0}{Z_{in} + Z_0}$ and $\Gamma_{in} = \frac{Z_{in} - Z_0}{Z_{in} + Z_0}$ into $|\Gamma_{in}\Gamma_r| = 1$, one obtains

$$Z_r + Z_{in} = 0$$

where

$$Z_r = R_r + jX_r$$

and

$$Z_{in} = R_{in} + jX_{in}.$$

Hence,

$$R_r = -R_{in} \tag{33}$$

and

$$X_r = -X_{in} \tag{34}$$

Equation (34) leads to the frequency of the oscillation. Equation (33) is the steady state equilibrium which is reached when the oscillation magnitude grows from noise levels to volts, and it starts affecting the regions with positive resistance.

In summary, the oscillation starts up with $R_{in} > R_r$, and $R_{in} < 0$. Because of the transistor's nonlinearity, as the magnitude grows, $R_r = -R_{in}$ is reached.

Then, for design purposes, $X_r = -X_{in}$ gives the resonator reactance. R_r is selected to be slightly greater than R_{in} for the start-up. As a result, Z_r can be determined.

3.1.3 Feedback:

Additionally, positive feedback is necessary to start and sustain oscillations. In other words, sufficient feedback will result s-parameters in equation (32) to yield a solution for Z_L for a given Z_{in}. Practical feedback circuit is a series feedback as shown in Figure 3.1.3.

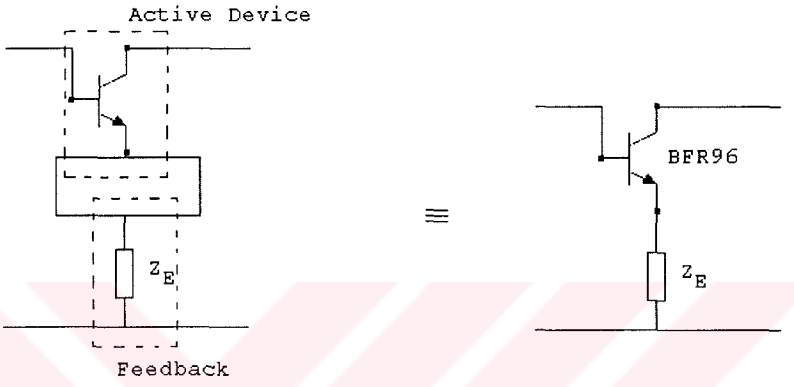


Figure 3.1.3 Feedback circuit.

Note that the feedback circuit Z_E contains a real load which is generally 50Ω. BFR96 is an RF transistor operating up to 2GHz ranges. It's used in RF amplifiers specifically in wide band antenna amplifiers. It has predominant features which are high power gain, low noise figure and high transition frequency.

3.1.4 DC Biasing:

Transistor biasing circuit is given in Figure 3.1.4. From the transistor's datasheet, DC bias conditions are selected for which I_C=15.2mA and V_{CE}=5V. It's also given that β of the transistor is 75, typically.

The inductor at the emitter serves as the path for DC and it also allows RF to flow into the load resistor R2.

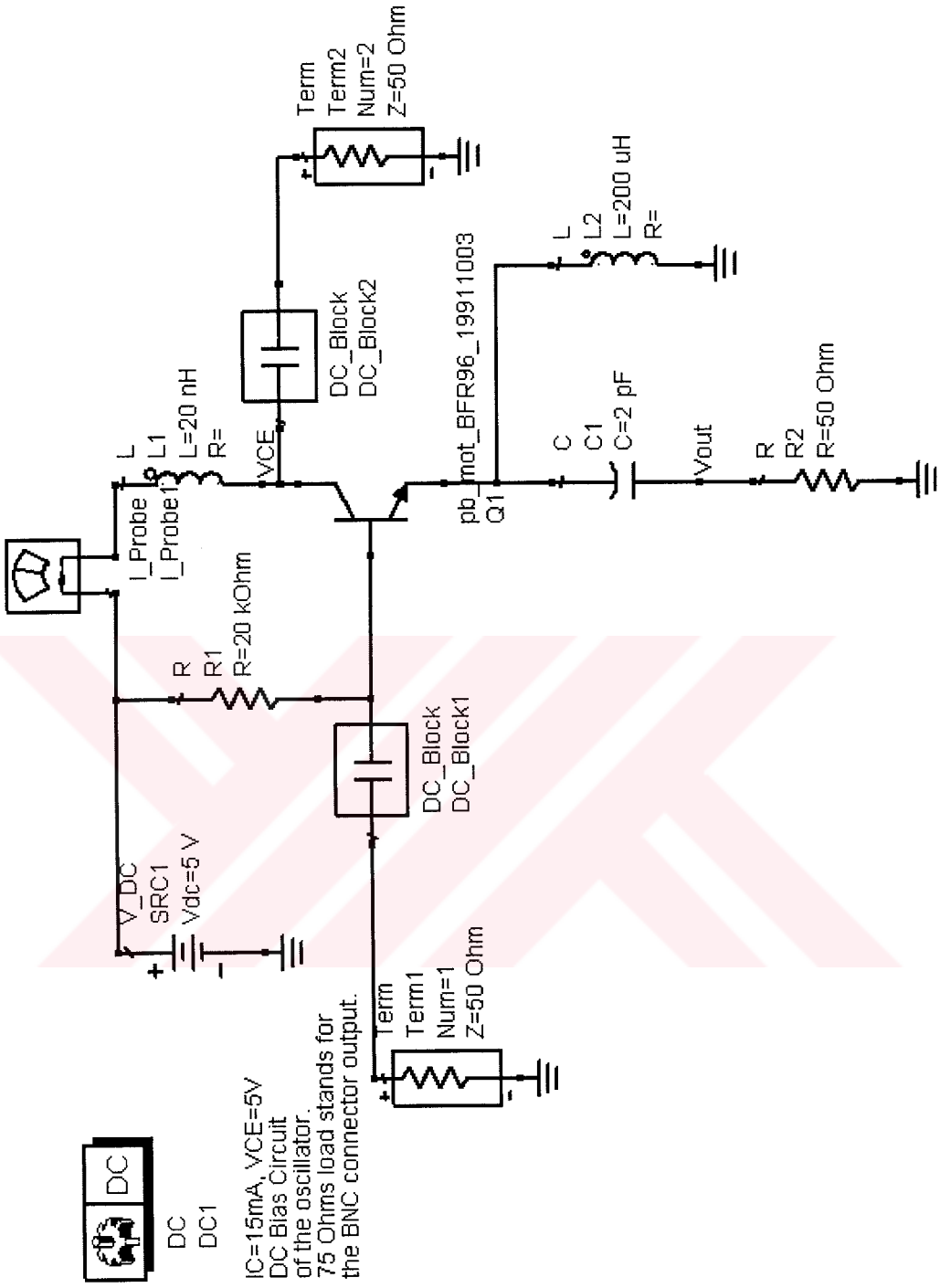


Figure 3.1.4 DC bias circuit.

In order to determine the bias resistance R_B, the following computation is carried out

$$I_B = \frac{I_C}{\beta} = \frac{15\text{mA}}{75} = 200\,\mu\text{A}.$$

Then,

$$R_B = \frac{(5-0.7)\text{V}}{I_B} = \frac{(5-0.7)\text{V}}{200\,\mu\text{A}} = 21500\,\Omega \approx 20\,\text{k}\Omega.$$

Therefore, taking R_B = 20kΩ will yield roughly the desired DC conditions. Also, an increase in supply voltage to 10V (V_{CE}=10V) will yield I_C to be about 50mA.

DC computer simulation results for the circuit in Figure 3.1.4 are shown below.

Table 3.1.4 DC bias conditions.

freq	VCE	I_Probe1.i
0.0000 Hz	5.000 V	15.21mA

that agrees with the computation results.

3.1.5 S-parameter Analysis:

Having established the DC conditions, s-parameter analysis can be performed in order to plot stability circles on the Smith Chart. Figure 3.1.5.1 is a circuit for such analysis. Note that s-parameter analysis is referenced to 50Ω impedances both at the input end and at the output end.

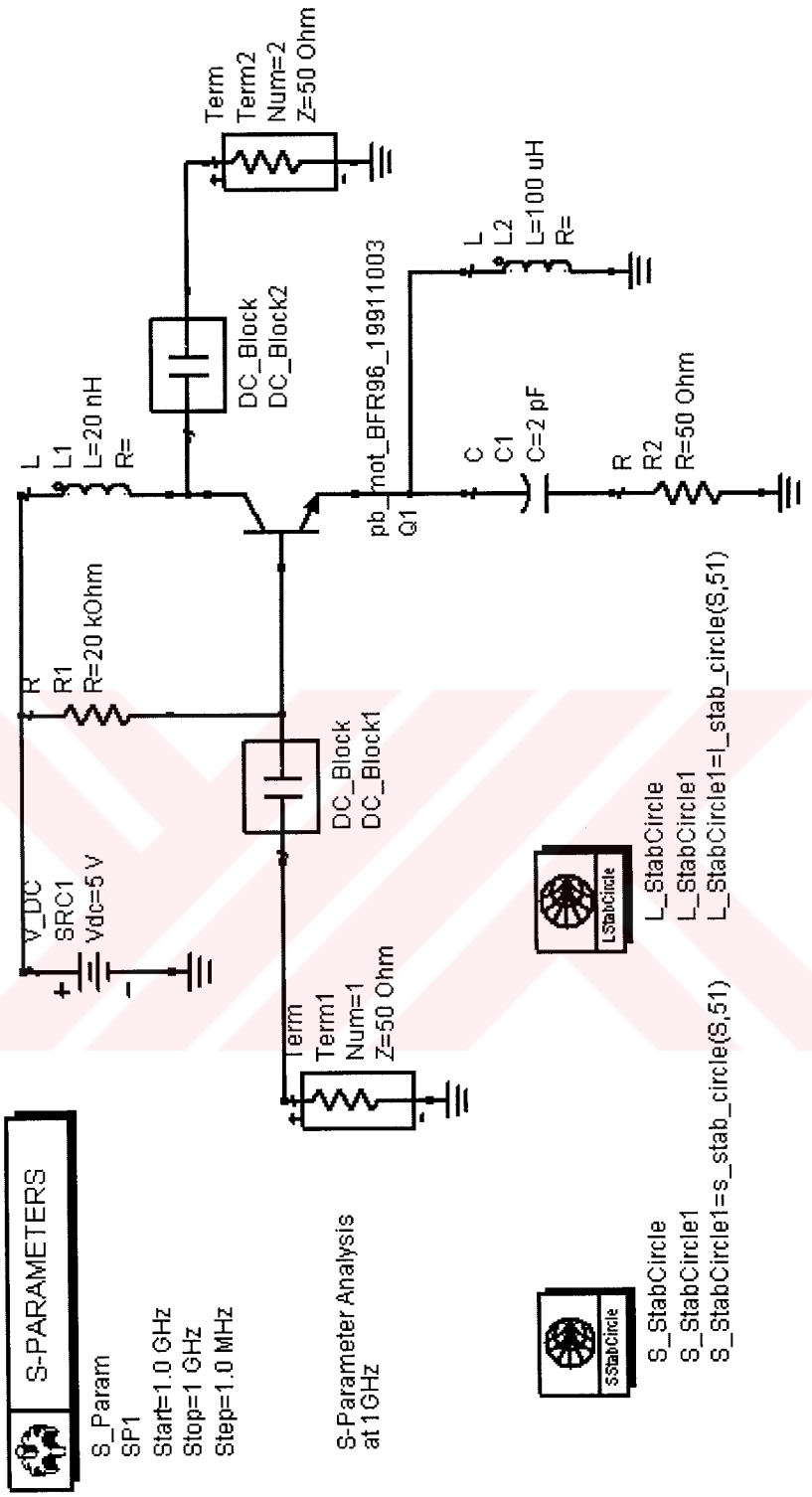


Figure 3.1.5.1 S-parameter analysis circuit.

Simulation is carried out for f=1GHz for the load stability circle (output) and the source (input) stability circle. Also, remembering that stability circles correspond to $|\Gamma_{in}| = 1$ circle on the load plane and $|\Gamma_{out}| = 1$ circle on the source plane (input plane) on the Smith Chart.

Later, in the implementation of this circuit, the output will be taken from the feedback resistor and connected to a coaxial cable. Therefore, the resistor R2=50Ω represents a BNC connector input impedance in reality.

Simulation results of stability circles for the circuit in Figure 3.1.5.1 are given on the Smith Chart below.

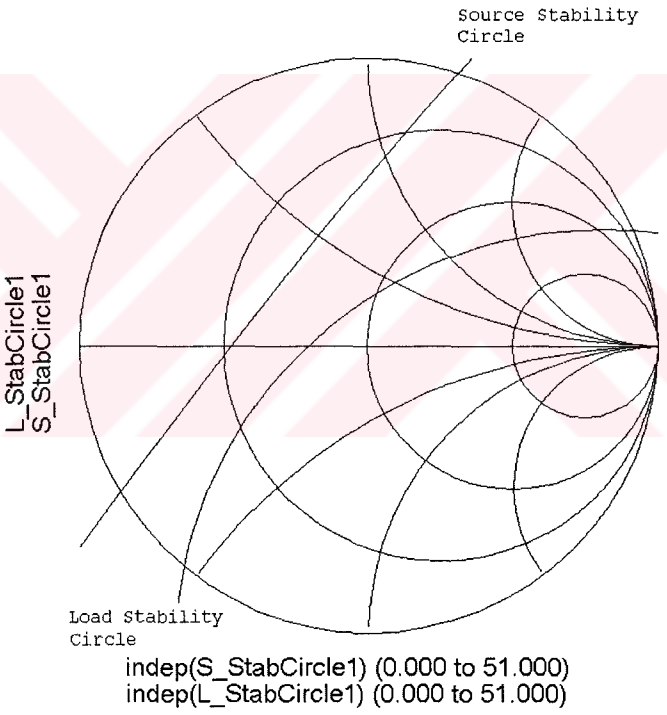


Figure 3.1.5.2 Stability circles.

As a result of the computer simulation, s-parameters for this circuit are given in the following table.

Table 3.1.5 S-parameters.

freq	S			
	S(1,1)	S(1,2)	S(2,1)	S(2,2)
1.000GHz	0.900 / -104.698	0.907 / 27.449	0.835 / 91.808	0.581 / -46.286

For the load stability circle, since $|s_{11}| < 1$, then the region where the center of the Smith chart is situated is the stable region. Similarly, for the source stability circle, since $|s_{22}| < 1$, then the region where the center is situated is the stable region.

In order for $|\Gamma_{in}| > 1$ $(R_{in} < 0)$, the load impedance must be inside the unstable region on Γ_L (or Z_L) plane. Therefore, Z_L=0Ω is a possible solution.

Writing equation (32) once more

$$\Gamma_{in} = s_{11} + \frac{s_{12}s_{21}\Gamma_L}{1-\Gamma_L s_{22}}$$

Then, substitute Z_L=0Ω ($\Gamma_L = -1$) in this equation

$$\Gamma_{in} = s_{11} + \frac{s_{12}s_{21}(-1)}{1-s_{22}(-1)}$$

where s parameters are already obtained in Table 3.1.5. Substitute them in the equation as well

$$\Gamma_{in} = 0.756\angle -103^0 + \frac{(0.851\angle 32^0)(0.856\angle 82^0)(-1)}{1-(0.513\angle -40^0)(-1)}$$

$$\Gamma_{in} = 1.24\angle -83^0$$

Substitute Γ_{in} in the following equation

$$Z_{in} = Z_0 \frac{1+\Gamma_{in}}{1-\Gamma_{in}}$$

or

$$Z_{in} = 50\frac{1+(1.24\angle -83^0)}{1-(1.24\angle -83^0)} = -12 - j54.74\,\Omega$$

Hence, the resonator should be chosen such that $|R_r| < |R_{in}|$ in this frequency range. Also, its Q high enough to eliminate X_{in}.

Let Rr=10 Ω and $X_r = -X_{in} = 54.74 = wL$, then

L=8.7nH at f=1GHz.

Therefore,

$$Z_r = 10 + j54.74\,\Omega.$$

Normalizing Z_r to 50 Ω,

$$\bar{z}_r = \frac{10+j54.74}{50} = 0.2 + j1.1\Omega$$

A plot of z_r on the Smith chart is given in the Figure 3.1.5.3. Stability circles and Z_L are also drawn for stability analysis.

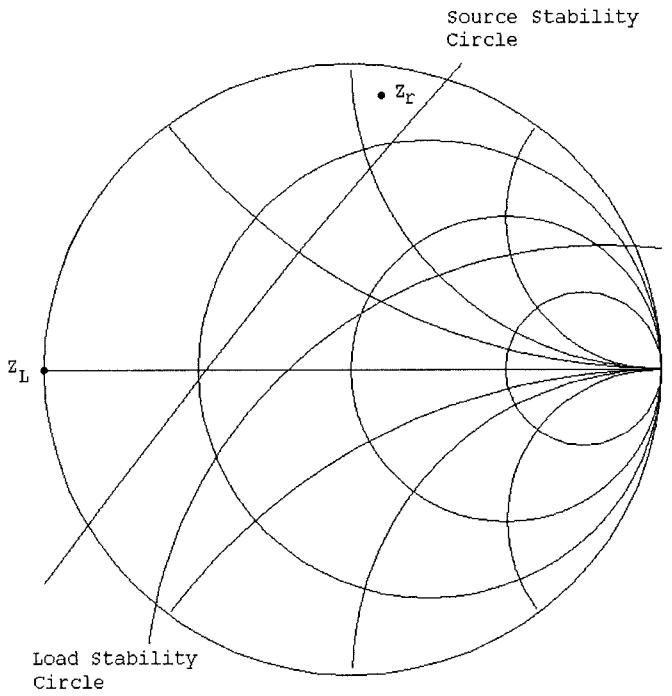


Figure 3.1.5.3 Resonator and load impedances.

Since $|s_{22}| < 1$, then the region where the center of the Smith chart is situated is the stable region. Therefore the source impedance is also inside the unstable region on Γ_{in} (or Z_{in}) plane.

Up to this point, Z_r and Z_L are obtained. Another important consideration with the oscillator circuit is the collector inductor. The value of 20nH is chosen arbitrary at this point. Nevertheless, it's also a reasonable value such that considering a micro strip line with length of 2cm (in fact, about the same length is used in the layout) in place of the inductor, then from the transmission line theory

$$\lambda = c/f = 3\times10^8/1\times10^9 = 30\,\text{cm}.$$

$$\lambda/2 = 15\text{cm}$$

which is a full around in the Smith Chart. Therefore at 2cm line length,

$$\theta = (360 \times 2)/15 = 48^0$$

degrees are covered. Since Z_L=0Ω, roughly 0.4H of inductance is asserted into the collector from the short circuited end of the Smith chart.

De-normalizing this value results

$$L = 0.4 \times 50 = 20\text{nH}.$$

this agrees with our simulation choice.

Also keeping in mind that the design has been possible through s-parameters after sufficient feedback was introduced. Without the feedback, stability circles may never cross the Smith chart and the system may remain unconditionally stable.

3.1.6 Harmonic Balance Analysis:

Harmonic balance analysis is performed to observe the output response in the frequency domain.

Simulation set-up scheme is shown in Figure 3.1.6.1. In this figure, there are a few points remarkable. First of all, Z_L=0Ω is placed at the load as evaluated from the s-parameter design. Secondly, for the source impedance, a special component, "OscPort", is placed with a series resonant circuit, "cResS". This resonant circuit represents the resonant impedance which was also obtained previously as R=10Ω, L=8.7nH or

$$Z_r = 10 + j54.74\,\Omega.$$

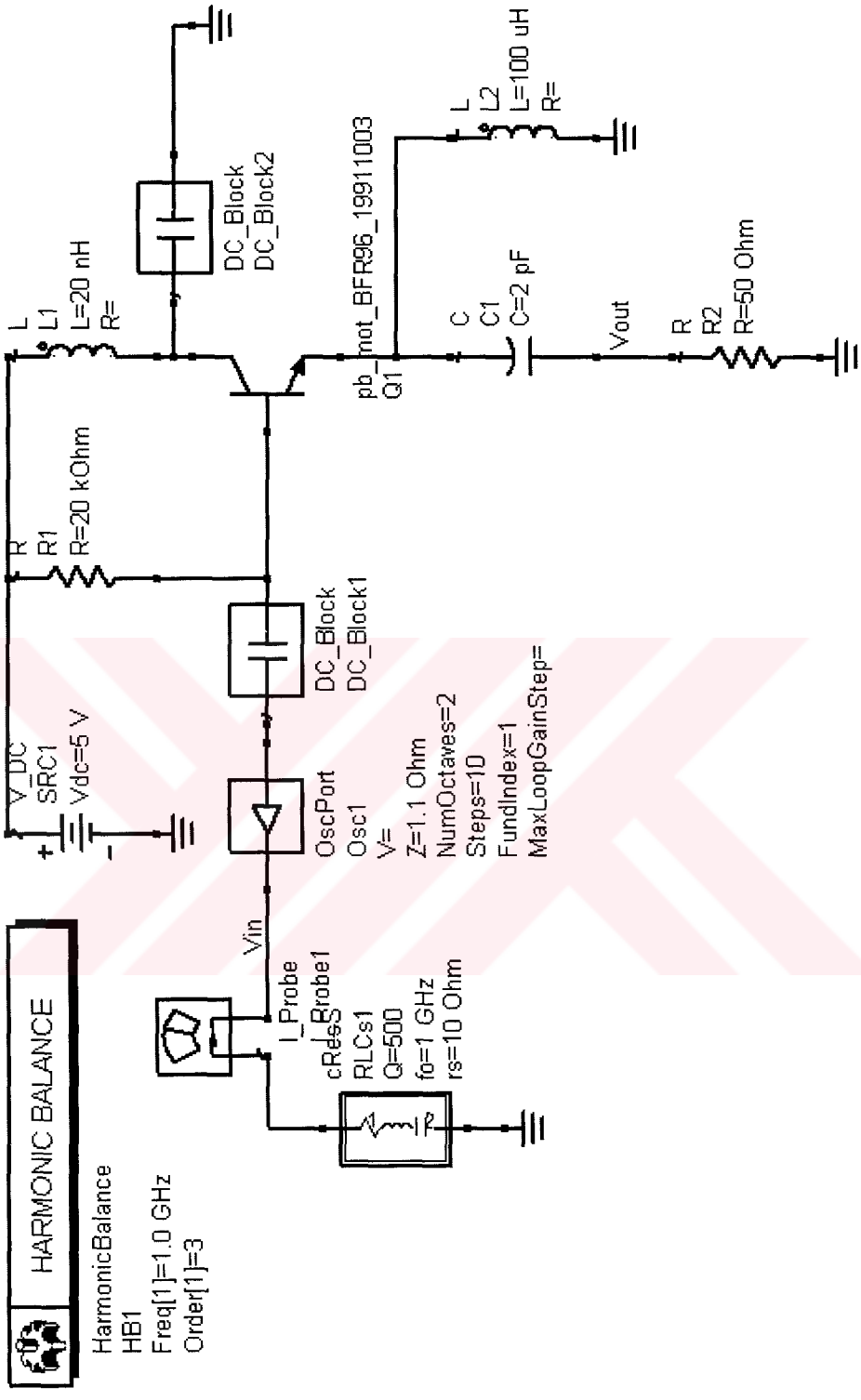


Figure 3.1.6.1 Harmonic balance analysis circuit.

Furthermore, a current measurement device, I_Probe, and a voltage marker V_{in} are placed at the source so that

$$Z_{in} = \frac{V_{in}}{I_Probe}$$

can be computed and verified that it aggress with the theoretically obtained

$$Z_{in} = -12 - j54.74\Omega$$

and

$$Z_r = 10 + j54.74\Omega.$$

at f=1GHz.

As a result of the simulation, the output voltage, V_{out}, is plotted in frequency and time domains for three of its harmonics. This is shown in Figure 3.1.6.2.

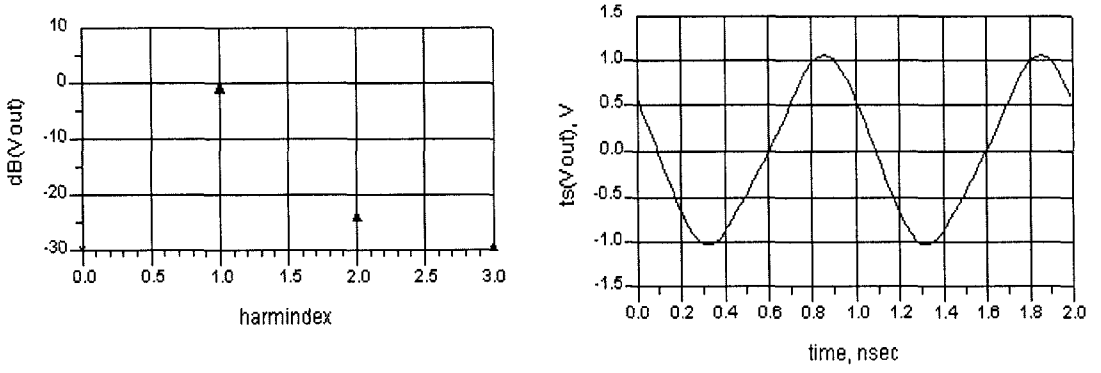


Figure 3.1.6.2 Harmonic balance simulations.

To verify the resonator impedance, a computer simulation is performed for the circuit in Figure 3.1.6.1 and the following results are obtained.

Table 3.1.6 Resonator impedance simulation.

Eqn Zr=Vin/I_Probe1.i

harmindex	Zr
0	<invalid>
1	49.789 / -101.587
2	7.561E3 / -90.076
3	1.341E4 / -90.043

Therefore at f=1GHz,

$$Z_{in} = 49.1\angle -101.587^0 = -9.86 - j48\Omega.$$

This is fairly closed to

$$Z_{in} = -12 - j54.74\Omega.$$

Furthermore, the output power of the oscillator can be evaluated as

$$P_{out} = \frac{1}{2}\frac{V_{peak}^2}{R} = \frac{1}{2}\frac{(1.2)^2}{50} \approx 15\,\text{mW}.$$

3.1.7 Time Domain (Transient) Analysis:

With the purpose of simulating the complete circuit behavior, time domain analysis is carried out for the set-up in the following figure. Also, in this circuit, Z_r is replaced with a series inductor and a resistor.

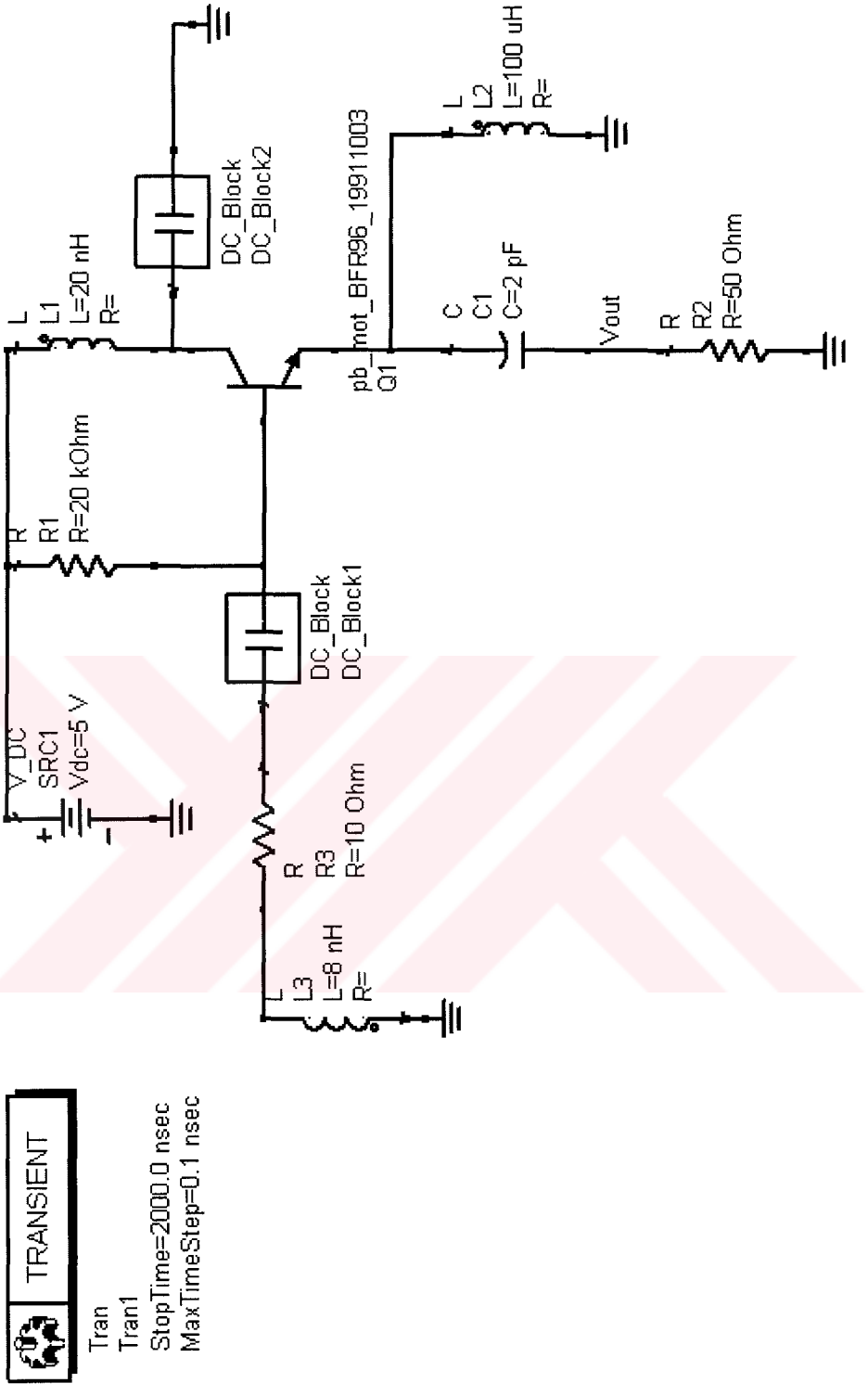


Figure 3.1.7.1 Time domain analysis circuit.

Simulation results for the time domain analysis are given in the Figure 3.1.7.2.

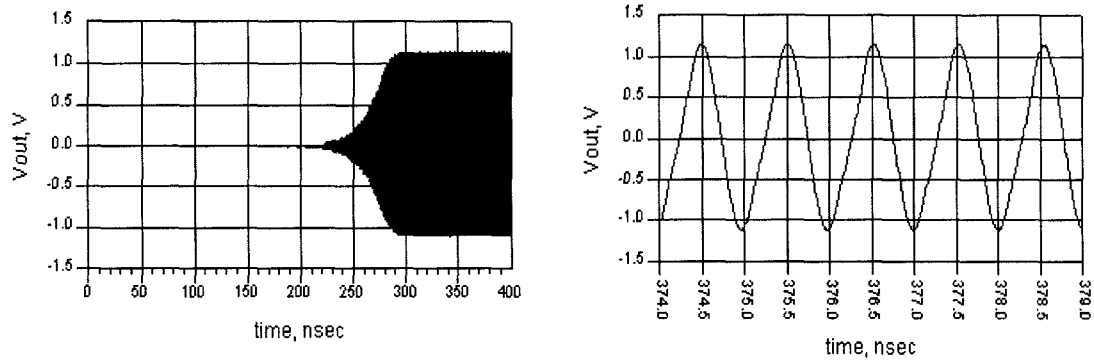


Figure 3.1.7.2 Time domain simulations.

It's also possible to obtain frequency domain translation of this response. This is shown in Figure 3.1.7.3.

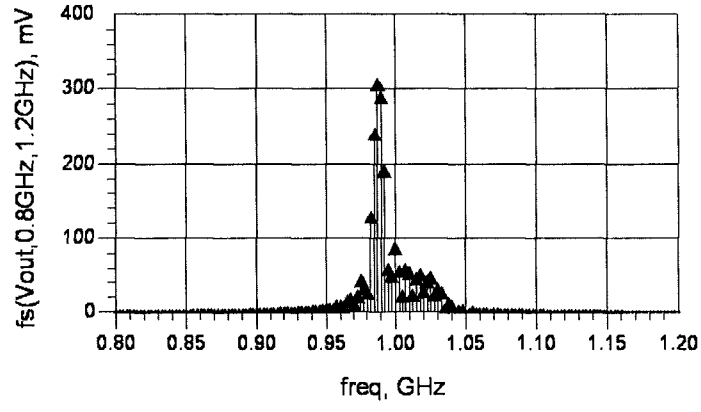


Figure 3.1.7.3 Frequency response of V_{out}.

In this graph, the residual frequency components are due to transient behavior of the oscillator. If the simulation is let run for longer periods, the response becomes sharper and gets closer to a delta function at 0.98GHz. The exact 1GHz response is possible via resonator inductance tuning. For example, for L=7.5nH, R=10 Ω, the resonance frequency settles right at 1GHz.

3.1.8 Frequency Control via Varactor Diodes:

Frequency of oscillation can be adjusted to a certain extend by modifying the resonator network reactance. Theory behind this concept follows that at every frequency, the core oscillator (with DC biasing and feedback) has different s-parameters and hence stability circles. At any frequency, as long as the device is unstable, there is always a $Z_{in}=R_{in}+jX_{in}$ where $R_{in}<0$. Conversely, when X_r is introduced as a resonator circuit $X_r=-X_{in}$ determines the frequency of oscillation.

The easiest method for altering resonator impedance is by connecting a varactor diode at the base of the oscillator. In the reverse biasing, the diode shows variable capacitance depending on the reverse voltage applied. Therefore, by changing the capacitance, it's possible to change the resonant frequency.

The diode used in the application is bb640, an RF varactor (UHF band), with 70pF capacitance deviation possible at 0-30V reverse voltage range at 1MHz. At 1GHz, a few pF deviations can be obtained.

Figure 3.1.8.1 shows the oscillator with varactor diode connected at the base. The simulation is carried out for the output voltage waveform with several different reverse voltage values across the diode. Results are shown in the following Figure 3.1.8.2.

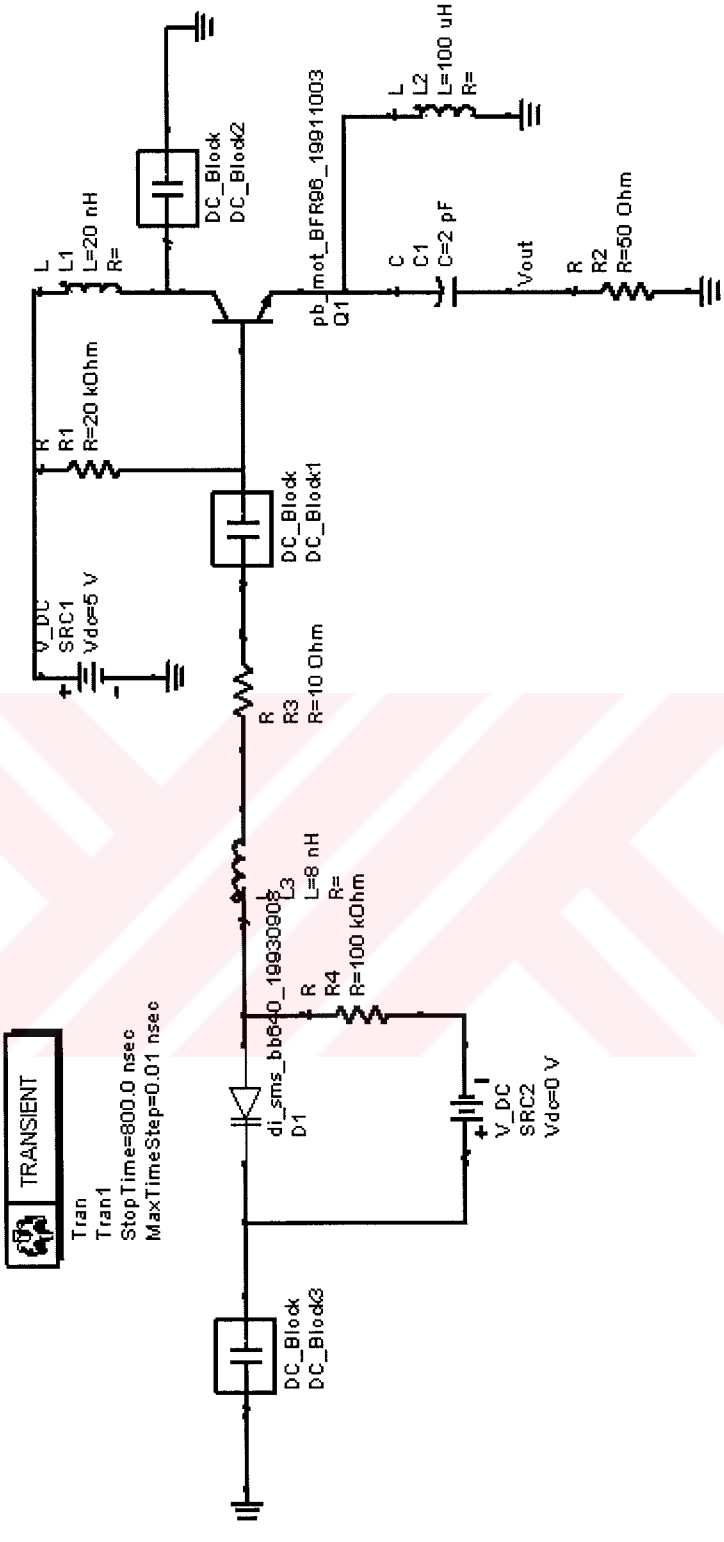


Figure 3.1.8.1 VCO circuit.

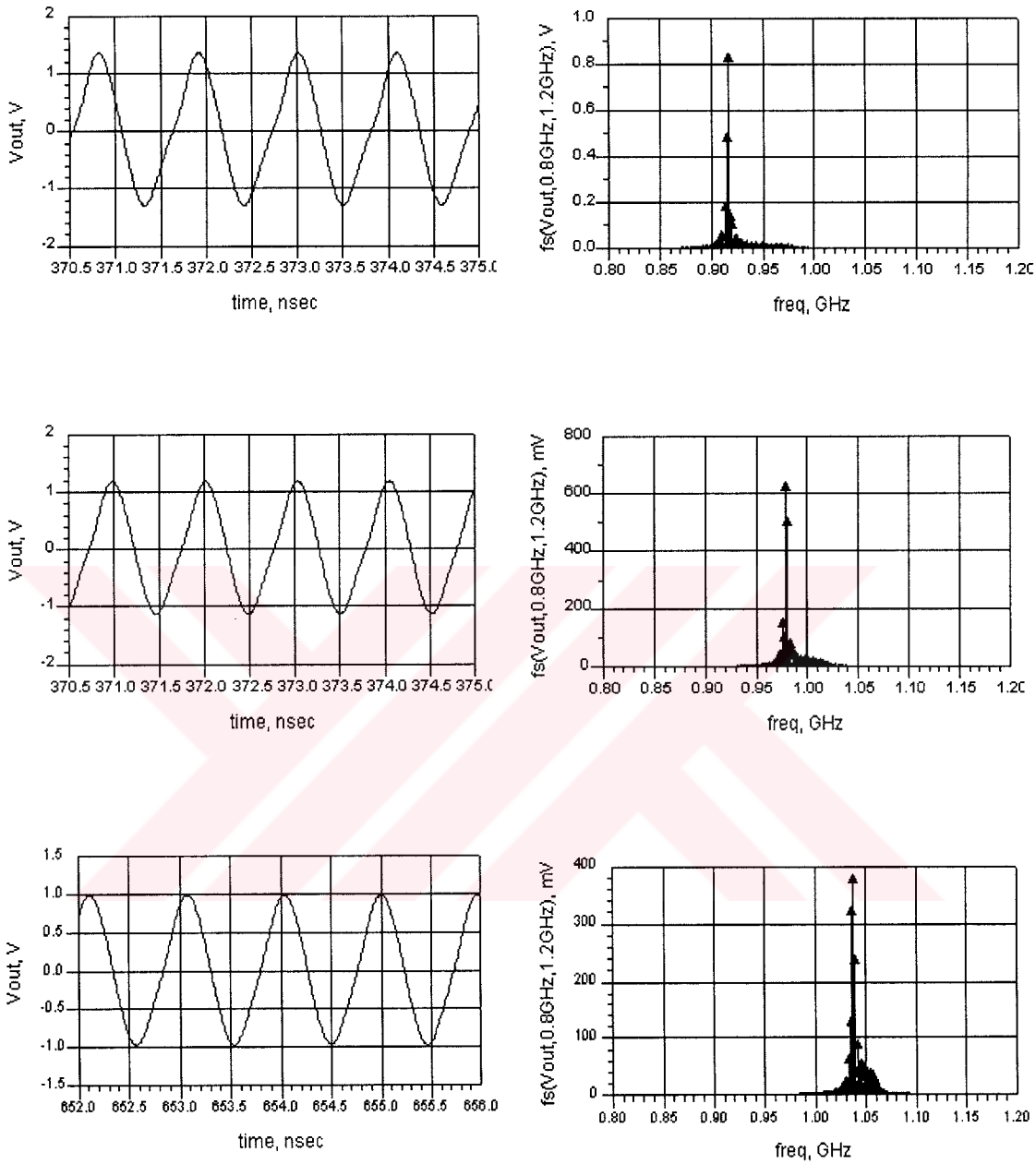


Figure 3.1.8.2 VCO outputs for V_r(V_DC SRC2)=0V,-6V,-12V.

3.2 Phase Locking Circuit Design:

In an attempt to simulate phase locking scheme , the simplest set-up can be formed by two oscillators. One oscillator represents the controlling signal (locking signal or injection signal), and the other represents the controlled output signal or the master signal. A diagram is given below.

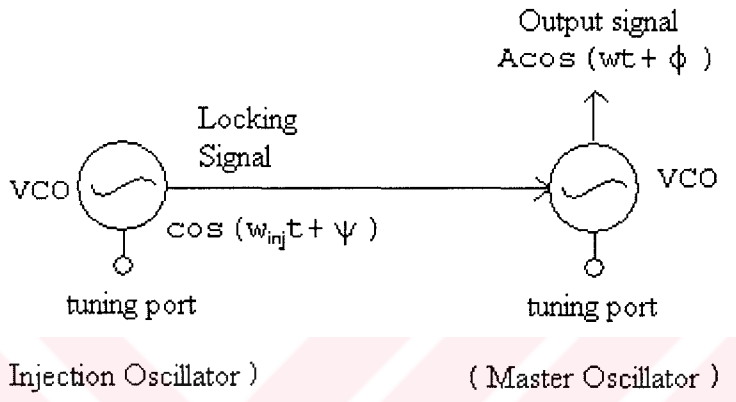


Figure 3.2.1 Phase locking test diagram.

In the first design of this scheme, a function generator from the software library is used as the locking oscillator. The VCO that was designed in the previous section is used as the master oscillator. Figure 3.2.2 shows this circuit set up. In this circuit, the injector generator amplitude is set to 2V which is greater than the master oscillator's amplitude which is about 1V. Clearly, this is for larger locking ranges. In the simulation, varactor diode reverse voltage (V_r) is varied from 0V to -14V, and the phase progressions are obtained in Figure 3.2.3.

Also, note that resonator network contains an inductor of 7nH which shifts the resonant frequency slightly higher in the frequency domain (getting closer to 1GHz) so that it's safely inside the locking range. Additionally, eliminating the base resistance is compensated by the diode internal resistance.

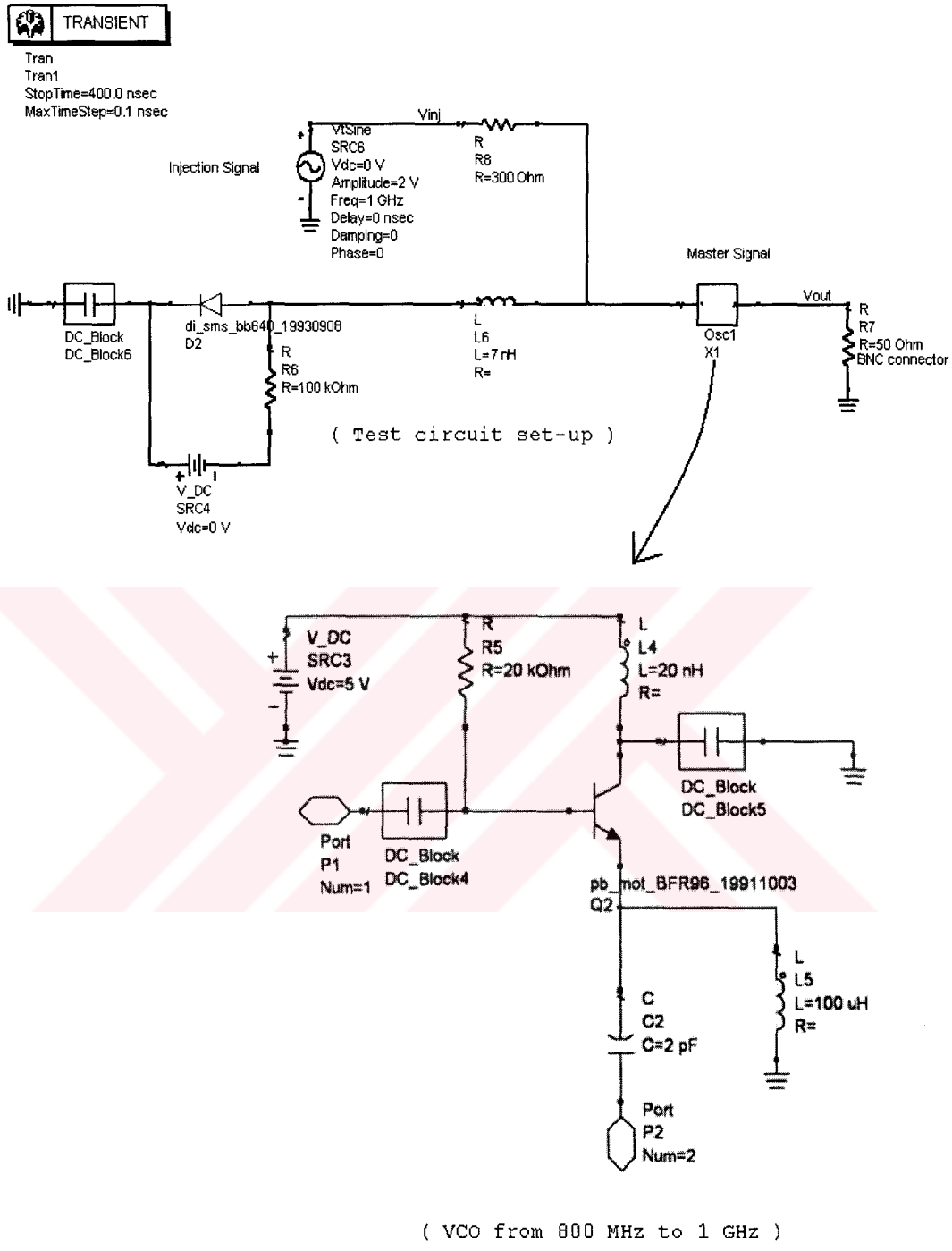


Figure 3.2.2 Phase locking test circuit.

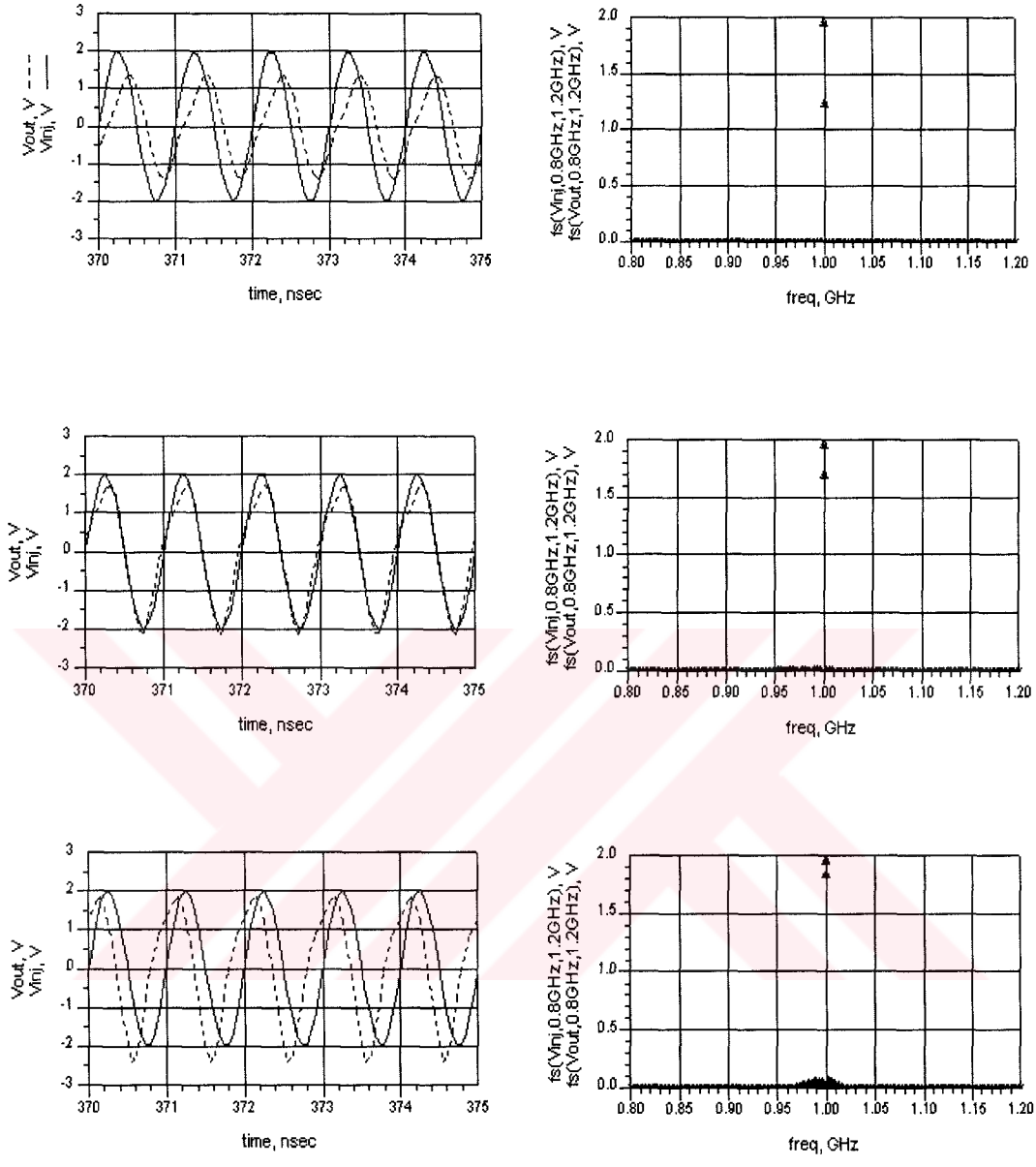


Figure 3.2.3 Phase Locking Simulation for V_r = 0,-10V,-14V.

Another important point is that the injection is made at the base of the master generator. This situation can be explained in terms of the feedback theory. The topology of the current series feedback is shown in Figure 3.2.4.

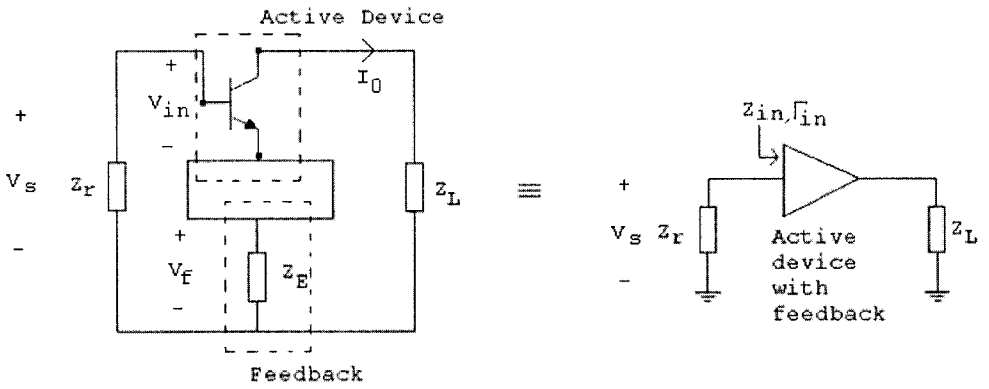


Figure 3.2.4 Current series feedback topology.

Now, inserting the injection voltage signal at the base indicates that base voltage is V_{inj}. In terms of the loop current I_0, the feedback impedance Z_E can be represented as an L-C resonator and the circuit can be shown as in Figure 3.2.4. [14] which is the start point of the earlier formulations. Hence the base connection is proven.

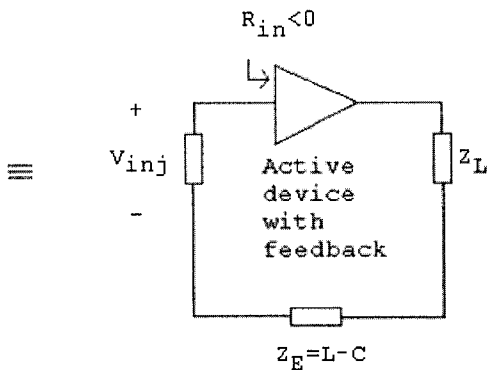


Figure 3.2.5 Feedback oscillator model.

Simulation results in Figure 3.2.3 shows that at V_r(SRC_4)=0V, $\phi \approx 90^0$, at V_r(SRC_4)=-10V, $\phi \approx 0^0$ and at V_r(SRC_4)= -14V, $\phi \approx -90^0$. Apparently, this is expected phase variation over the locking range.

In the next simulation, the function generator from the software library is also replaced by the VCO. Once again, the amplitude of the control signal is kept at 2V which is higher than the master signal amplitude whose value is 1V and the injection is made via 200Ω resistor. This resistor plays an important role in terms of the oscillation conditions and the locking range. Remembering the Adler's locking range equation

$$w_{inj} = w_0 \pm \Delta w_m$$

$$\Delta w_m = \frac{w_0}{2Q} \frac{A_{inj}}{A}$$

with A_{inj} and A are being the injection and master oscillator amplitudes respectively. Thus, for larger injection frequency ranges, it requires that we need larger injection amplitudes and smaller master signal amplitudes. Signal amplitudes can be controlled by varying the supply voltages. However, caution needs to be taken since setting them too low may result in no oscillation at all, or conversely, turning them too high may extend the DC points and saturation or damaging may occur. Typically, 8V-10V supply voltage for the injection oscillator and 5V-6V for the master oscillator enables good lockings. Under these circumstances, 200 Ω coupling resistor maintains roughly 50 Ω for the load impedance providing a constant load and sufficient current to the master network that maintains V_{inj} amplitude large enough.

In order to ensure that the system is inside the locking range, the injection oscillator's varactor diode voltage is kept at a mid-value such as -4V or -7V. This gives maximum phase control when the master varactor diode varies between 0V to -12V. Circuit diagram is given on the next page in Figure 3.2.6. Figure 3.2.7 shows the simulation results for which V_r(SRC_2)= 0V, $\phi \approx 90^0$, V_r= -6V, $\phi \approx 0^0$, V_r= -10V, $\phi = -90^0$, and V_r= -14V (Out of Locking).

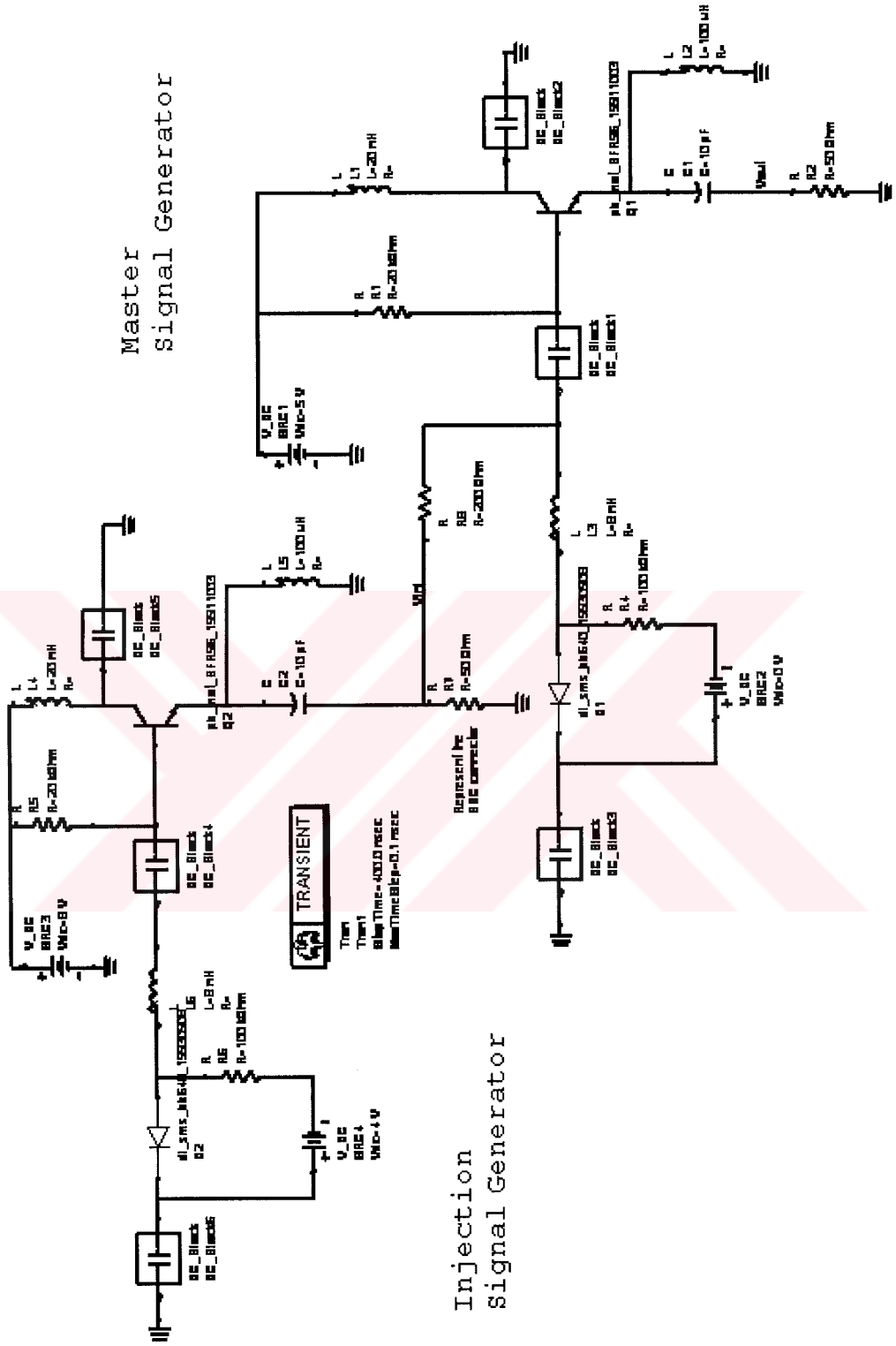


Figure 3.2.6 Phase locking circuit.

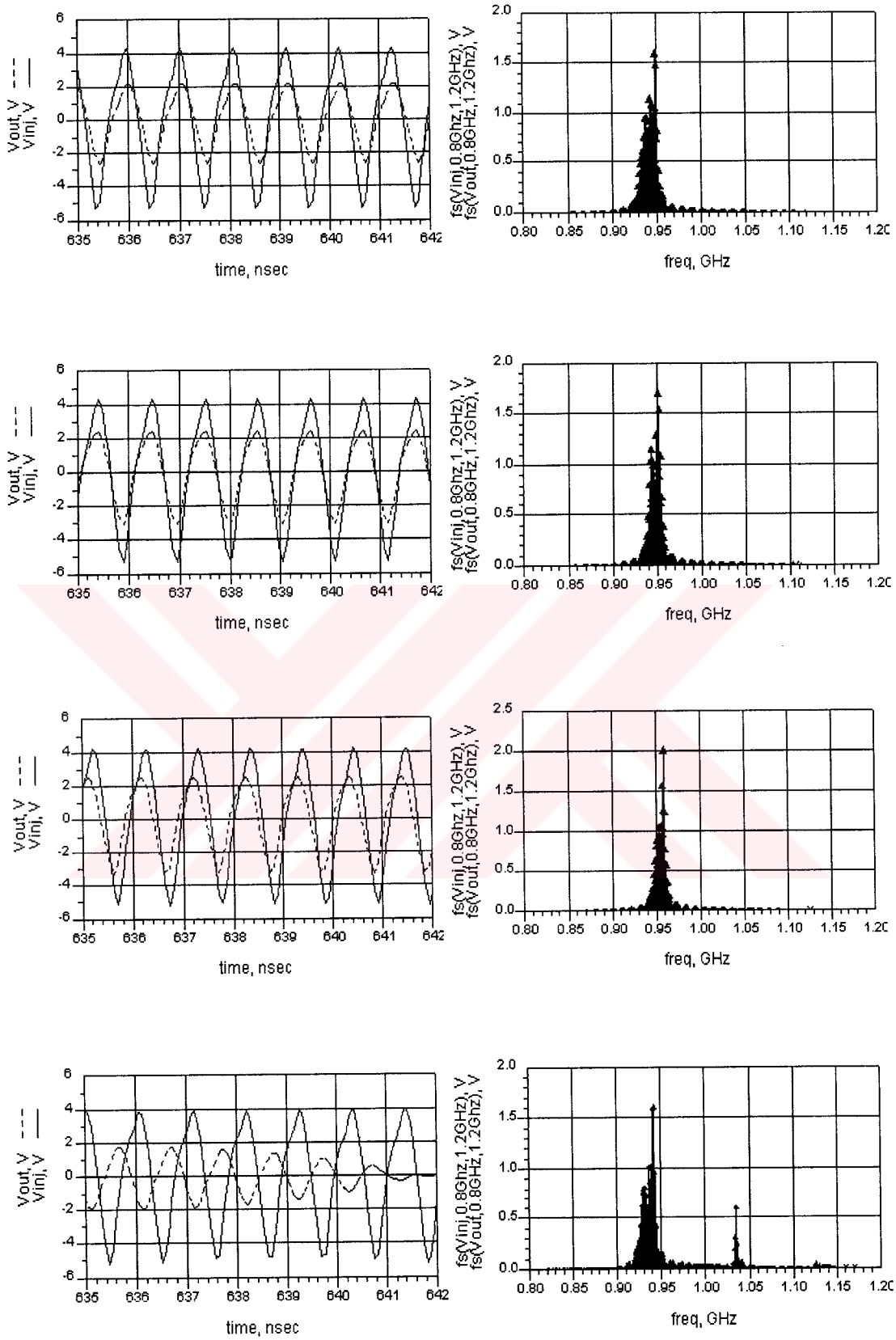


Figure 3.2.7 Phase Locking Simulations for V_r = 0,-6V,-10V,-14V.

CHAPTER 4

EXPERIMENTAL IMPLEMENTATION

4.1 VCO Layout and Simulations:

In s-domain analysis techniques, short circuited line of length ℓ is analogous to series inductance of L. [12]

This is illustrated below.

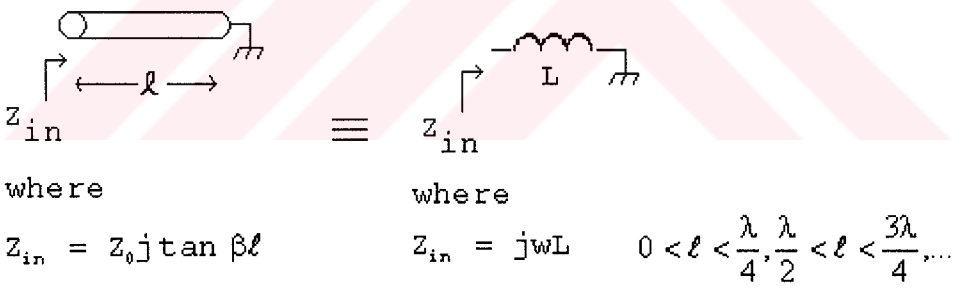


Figure 4.1.1 S-domain analysis.

Therefore, to introduce inductors in the VCO, micro strip lines of various lengths can be used. Starting from the collector inductance of 20nH, the aim is to find the micro strip line length corresponding to such inductance from the short circuited end as shown in Figure 4.1.2.

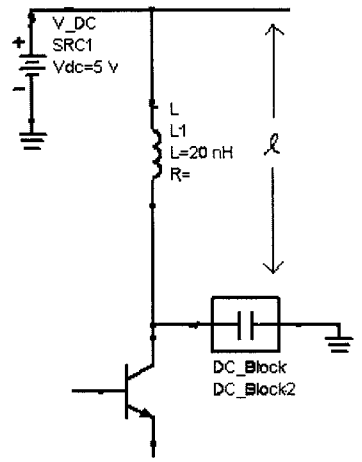


Figure 4.1.2 Collector inductance length.

Following that

$$Z_{in} = Z_0 j \tan \beta \ell = jwL$$

$$Z_0 \tan \beta \ell = wL$$

where $Z_0 = 50\,\Omega$, $\beta = w\sqrt{LC}$ rad/m, $w = 2\pi \times 10^9$ rad/sec and $L = 20 \times 10^{-9}$ H.

In order to find L and C (per unit inductance and capacitance of the micro-strip line), several line parameters must be known in advance [15]

d = thickness = 1mm.

w = width = 2mm.

$\varepsilon_r = 4$

Then,

$$L = \mu \frac{d}{w} = 4\pi \times 10^{-7} \frac{0.001}{0.002} = 2\pi \times 10^{-7} \text{H}.$$

$$C = \varepsilon \frac{w}{d} = \varepsilon_0 \varepsilon_r \frac{w}{d} = \frac{10^{-9}}{36\pi} \times 4 \times \frac{0.002}{0.001} = 71 \text{pF}$$

$$\beta = w\sqrt{LC} = (2\pi \times 10^{9})\sqrt{(2\pi \times 10^{-7})(71 \times 10^{-12})} = 42$$

Substituting the values in the impedance equation

$$(50)\tan(42)\ell = (2\pi \times 10^{9})(20 \times 10^{-9})$$

$$\therefore \ell \approx 30\text{mm}.$$

If somewhat shorter line, like 12mm is used, the inductance changes to 4nH. However, this doesn't make considerable difference on the stability analysis and hence no changes occur on the oscillation process. Moreover, the load is short circuited for RF and the line length is irrelevant. 12 mm line also makes the design much easier to implement on the board.

Similarly, for the base inductance of 8nH, the line length required is

$$(50)\tan(42)\ell = (2\pi \times 10^{9})(8 \times 10^{-9})$$

$$\therefore \ell \approx 20\text{mm}.$$

Figure 4.1.3 shows the base inductance and its accompanying length.

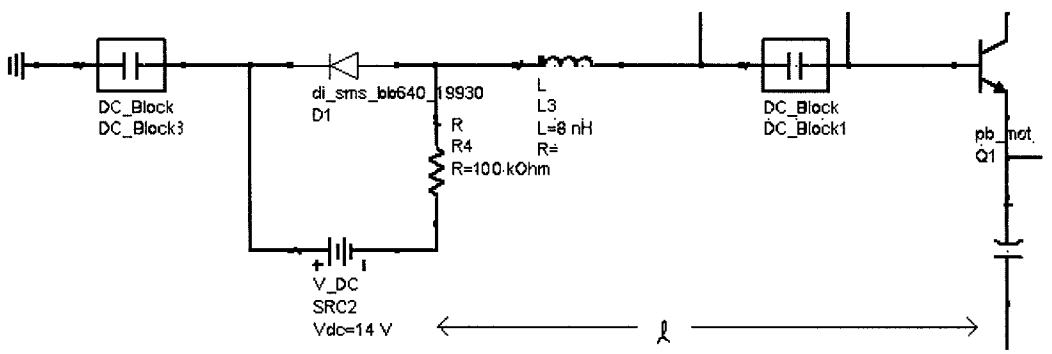


Figure 4.1.3 Base inductance length.

Somewhat longer line, like $\ell = 30\text{mm.}$, increases the inductance slightly. This, in the effect, reduces the resonance frequency. In fact, this is what happens in the real design especially after the varactor diode is introduced, the total line length at the base increases to 25-30mm which pulls the resonator down to 800MHz ranges. Since the oscillators are identical, this doesn't produce a problem as far as the locking phenomena is concerned.

Turning into the emitter side, there is a capacitor of 2pF. Figure 4.1.4 shows the emitter inductance length.

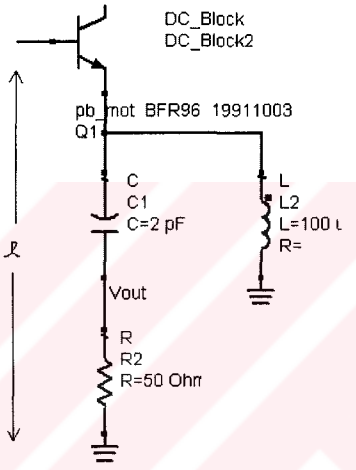


Figure 4.1.4 Emitter inductance length.

Introducing a line length of 6mm at the emitter in the layout, the inductive contribution referenced to ground becomes

$$L = \frac{(50)\tan(42)(0.006)}{(2\pi \times 10^{9})} \approx 2\text{nH}.$$

In the overall effect, in order to have a capacitance of C such that

$$\frac{1}{wC} = \frac{1}{(1\times 10^{9})(2\times 10^{-12})}$$

and considering a series connection of impedances along the emitter line such that

$$\frac{1}{wC} = \frac{1}{(1\times10^{9})(2\times10^{-12})} = wL + \frac{1}{wC_2}$$

where L=2nH (due to the line), then

$$C_2 \approx 2\text{pF}.$$

Therefore, the insertion of 6mm line at the emitter does not affect the impedance very much and it's safe to use 2pF capacitor as unchanged.

Nevertheless, in the following chapter with the addition of a BNC connector, the total line length increases to about 20mm. This total length creates

$$L = \frac{(50)\tan(42)(0.02)}{(2\pi\times10^{9})} \approx 10\text{nH}$$

inductance from the short circuited end (ground).

In the overall effect, in order to have a capacitance of C such that

$$\frac{1}{wC} = \frac{1}{(1\times10^{9})(2\times10^{-12})}$$

and considering a series connection of impedances along the emitter line such that

$$\frac{1}{wC} = \frac{1}{(1\times10^{9})(2\times10^{-12})} = wL + \frac{1}{wC_2}$$

where L=10nH, then

$$C_2 \approx 10\text{pF}$$

capacitance is needed so that with the contribution of the line length inductance, the effective capacitance at the base is 2pF.

Therefore, the line lengths for a single oscillator at the three junctions of the transistor can be summarized as

$$\ell_c = 12\text{mm.}$$

$$\ell_b = 20\text{mm.}$$

$$\ell_e = 6\text{mm. (20mm with the BNC connector)}$$

For these given line lengths, the oscillator layout is drawn on a computer program. Additionally, by converting the layout into circuit representation, an equivalent circuit schematic is obtained. Both the layout and the equivalent circuit are shown in Figure 4.1.5 and Figure 4.1.6 respectively. Then, the simulation is run for several reverse voltage values across the master oscillator diode. The output voltage versus time graphs are obtained. These results are given in Figure 4.1.7.

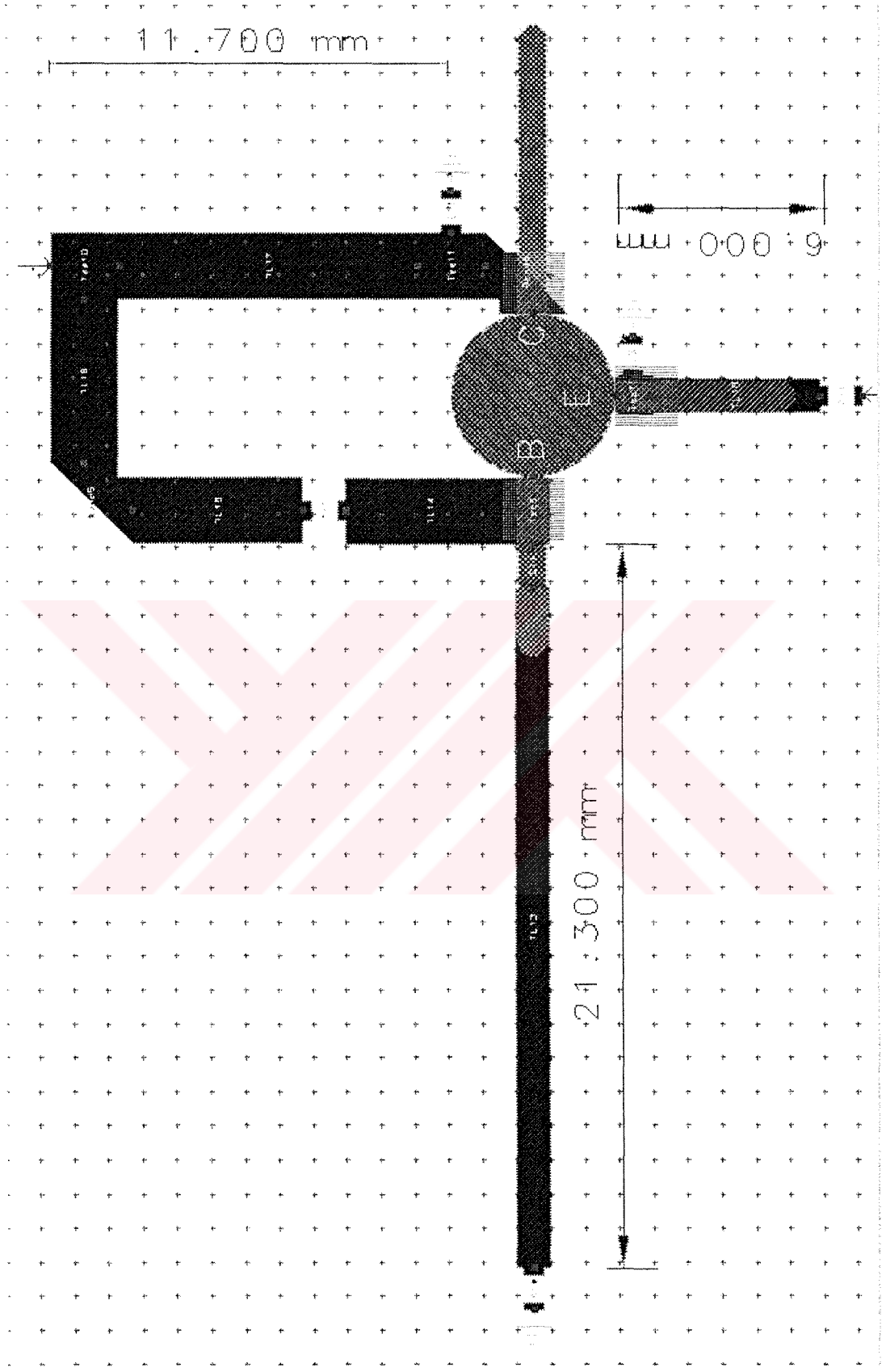


Figure 4.1.5 VCO Layout.

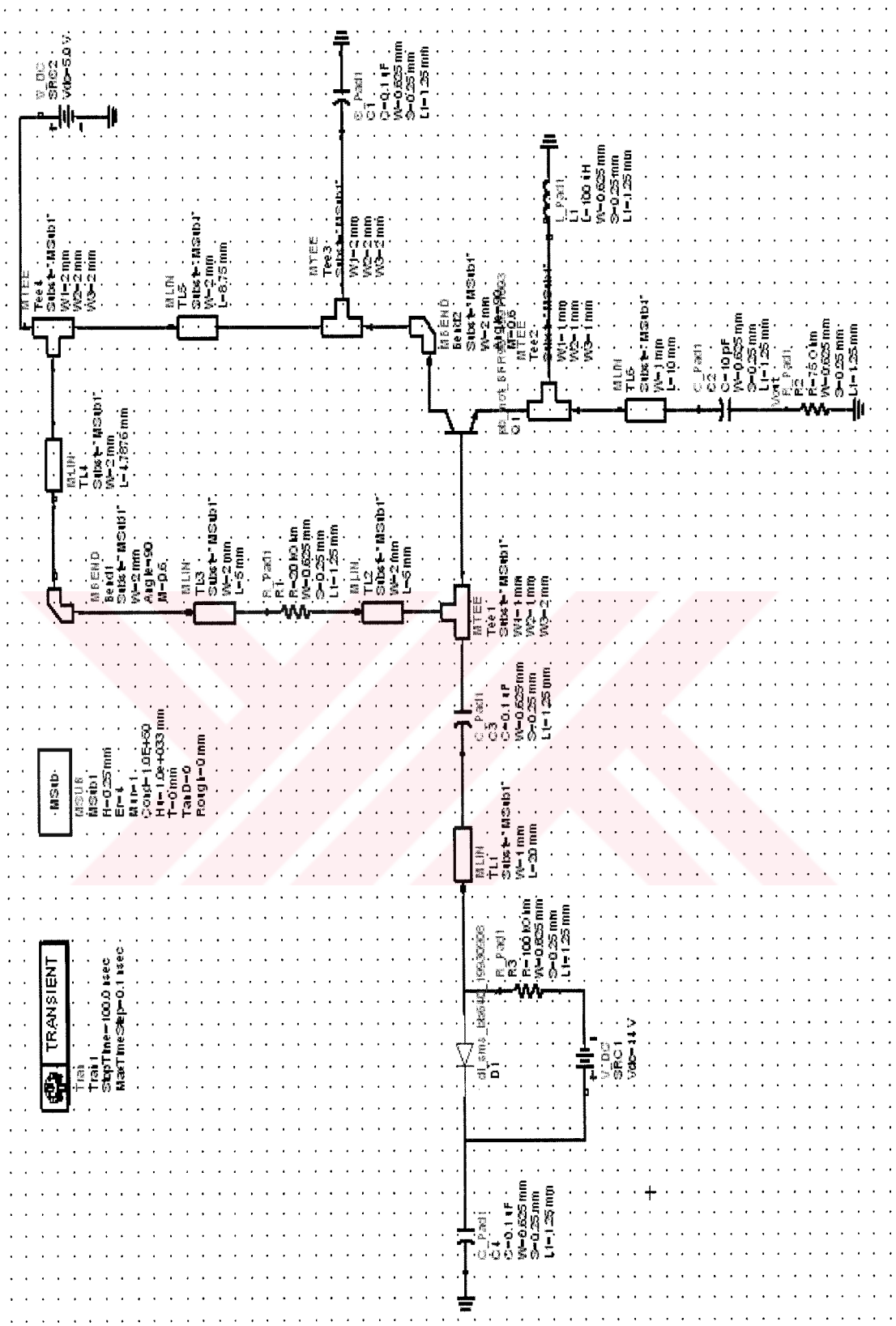


Figure 4.1.6 VCO Schematics.

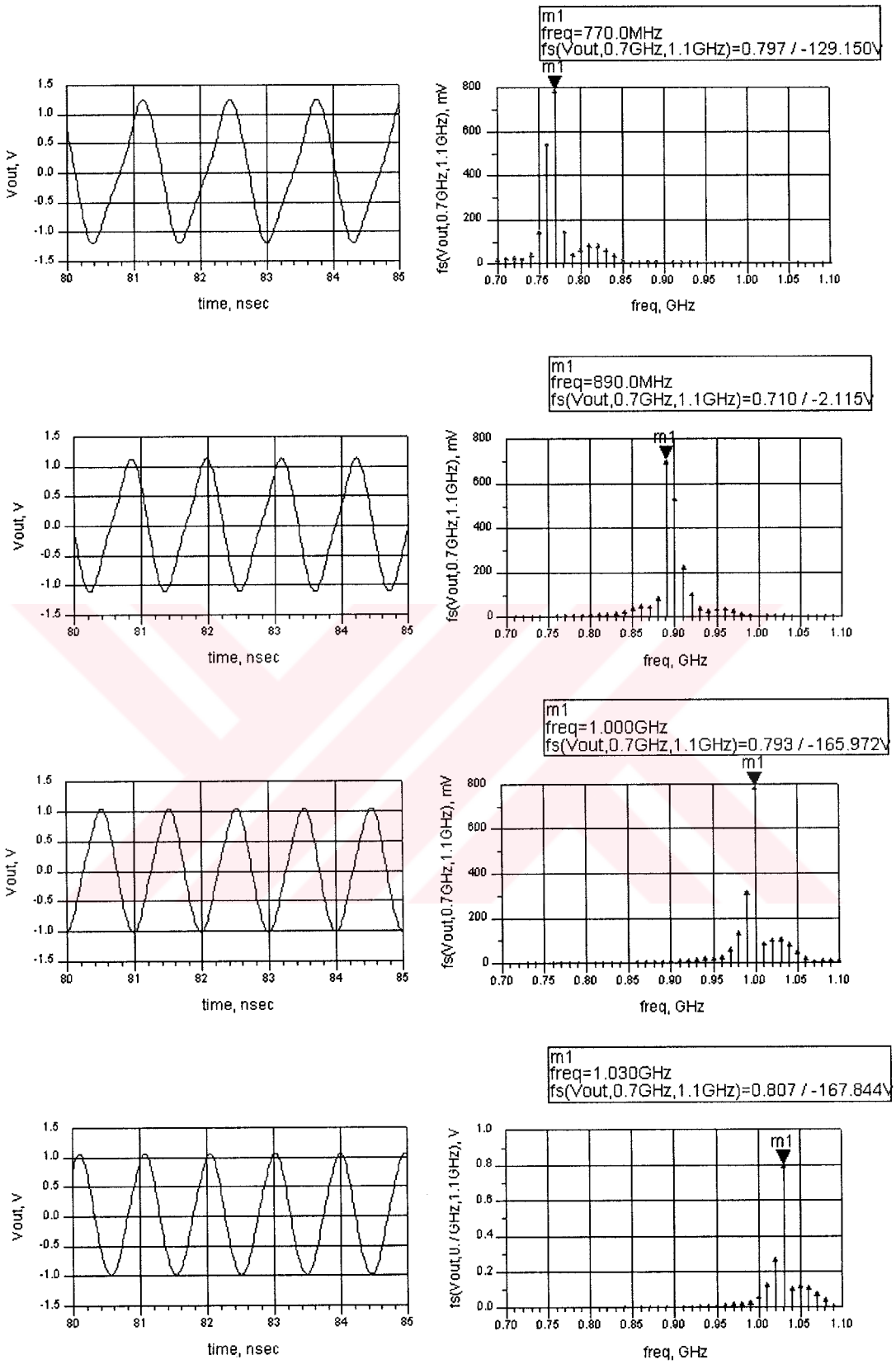


Figure 4.1.7 VCO Layout simulations for V_r (SRC_2)= 0,-6V,-12V,-14V.

Results of this simulation shows that frequency can be controlled in a wide bandwidth of 800MHz to 1GHz.

Also, the relative permittivity of the micro-strip substrate is taken to be 4. In fact, this is the permittivity obtained from the real circuit. Computations regarding permittivity are explained in the following chapter.

It was mentioned previously that when the BNC connector is connected as a 50Ω load at the emitter, the line length was modified to 20mm. In the real implementation of the circuit, this is accomplished by introducing a 14mm. straight line at the emitter connected to a 3mm tee-line and 3mm welding which all together add about 20mm. On the other hand, the micro strip at the base of the transistor is also set to 30mm taking account for the diode connection lengths.

After these modifications, the circuit schematic is re-drawn in Figure 4.1.8. for

$$\ell_{base} \quad 30 \text{ mm.}$$

$$\ell_{emitter} \quad 20 \text{ mm.}$$

Simulation is run for the varactor voltage V_r versus the oscillation frequency. The results are tabulated in Table 4.1.1.

The table shows that the frequency of oscillations can be controlled over the range 700MHz to 1GHz. This corresponds to reverse voltage values of 0V to -12V across the diode.

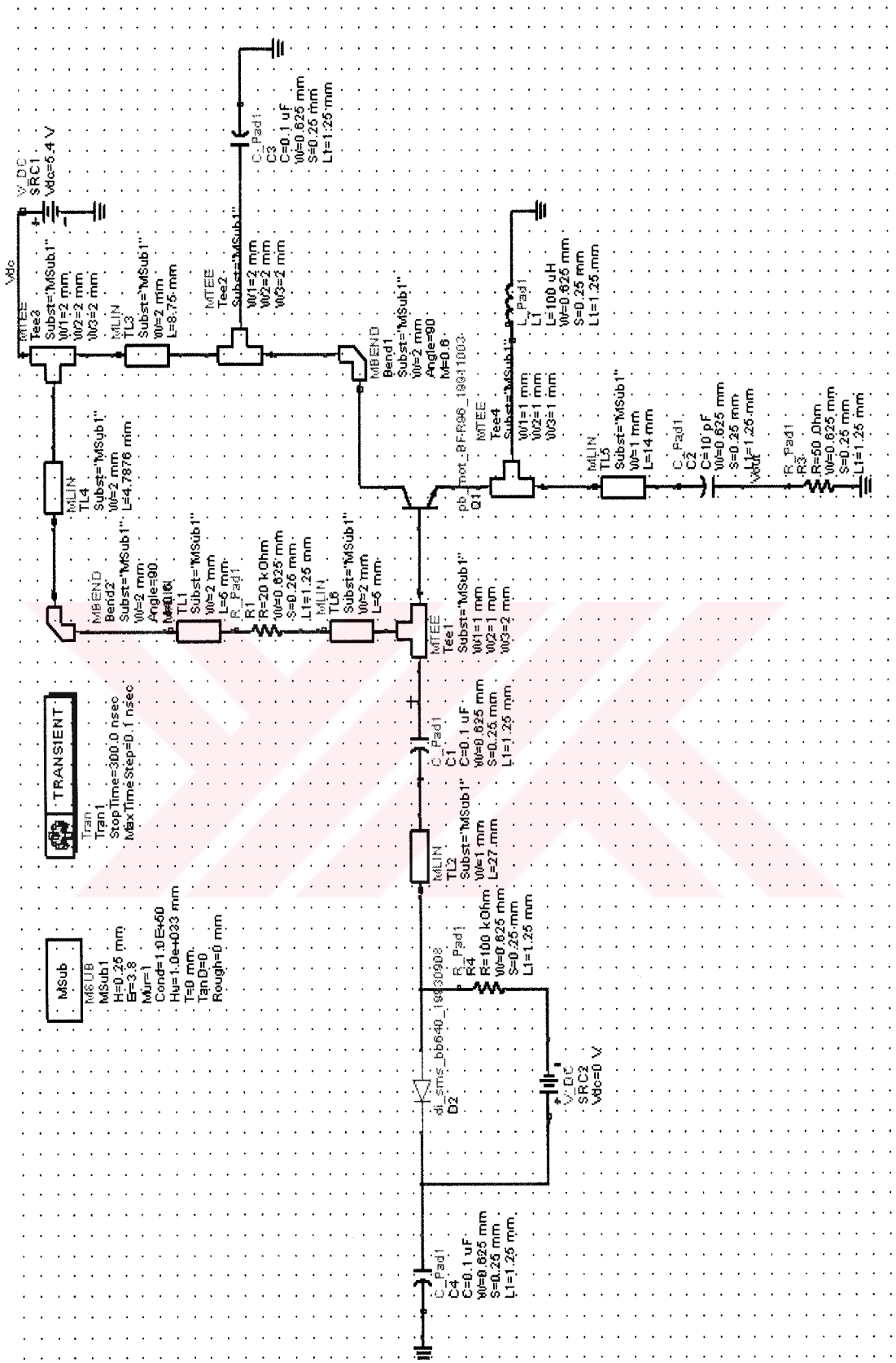


Figure 4.1.8 Modified VCO layout.

Table 4.1.1 Voltage versus frequency values.

V_r (SRC_2)	Frequency(MHz)	V_r (SRC_2)	Frequency(MHz)
0 V	670	7 V	830
0.5 V	690	7.5 V	840
1 V	700	8 V	850
1.5 V	710	8.5 V	860
2 V	720	9 V	870
2.5 V	730	9.5 V	880
3 V	740	10 V	890
3.5 V	760	10.5 V	900
4 V	770	11 V	900
4.5 V	780	11.5 V	910
5 V	790	12 V	920
5.5 V	800	14 V	950
6 V	810	20 V	980
6.5 V	820	30 V	990

In all cases, amplitude of 1V is recorded.

4.2 Phase Locking Circuit Layout:

All the theory and circuit details about phase locking phenomena have been given in chapter 3.2.

In order to develop the phase locking test circuit layout, two of the previously designed VCO s can be connected via 200Ω resistor. This is shown in the following figure.

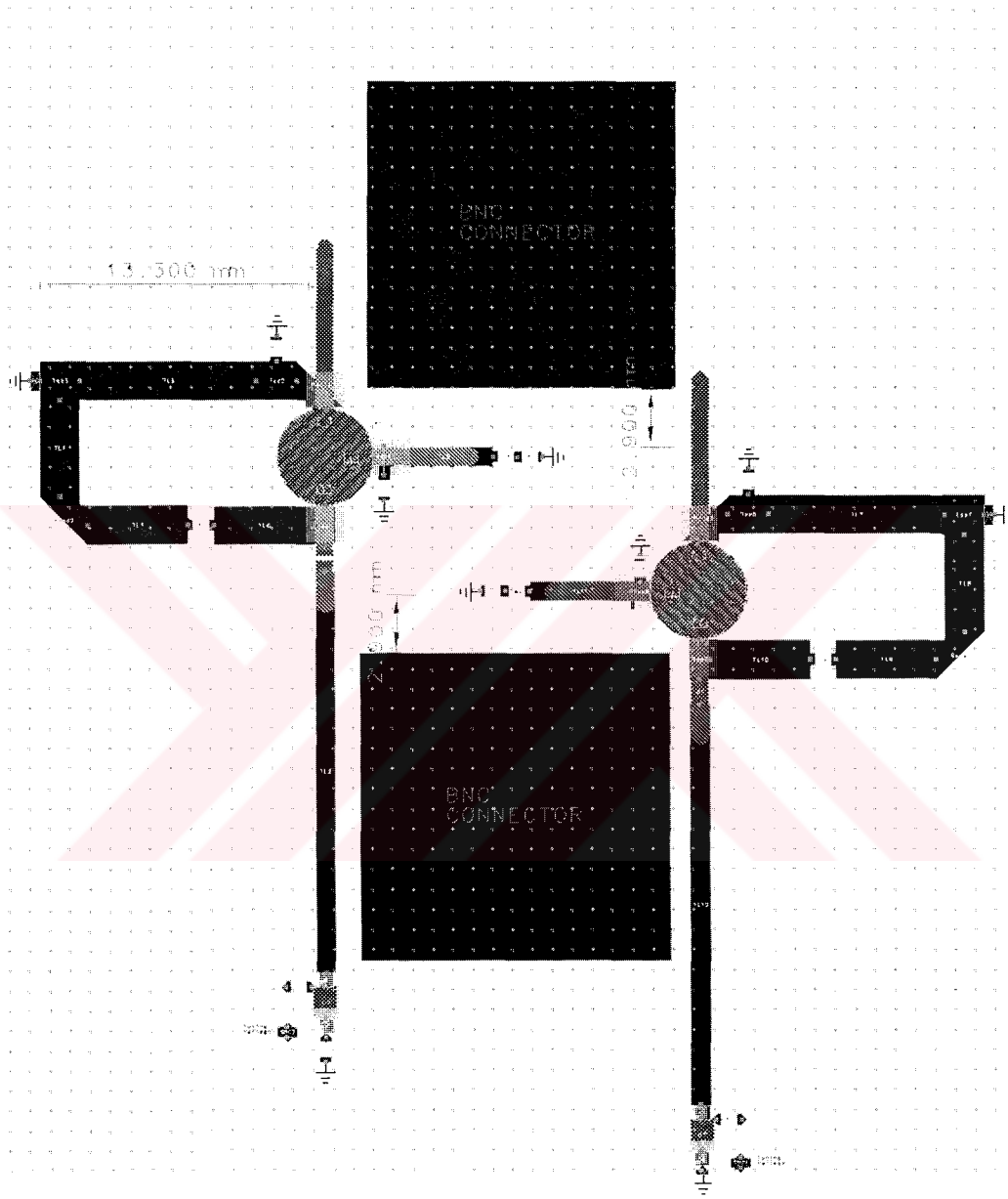


Figure 4.2.1 Phase locking circuit layout.

Before starting the simulation, the schematic equivalent circuit of this layout needs to be obtained. Figure 4.2.2 shows this equivalent circuit. On this schematic circuit, the micro-strip line at the emitter is modified. Originally, the emitter line was 6mm with 2pF capacitance driving the 50Ω load. In this real design, as a result of the BNC connection, this length is now 20mm (Refer to Chapter 4.1, VCO Layout). To compensate for the difference, 10pF capacitance driving the BNC connector is connected. Also note that, this 20mm length is distributed as 14mm straight line that is connected to 3mm tee line and to other components as well.

4.3 Phase Locking Circuit Simulations:

Simulation Results of the phase locking layout circuit is given in the following figure.

For V_r = master varactor voltage (SRC_2)= 0V, $\varphi=-90^0$.

At V_r = 6V,

$\varphi=-69^0$.

At V_r = 10V,

$\varphi=0^0$.

At V_r = 14V,

$\varphi=87^0$.

As a result, the master oscillator is locked at f=830MHz with a phase variation roughly from -90^0 to 90^0 as expected.

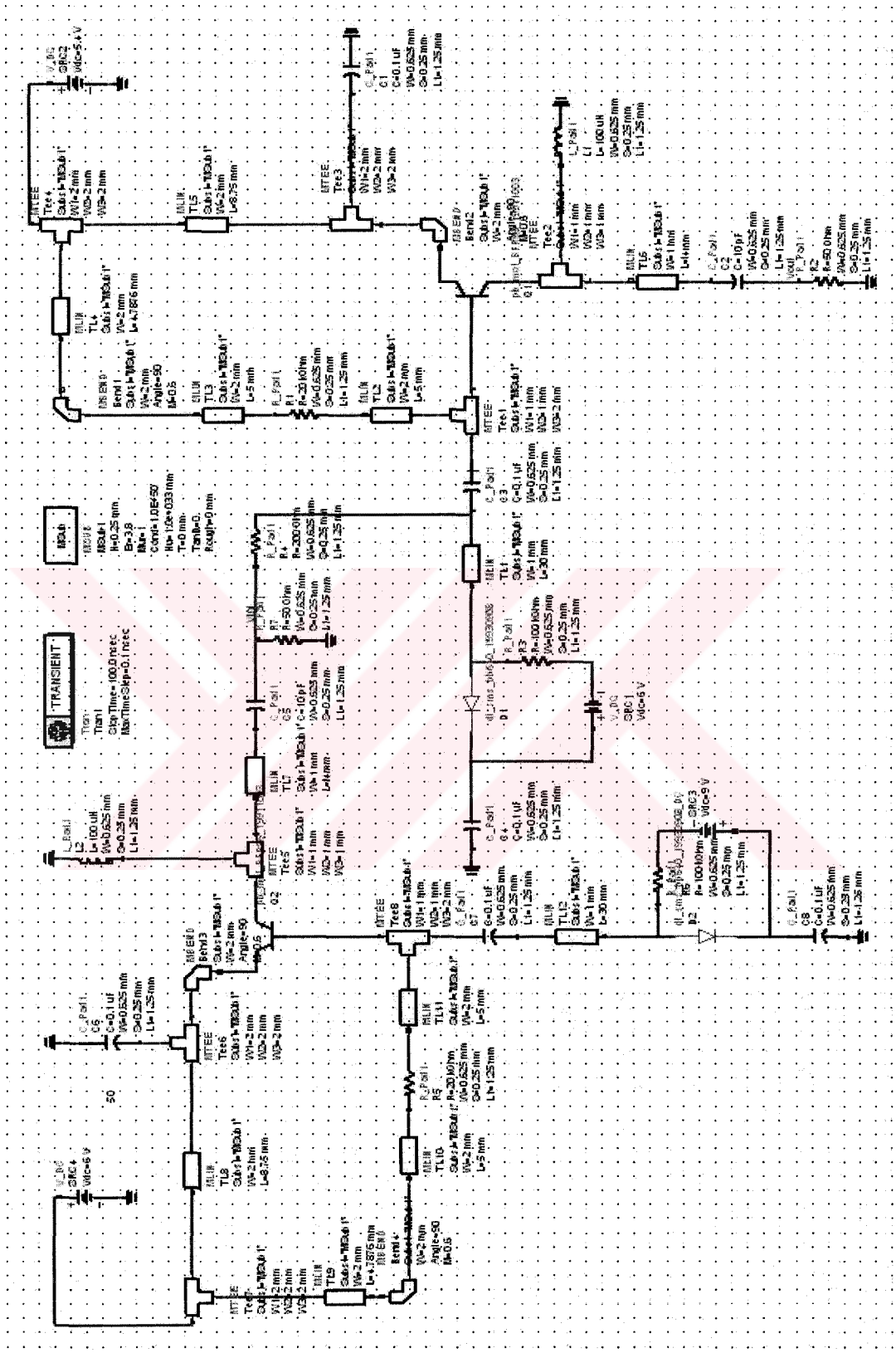


Figure 4.2.2 Phase locking schematics.

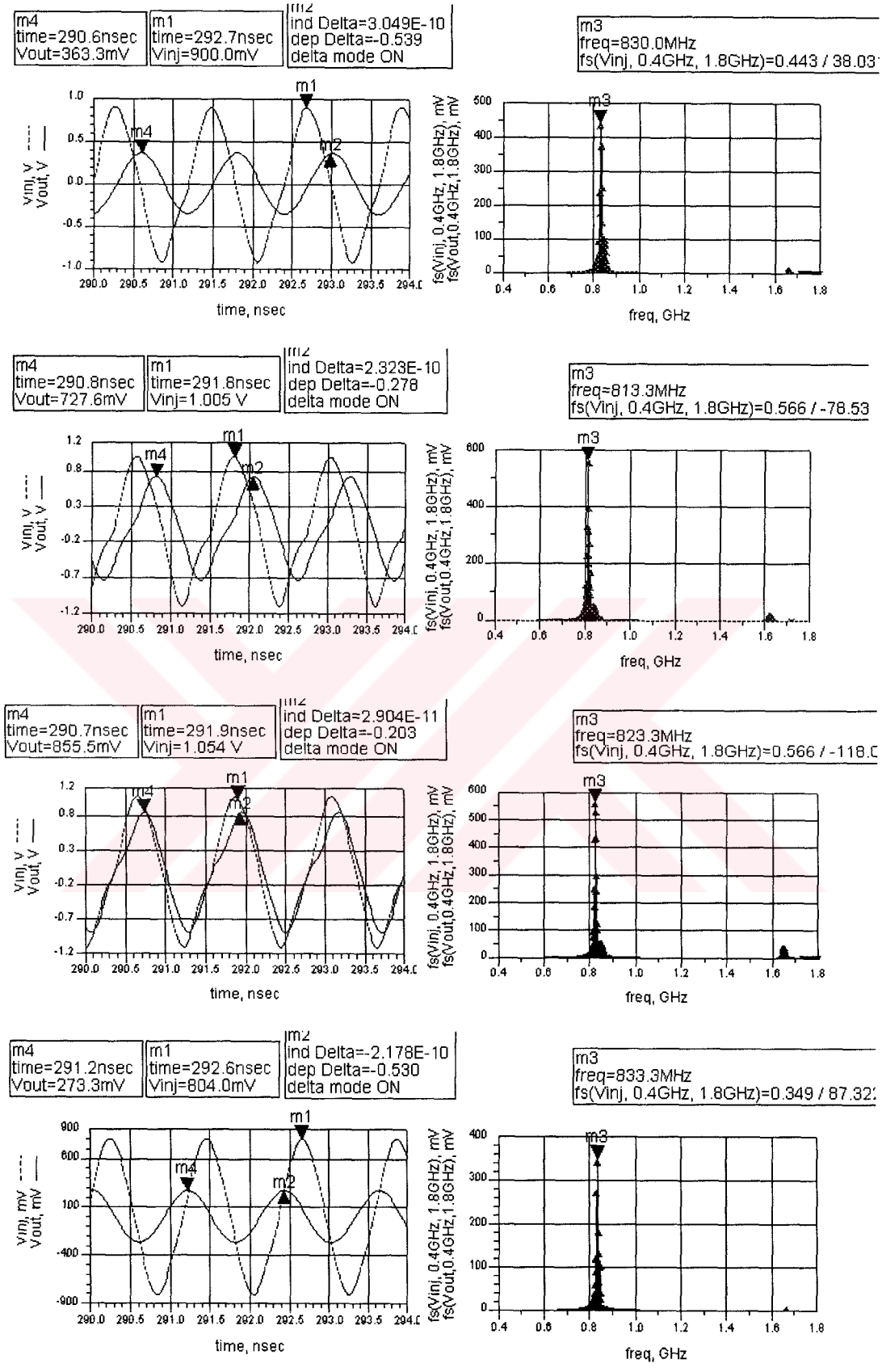


Figure 4.3.1 Phase locking simulations.

4.4 Permittivity Calculations:

Relative permittivity is taken to be 3.8. In order to obtain this value, a piece of metal-coated substrate is cut in 1 by 1 cm^2 shape. Then, it's connected to a sensitive precision LCR meter. The capacitance is measured and the permittivity is obtained from the following computations.

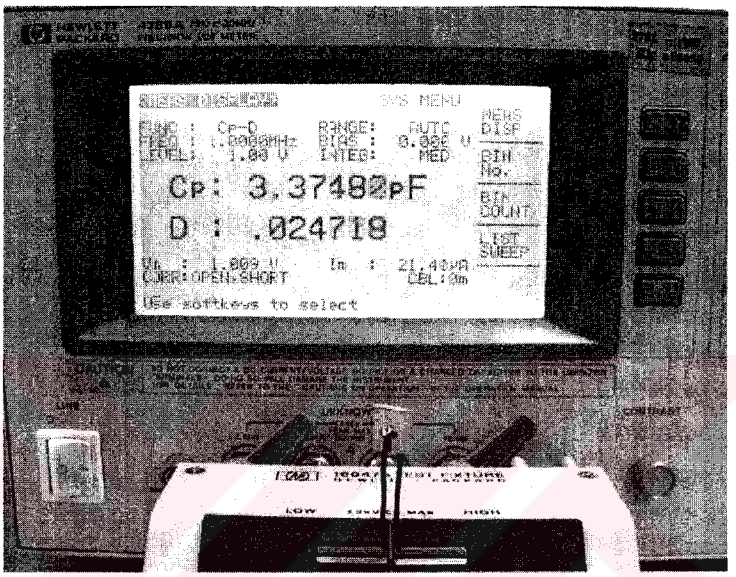


Figure 4.4.1 LCR meter measurement.

$C = \varepsilon \frac{S}{d}$ for a parallel plate capacitor.

where

d=1mm. is the thickness of the substrate and

$S=(0.01)^2$ m^2 is the plate area.

Following that

$$C = \varepsilon_0 \varepsilon_r \frac{S}{d} = 3.37 \times 10^{-12}$$

$$\varepsilon_r = \frac{3.37 \times 10^{-12} \times (0.001)}{(0.01)^2 \times \varepsilon_0} = 3.8$$

As a result, the permittivity can be taken as 3.8. On the other hand, the permittivity of 4 can also be used. This is due to the fact that the LCR meter slightly fluctuates in its value in reality. This puts the permittivity in the range of 3.8 to 4. In terms of calculations, neither value does cause a significant difference. Hence, in some parts of the simulations the permittivity is taken as 4.

CHAPTER 5

MEASUREMENT RESULTS

5.1.1 Realization of the VCO:

In accordance to the VCO layout in chapter 4.1, The oscillator is implemented on a board with 1 mm. thickness and permittivity 3.8 and the bottom surface being the ground plane. Through the BNC connector, the output waveform is observed on Tektronix 492 spectrum analyzer for the frequency control. The diode reverse voltage is set to 0V, -6V, -12V and three different frequency of oscillations are obtained. Figure 5.1.1 shows the VCO implementation of the oscillator. Figure 5.1.2 shows the spectrum analyzer results for the output amplitude in dB scale versus the frequency. Noting that the central dot on the screen corresponds to 1GHz and the horizontal axis is divided in steps of 200MHz per division. The circuit gives the frequency control roughly over 800MHz to 1GHz as expected.

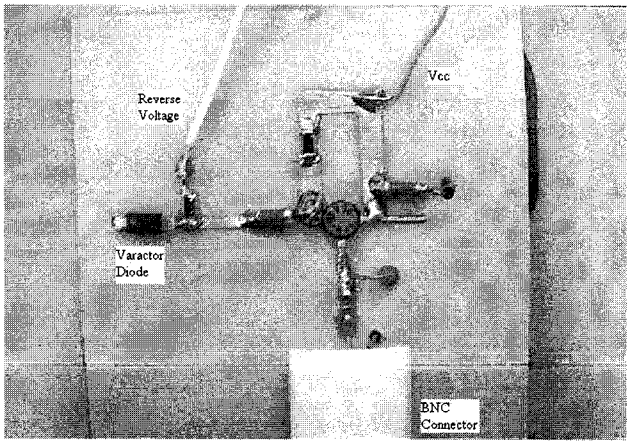


Figure 5.1.1 VCO Implementation.

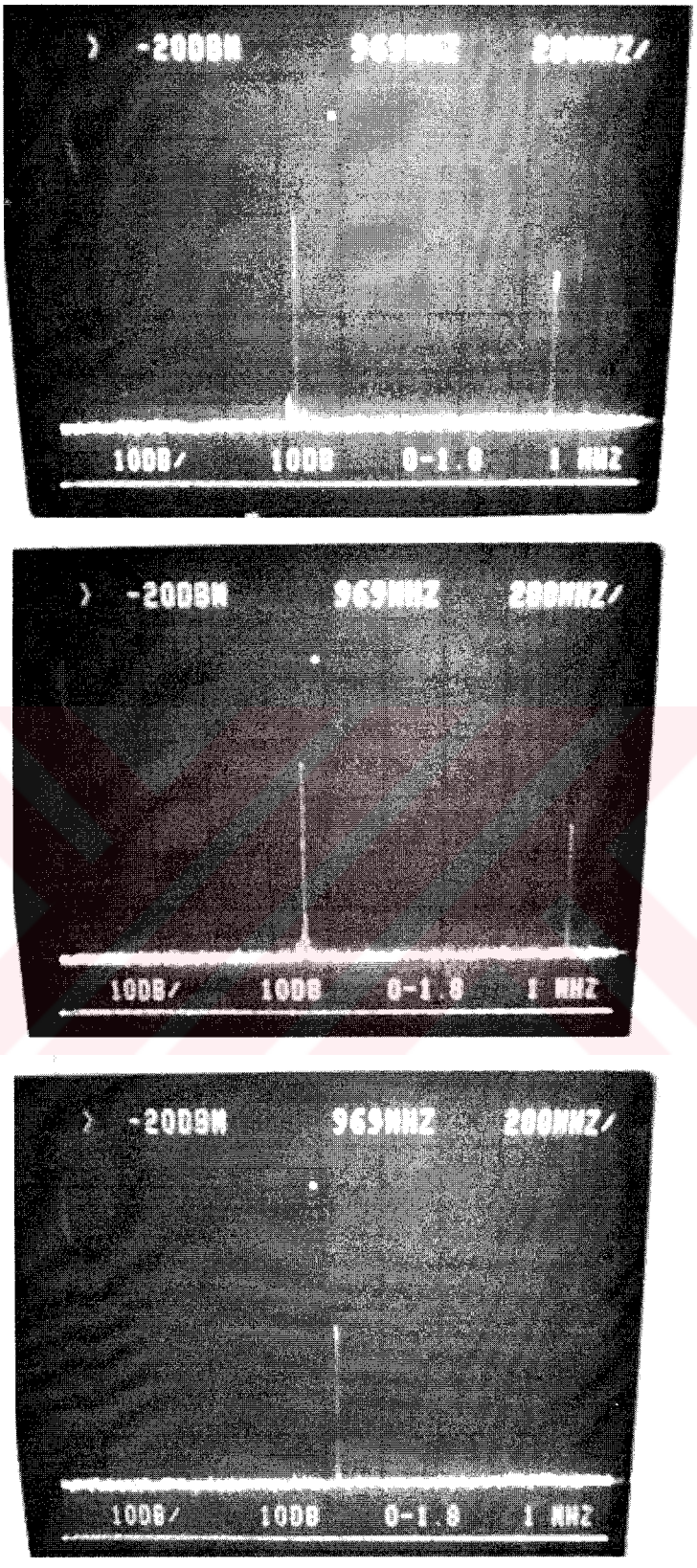


Figure 5.1.2 VCO Measurements for Vr=0V,-6V,-12V.

5.2 Realization of the Phase Locking Circuit:

The phase locking experimental circuit is realized in accordance with the computer design in chapter 4.2. Figure 5.2.1 shows this implementation. Here, again the V_{CC} supplies are protected from RF due to short circuited loads.

5.2 Measurement Results:

In this section, the real measurements are compared with theoretical formulations and computer simulations. Then, the results are tabulated.

First, define

V_{is}=Supply voltage of the control signal (injection oscillator).

V_{ms}=Supply voltage of the master signal (the oscillator being controlled).

V_{it}= Varactor diode tuning voltage of the control signal (injection oscillator).

V_{mt}= Varactor diode tuning voltage of the master signal (the oscillator being controlled).

In the first set of measurements, the following quantities are taken as constants.

V_{ms} = 5.4V, V_{is} = 8V, V_{it} = 0-2-4-6-8-10V.

Then, V_{mt} is varied from 0V to -12V for each V_{it}.

In the second set of measurements,

V_{ms} = 5.4V, V_{is} = 8V, V_{mt} = 0-2-4-6-8-10V. are constants and V_{it} is varied from 0V to -12V for each V_{mt}.

In the third set of measurements, only supply voltages are varied for the widest locking range set up i.e. V_{ms} = 5.4V, V_{is} = 8V, V_{it} = 9V, V_{mt} = 0-12V.

Results are given in a table. In this table, simulation results are obtained from the phase locking circuit in chapter 4.3. The real measurements are obtained by Agilent infiniium 500MHz oscilloscope. Theoretical computations are performed based on the phase locking phenomena.

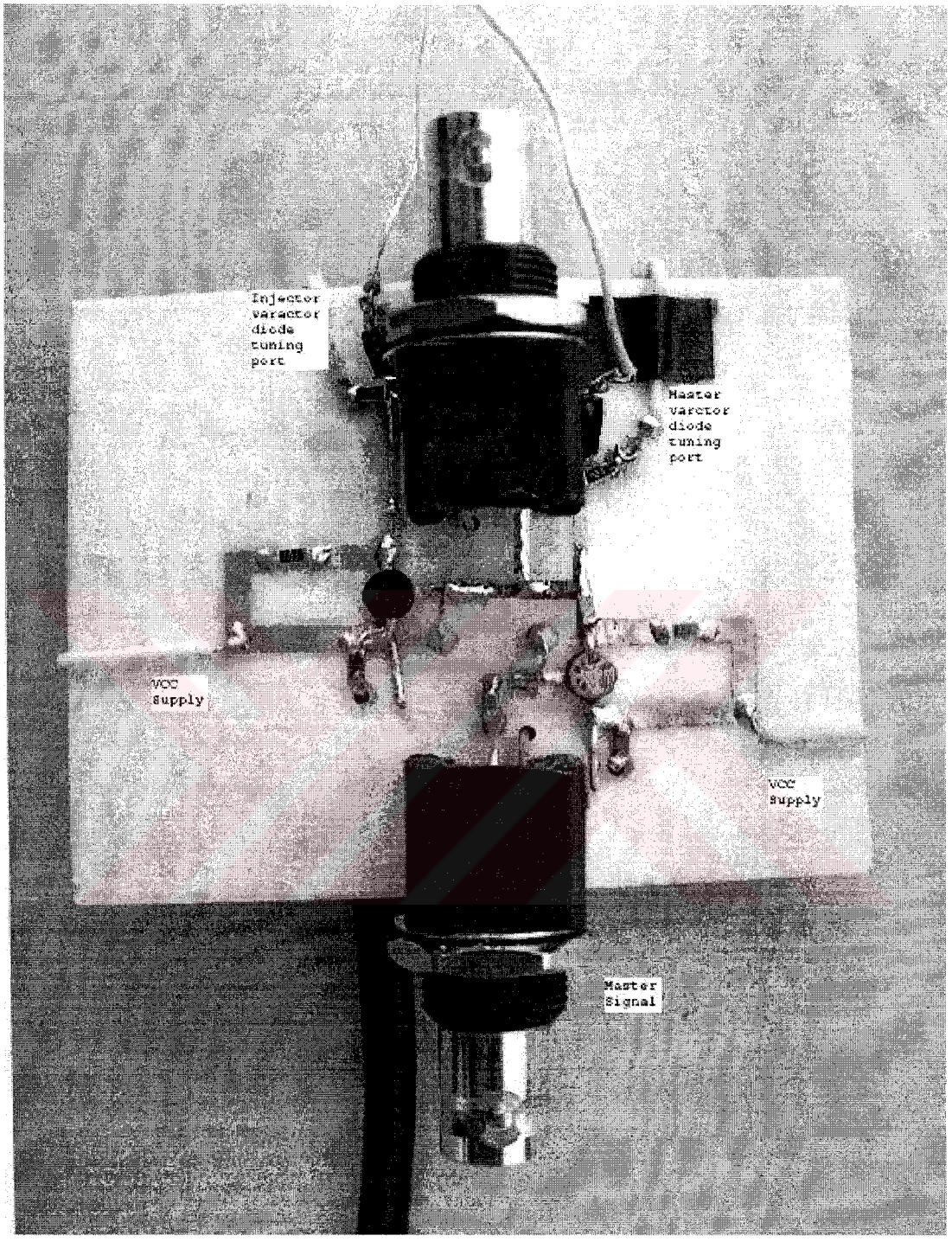


Figure 5.2.1 Phase locking test circuit.

Theoretical range computations can be carried out by starting with the Adler's range equation

$$w_{inj} = w_0 \pm \Delta w_m \quad \text{where} \quad \Delta w_m = \frac{w_0}{2Q}\frac{A_{inj}}{A}$$

In the first step, w_0 (free-running frequency of the master oscillator) is varied and w_{inj} is kept constant.

Having the diode voltage, the frequency w_{inj} can be obtained from table 4.1.1. Also, A_{inj} is roughly 2V and A=1V in all simulations. Then, the quality factor of the resonator can be evaluated as follows:

The resonator network consists of an inductor of 8nH and a capacitor of

$$-j54.74\,\Omega = -j\frac{1}{wC}$$

or C=3pF as shown in figure 5.2.1.

Ploting the frequency response of this circuit, the graphs in figure 5.2.2 are obtained.

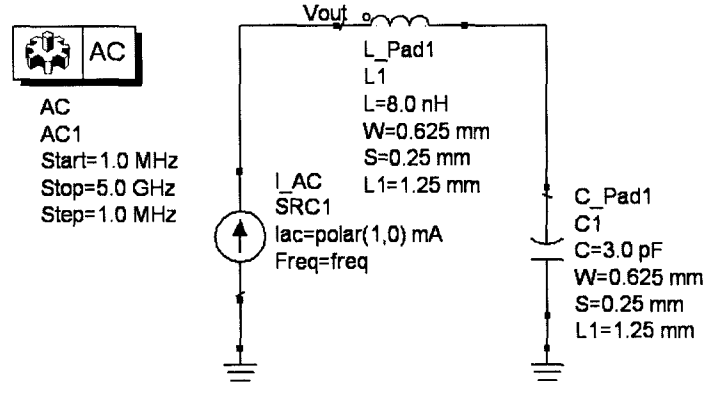


Figure 5.2.2.1 Resonator circuit.

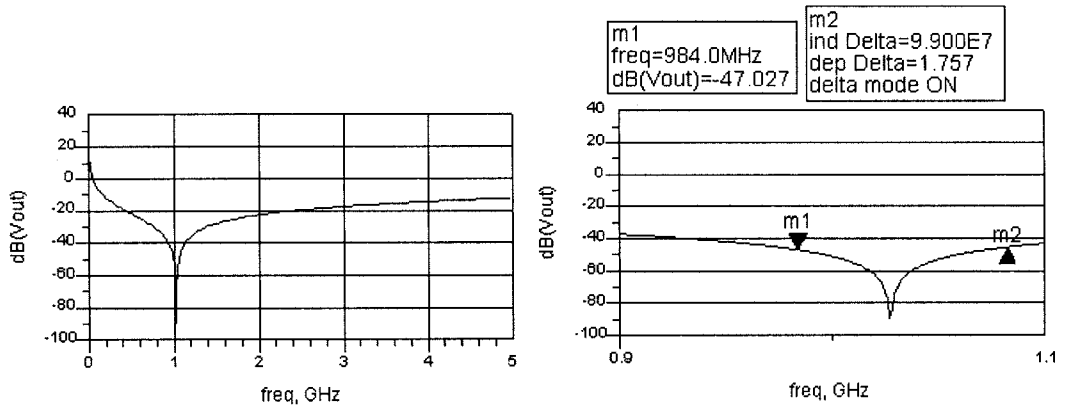


Figure 5.2.2.2 Resonator circuit response.

where

$$Q = \frac{w_0}{B}$$

and B is the bandwidth. Observing from the graph B is roughly equal to 100MHz.

Therefore,

$$Q = \frac{w_0}{B} = \frac{1\times10^9}{100\times10^6} = 10$$

Considering the Adler's equation

$$w_{inj} = w_0 \pm \Delta w_m$$

$$w_{inj} = w_0 \pm (\frac{w_0}{2Q}\frac{A_{inj}}{A}) = w_0(1 \pm \frac{1}{2Q}\frac{A_{inj}}{A})$$

Solving the last equation for w_0 gives the following expression

$$w_0 = w_{inj} / (1 \pm \frac{1}{2Q}\frac{A_{inj}}{A}).$$

Substituting all the parameters on the right hand side of this final equation gives the range for w_0. For this frequency range, from table 4.1.1, the corresponding voltage ranges can be found. Then, assuming a linear phase variation from -90^0 to 90^0 in this range, the theoretical phase values can be obtained.

As an example, for the first set of circuit, where the parameters are defined as

$$V_{is}= 8V.$$

$$V_{ms}= 5.4V.$$

$$V_{it}= 0V. \text{ or } f_{inj}=670MHz.$$

Then,

$$f_0 = (670\times10^6)/(1\pm\frac{1}{20}\frac{2}{1}) \approx 610MHz - 740MHz.$$

which corresponds to a voltage range 0V-3V.

Therefore, theoretically, we expect the locking to occur at V_{mt}=0V-3V.

Table 5.2.3 1st Set of Measurements i

Vis=8V		Vms=5.4V		Vit=0V	R=200Ω					Theory:
		Simulation Results				Test Results				Locking
		Phase	Amplitudes			Phase	Amplitudes(V)			Range
Vmt		ΔΦ	Vi	Vo	f(MHz)	ΔΦ	Vi	Vo	f(MHz)	f(MHz)
0	V	0	1.37	1.49	670	60	2.78	2.17	745	610
-0.5	V	-10	1.26	1.45	680	54	2.74	2.15	745	
-1	V	-21	1.13	1.38	690	46	2.73	2.1	745	
-1.5	V	-85	0.92	0.5	685	38	2.68	2.08	745	
-2	V	-85	0.93	0.5	680	31	2.64	2	745	
-2.5	V	-90	0.98	0.4	680	27	2.6	1.92	742	
-3	V	-90	0.98	0.4	680	20	2.58	1.78	740	740
-3.5	V	-90	0.98	0.3	680	11	2.57	1.6	738	
-4	V	-90	0.98	0.3	670	7	2.56	1.46	738	
-4.5	V	-90	0.98	0.28	670	7	2.56	1.25	738	
-5	V	-90	0.98	0.25	670	7	2.56	1.12	738	
-5.5	V	-90	0.98	0.22	670	7	2.56	1	738	
-6	V	-90	0.98	0.2	670	7	2.56	0.95	738	
-6.5	V	-90	0.98	0.18	670	7	2.56	0.7	738	
-7	V	-90	0.98	0.15	670	7	2.56	0.6	738	
-7.5	V	-90	0.98	0.13	670	7	2.56	0.55	738	
-8	V	-90	0.98	0.12	670	7	2.56	0.5	738	
-8.5	V	-90	0.98	0.11	670	7	2.56	0.45	738	
-9	V	-90	0.98	0.1	665	7	2.56	0.4	738	

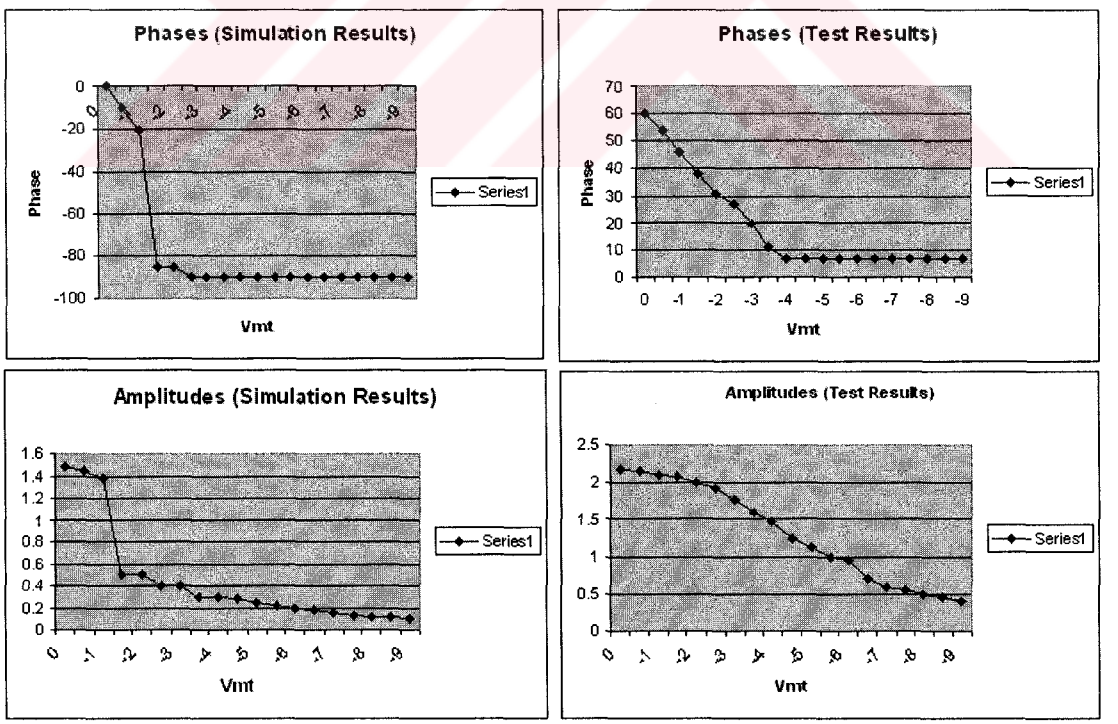


Figure 5.2.3 Phase and Amplitude plots i.

Table 5.2.4 1st Set of Measurements ii

Vis=8V		Vms=5.4V		Vit=2V	R=200Ω					Theory:
		Simulation Results				Test Results				Locking
		Phase	Amplitudes			Phase	Amplitudes(V)			Range
Vmt		ΔΦ	*Vi*	*Vo*	f(MHz)	ΔΦ	*Vi*	*Vo*	f(MHz)	f(MHz)
0	V	30	1.35	1.32	700	54	2.63	2.35	766	650
-0.5	V	20	1.3	1.32	700	50	2.63	2.35	766	
-1	V	10	1.25	1.31	700	41	2.61	2.35	766	
-1.5	V	5	1.2	1.31	700	37	2.6	2.31	765	
-2	V	0	1.18	1.31	720	32	2.6	2.28	763	
-2.5	V	-5	1.16	1.31	720	25	2.6	2.24	763	
-3	V	-15	1.16	1.3	735	14	2.56	2.18	764	
-3.5	V	-64	0.94	0.55	730	7	2.52	2.02	763	
-4	V	-60	0.93	0.5	725	0	2.48	1.82	763	
-4.5	V	-60	0.93	0.4	725	-3	2.43	1.75	763	
-5	V	-60	0.93	0.3	725	-3	2.41	1.35	762	
-5.5	V	-60	0.93	0.28	725	-3	2.4	1.21	763	800
-6	V	-60	0.93	0.28	720	-3	2.4	1.16	763	
-6.5	V	-60	0.93	0.25	720	-3	2.4	0.83	763	
-7	V	-60	0.93	0.2	720	-3	2.4	0.8	763	
-7.5	V	-60	0.93	0.18	720	-3	2.4	0.75	763	
-8	V	-60	0.93	0.15	720	-3	2.4	0.7	763	
-8.5	V	-60	0.93	0.12	720	-3	2.4	0.6	763	
-9	V	-60	0.93	0.1	720	-3	2.4	0.5	763	

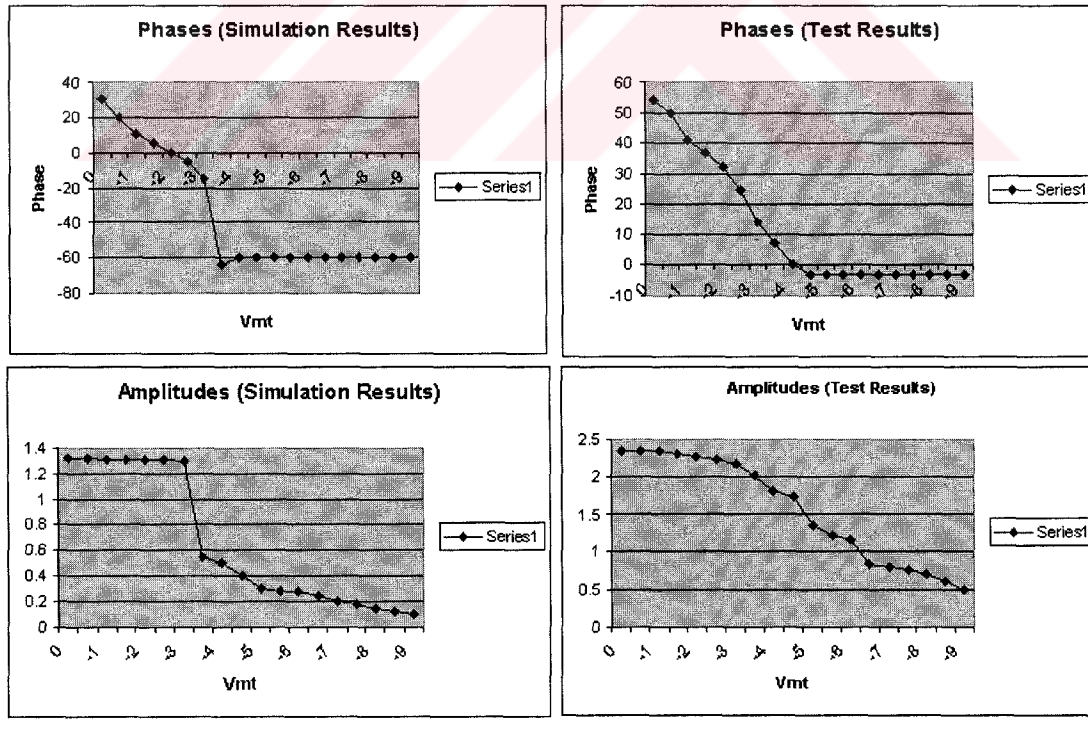


Figure 5.2.4 Phase and Amplitude plots ii.

Table 5.2.5 1st Set of Measurements iii

Vis=8V		Vms=5.4V		Vit=4V	R=200Ω					Theory:
		Simulation Results				Test Results				Locking
		Phase	Amplitudes			Phase	Amplitudes(V)			Range
Vmt		ΔΦ	Vi	Vo	f(MHz)	ΔΦ	Vi	Vo	f(MHz)	f(MHz)
0	V	50	1.11	1.15	740	60	2.58	2.31	770	700
-0.5	V	46	1.11	1.15	740	53	2.58	2.32	780	
-1	V	42	1.11	1.15	740	48	2.58	2.31	782	
-1.5	V	37	1.11	1.15	740	41	2.58	2.31	781	
-2	V	34	1.21	1.28	745	32	2.58	2.29	778	
-2.5	V	30	1.21	1.28	745	27	2.58	2.28	777	
-3	V	20	1.21	1.28	745	22	2.57	2.2	778	
-3.5	V	10	1.21	1.28	745	8	2.56	2.13	780	
-4	V	0	1.25	1.3	765	0	2.52	2.07	780	
-4.5	V	-10	1.24	1.3	765	-15	2.47	1.76	780	
-5	V	-20	1.2	1.28	775	-21	2.4	1.51	779	
-5.5	V	-65	0.9	0.6	785	-24	2.36	1.26	780	
-6	V	-65	0.9	0.46	780	-24	2.36	1.18	780	
-6.5	V	-65	0.9	0.4	780	-24	2.36	0.88	780	
-7	V	-65	0.9	0.35	780	-24	2.36	0.8	780	
-7.5	V	-65	0.9	0.3	780	-24	2.36	0.75	780	
-8	V	-65	0.9	0.25	780	-24	2.36	0.7	780	850
-8.5	V	-65	0.9	0.22	780	-24	2.36	0.65	780	
-9	V	-65	0.9	0.2	770	-24	2.36	0.5	780	

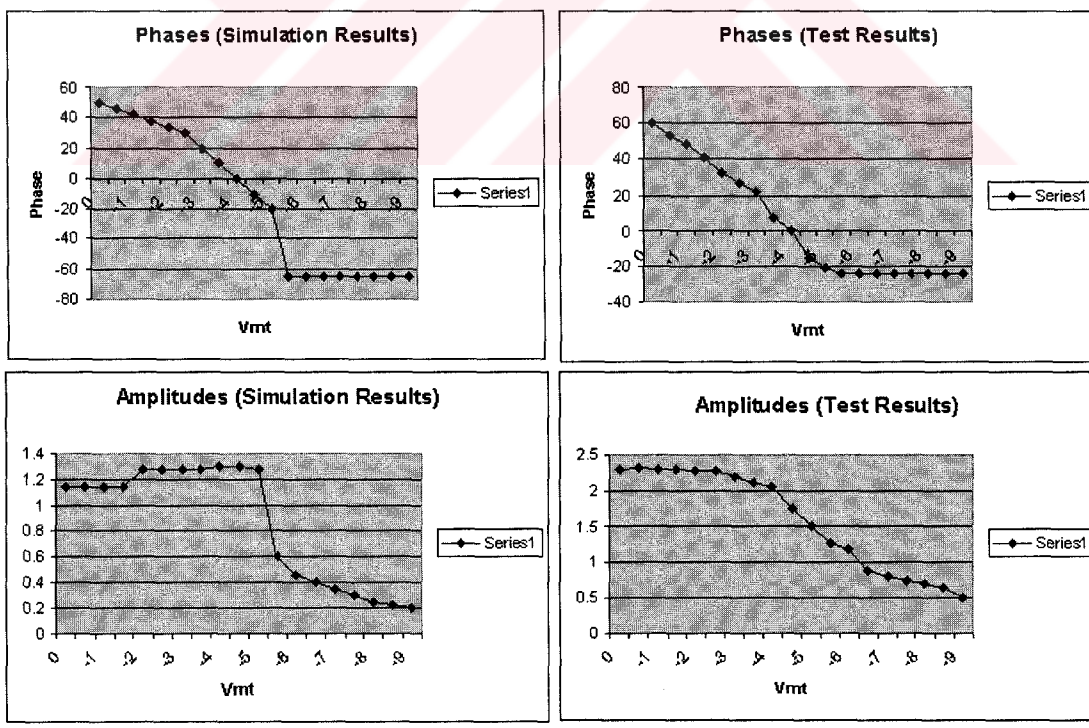


Figure 5.2.5 Phase and Amplitude plots iii.

Table 5.2.6 1st Set of Measurements iv

Vis=8V		Vms=5.4V		Vit=6V	R=200Ω					Theory:
		Simulation Results				Test Results				Locking
		Phase	Amplitudes			Phase	Amplitudes(V)			Range
Vmt		ΔΦ	*Vi*	*Vo*	f(MHz)	ΔΦ	*Vi*	*Vo*	f(MHz)	f(MHz)
0	V	90	1	0.9	785	47	2.27	1.9	810	
-0.5	V	82	1	0.9	785	45	2.25	1.95	806	
-1	V	78	1	0.9	785	39	2.26	1.97	803	
-1.5	V	70	1	0.9	785	35	2.27	1.96	806	
-2	V	65	1.1	1.1	780	29	2.23	1.96	807	
-2.5	V	64	1.1	1.1	780	22	2.22	1.94	807	730
-3	V	58	1.1	1.1	780	13	2.19	1.94	807	
-3.5	V	55	1.1	1.1	780	9	2.16	1.9	813	
-4	V	53	1.18	1.3	790	0	2.14	1.87	815	
-4.5	V	40	1.18	1.3	790	-13	2.02	1.86	812	
-5	V	30	1.18	1.3	790	-31	1.9	1.75	816	
-5.5	V	20	1.16	1.3	790	-38	1.81	1.64	815	
-6	V	0	1.15	1.3	810	-59	1.74	1.45	826	
-6.5	V	0	1.14	1.3	810	-59	1.74	1.05	825	
-7	V	0	1.14	1.3	820	-59	1.74	0.875	820	
-7.5	V	-47	0.4	0.4	820	-59	1.74	0.85	818	
-8	V	-64	0.7	0.4	830	-59	1.74	0.8	818	
-8.5	V	-64	0.7	0.35	820	-59	1.74	0.7	818	
-9	V	-64	0.7	0.3	820	-59	1.74	0.6	818	900

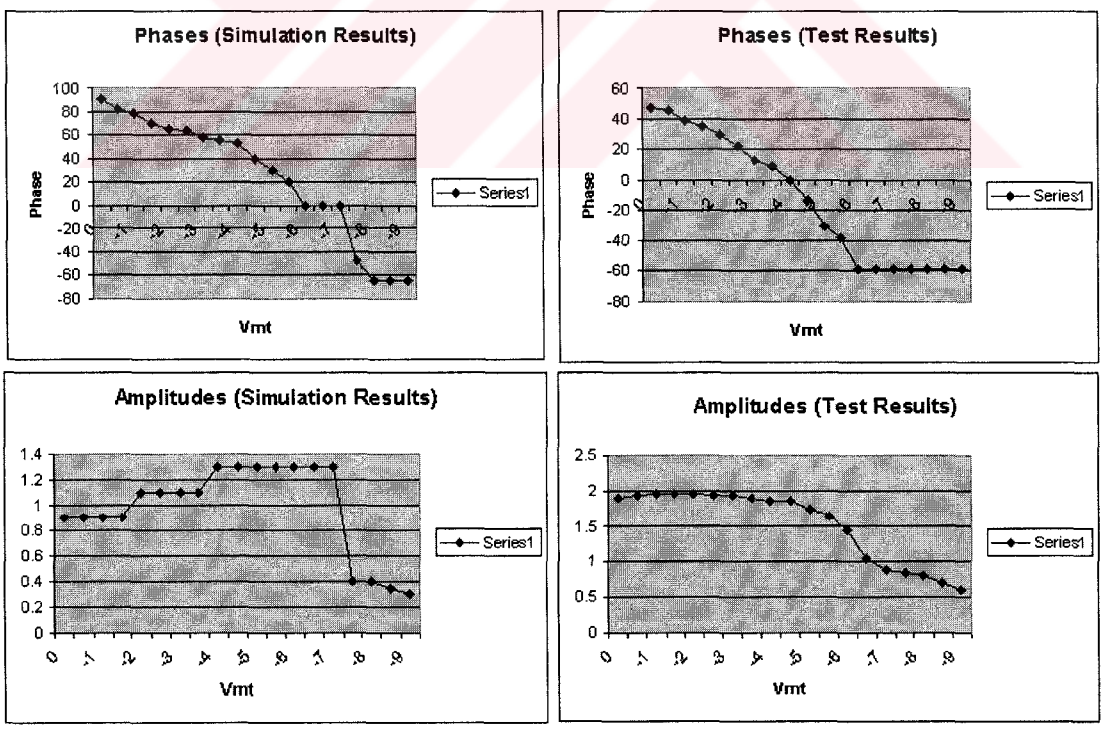


Figure 5.2.6 Phase and Amplitude plots iv.

Table 5.2.7 1st Set of Measurements v

Vis=8V		Vms=5.4V		Vit=8V	R=200Ω					Theory:
		Simulation Results				Test Results				Locking
		Phase	Amplitudes			Phase	Amplitudes(V)			Range
Vmt		ΔΦ	*Vi*	*Vo*	f(MHz)	ΔΦ	*Vi*	*Vo*	f(MHz)	f(MHz)
0	V	100	0.9	0.5	835	49	1.6	1.66	851	
-0.5	V	95	0.9	0.6	835	46	1.6	1.71	855	
-1	V	90	0.9	0.7	835	40	1.61	1.72	850	
-1.5	V	90	0.9	0.7	835	32	1.61	1.78	850	
-2	V	86	0.95	0.8	830	29	1.62	1.82	845	
-2.5	V	80	1	1	830	26	1.63	1.83	844	
-3	V	72	1	1	830	20	1.64	1.86	842	
-3.5	V	68	1	1	830	14	1.65	1.88	842	
-4	V	64	1	1	825	0	1.66	1.9	841	770
-4.5	V	60	1	1	825	-8	1.66	1.89	838	
-5	V	55	1	1	825	-12	1.67	1.89	837	
-5.5	V	50	1	1	825	-24	1.67	1.86	837	
-6	V	43	1	1.2	835	-41	1.67	1.78	834	
-6.5	V	35	1	1.2	835	-71	1.65	1.55	838	
-7	V	30	1	1.2	835	-89	1.61	1.1	850	
-7.5	V	25	1	1.2	835	-89	1.6	1	851	
-8	V	15	1	1.2	855	-89	1.6	0.95	851	
-8.5	V	10	1	1.2	855	-89	1.6	0.85	851	
-9	V	0	1	1.2	855	-89	1.6	0.6	851	
-12		-72	0.5	0.2	865					940

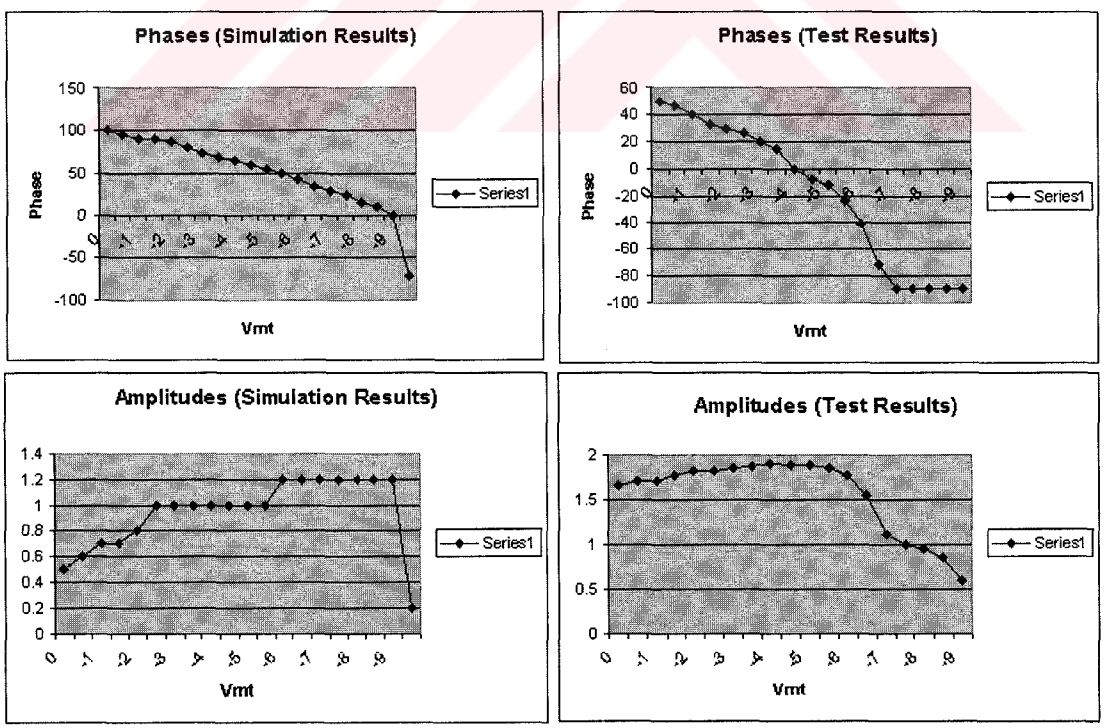
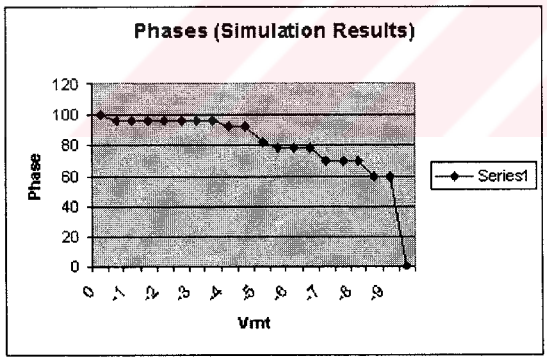
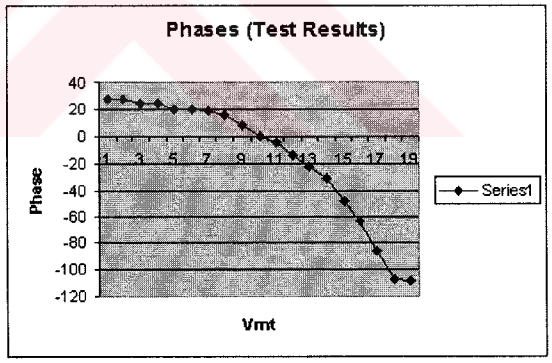


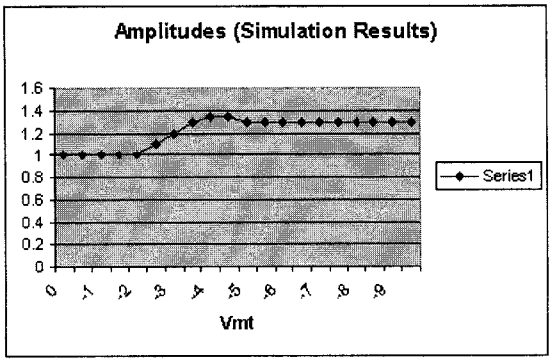
Figure 5.2.7 Phase and Amplitude plots v.

Table 5.2.8 1st Set of Measurements vi

Vis=8V		Vms=5.4V		Vit=10V		R=200Ω				Theory:
		Simulation Results				Test Results				Locking
		Phase	Amplitudes			Phase	Amplitudes(V)			Range
Vmt		ΔΦ	Vi	Vo	f(MHz)	ΔΦ	Vi	Vo	f(MHz)	f(MHz)
0	V	100	0.6	1	883	27	1.21	1.17	882	
-0.5	V	96	0.7	1	883	27	1.24	1.22	878	
-1	V	96	0.7	1	883	24	1.24	1.24	878	
-1.5	V	96	0.7	1	883	24	1.26	1.31	877	
-2	V	96	0.75	1	883	20	1.23	1.36	875	
-2.5	V	96	0.8	1.1	883	20	1.3	1.37	875	
-3	V	96	0.9	1.2	875	19	1.29	1.45	873	
-3.5	V	96	0.95	1.3	875	16	1.31	1.5	874	
-4	V	92	1	1.35	875	8	1.31	1.53	870	
-4.5	V	92	1.1	1.35	875	0	1.33	1.59	871	
-5	V	82	1.3	1.3	875	-5	1.32	1.63	872	
-5.5	V	78	1.4	1.3	875	-14	1.31	1.65	872	800
-6	V	78	1.4	1.3	875	-22	1.3	1.7	870	
-6.5	V	78	1.4	1.3	875	-31	1.29	1.71	867	
-7	V	70	1.4	1.3	875	-48	1.23	1.71	867	
-7.5	V	70	1.4	1.3	875	-64	1.21	1.68	866	
-8	V	70	1.4	1.3	875	-86	1.56	1.1	881	
-8.5	V	60	1.4	1.3	875	-107	1.07	1.1	876	
-9	V	60	1.4	1.3	875	-108	1.11	0.8	886	
-12		0	1.4	1.3	875					980







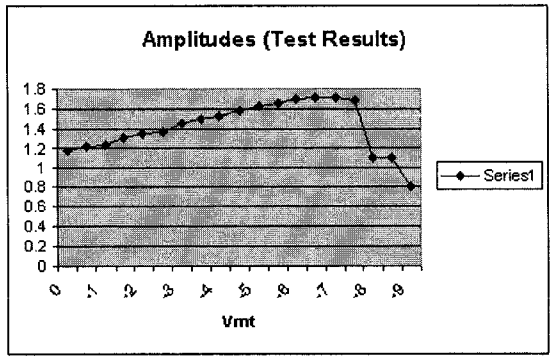


Figure 5.2.8 Phase and Amplitude plots vi.

Table 5.2.9 2nd Set of Measurements i (V_{mt} is constant, V_{it} is variable)

Vis=8V		Vms=5.4V		Vmt=0V		R=200Ω			
		Simulation Results				Test Results			
		Phase	Amplitudes			Phase	Amplitudes(V)		
Vit		ΔΦ	*Vi*	*Vo*	f(MHz)	ΔΦ	*Vi*	*Vo*	f(MHz)
0	V	23	1.4	1	660	57	2.79	2.16	742
-0.5	V	27	1.4	1	665	55	2.72	2.23	751
-1	V	38	1.33	0.93	680	60	2.7	2.3	755
-1.5	V	40	1.26	0.9	690	59	2.67	2.34	760
-2	V	47	1.2	0.85	700	59	2.65	2.36	765
-2.5	V	55	1.1	0.81	710	59	2.66	2.36	767
-3	V	63	1	0.78	720	60	2.65	2.36	770
-3.5	V	68	1	0.76	730	60	2.63	2.34	776
-4	V	80	1	0.7	745	60	2.63	2.32	781
-4.5	V	85	1	0.7	765	61	2.6	2.31	782
-5	V	85	1	0.6	775	61	2.57	2.21	789
-5.5	V	90	1	0.6	785	62	2.48	2.1	797
-6	V	90	1	0.5	795	50	2.17	1.9	810
-6.5	V	90	0.9	0.45	810	45	1.84	1.79	815
-7	V	90	0.9	0.4	820	46	1.7	1.75	826
-7.5	V	90	0.9	0.4	830	47	1.63	1.71	836
-8	V	90	0.85	0.37	845	47	1.6	1.65	841
-8.5	V	90	0.85	0.35	870	47	1.6	1.57	850
-9	V	90	0.8	0.3	880	43	1.59	1.49	856
-11	V	90	0.7	0.25	895	45	0.909	0.99	900

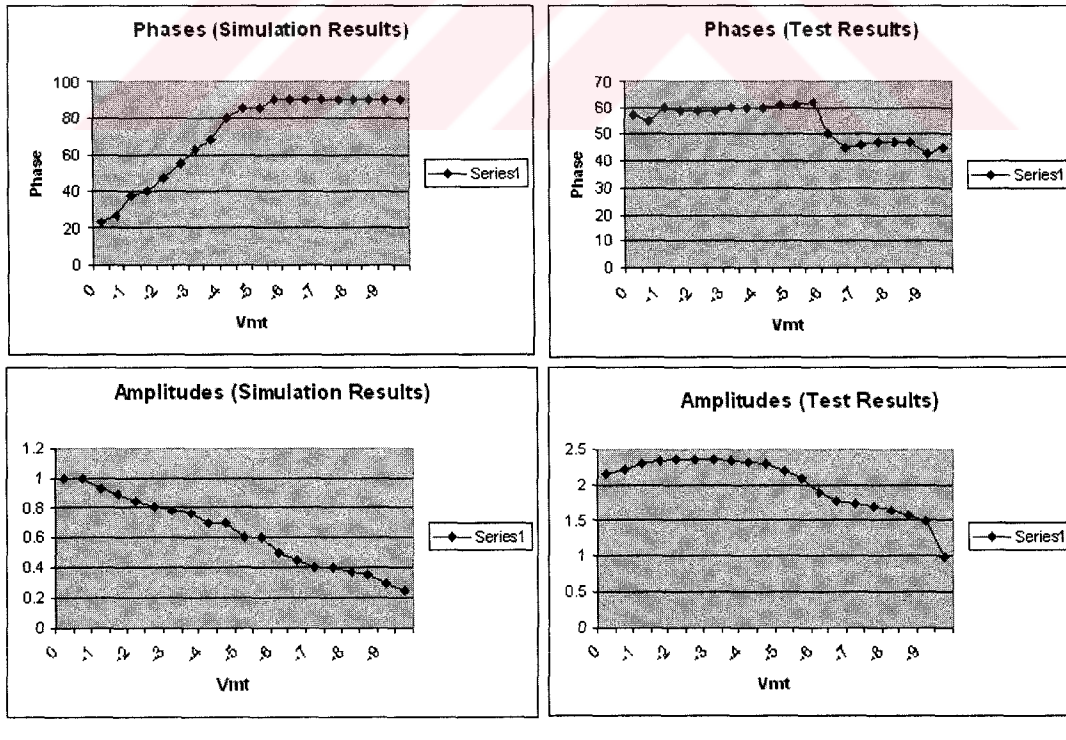


Figure 5.2.9 Phase and Amplitude plots 2-i.

Table 5.2.10 2nd Set of Measurements ii

Vis=8V		Vms=5.4V		Vmt=2V		R=200Ω			
		Simulation Results				Test Results			
		Phase	Amplitudes			Phase	Amplitudes(V)		
Vit		ΔΦ	*Vi*	*Vo*	f(MHz)	ΔΦ	*Vi*	*Vo*	f(MHz)
0	V	-14	1.1	1	680	31	2.64	2	742
-0.5	V	0	1.1	0.98	690	31	2.61	2.1	749
-1	V	5	1.1	0.96	700	31	2.62	2.22	759
-1.5	V	10	1.1	0.94	705	32	2.63	2.25	762
-2	V	22	1.1	0.92	710	32	2.62	2.28	767
-2.5	V	30	1	0.9	720	32	2.62	2.29	770
-3	V	40	1	0.88	730	32	2.63	2.29	775
-3.5	V	50	1	0.85	740	32	2.62	2.29	778
-4	V	62	1	0.83	745	32	2.6	2.29	782
-4.5	V	65	1	0.8	760	32	2.58	2.27	785
-5	V	70	1	0.75	770	33	2.56	2.21	790
-5.5	V	75	1	0.7	780	33	2.38	2.1	796
-6	V	78	1	0.67	790	26	2.1	1.97	805
-6.5	V	80	1	0.6	800	26	1.84	1.89	813
-7	V	90	0.9	0.55	820	27	1.75	1.87	820
-7.5	V	90	0.9	0.5	830	27	1.66	1.84	835
-8	V	90	0.9	0.47	840	27	1.63	1.8	844
-8.5	V	90	0.8	0.4	860	28	1.63	1.74	854
-9	V	90	0.8	0.3	880	28	1.61	1.65	857
-11	V	90	0.73	0.28	895	29	0.904	1.15	900

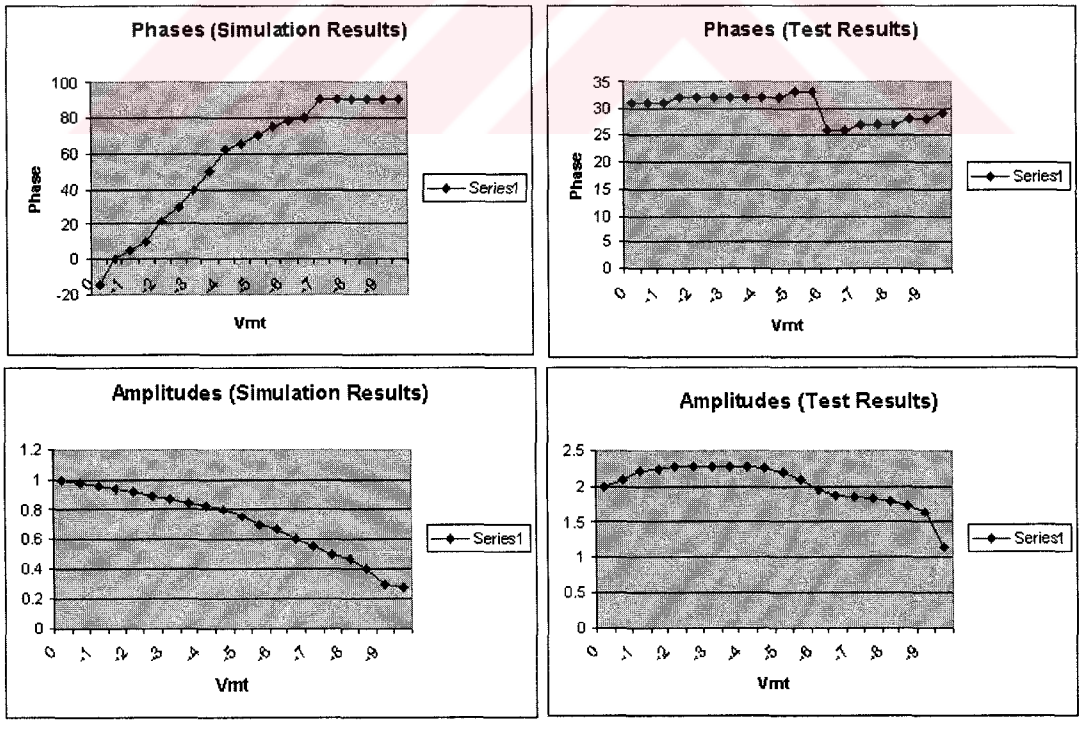


Figure 5.2.10 Phase and Amplitude plots 2-ii.

Table 5.2.11 2nd Set of Measurements iii

Vis=8V		Vms=5.4V		Vmt=4V		R=200Ω			
		Simulation Results				Test Results			
		Phase	Amplitudes			Phase	Amplitudes(V)		
Vit		ΔΦ	*Vi*	*Vo*	f(MHz)	ΔΦ	*Vi*	*Vo*	f(MHz)
0	V	-90	1	0.3	675	9	2.54	1.45	739
-0.5	V	-70	1	0.5	690	9	2.46	1.58	746
-1	V	-40	1	0.7	700	0	2.43	1.68	755
-1.5	V	-20	1	0.8	710	0	2.43	1.74	760
-2	V	0	1	0.9	725	0	2.45	1.8	763
-2.5	V	10	1	0.9	730	0	2.47	1.86	769
-3	V	20	1	0.9	740	0	2.49	1.93	773
-3.5	V	30	1	0.9	750	0	2.51	1.97	776
-4	V	40	1.1	0.88	755	0	2.53	2.01	780
-4.5	V	45	1.1	0.85	765	0	2.52	2.03	786
-5	V	50	1.1	0.8	770	0	2.41	2	794
-5.5	V	60	1.1	0.8	780	0	2.26	1.94	802
-6	V	68	1	0.78	790	-4	2	1.88	813
-6.5	V	75	1	0.75	800	-4	2	1.87	817
-7	V	80	1	0.7	810	0	1.7	1.89	824
-7.5	V	85	1	0.65	820	0	1.66	1.89	830
-8	V	90	0.9	0.6	835	0	1.66	1.88	840
-8.5	V	90	0.8	0.5	850	5	1.66	1.86	850
-9	V	90	0.75	0.4	870	5	1.64	1.8	857
-11	V	90	0.75	0.36	895	5	0.919	1.28	885

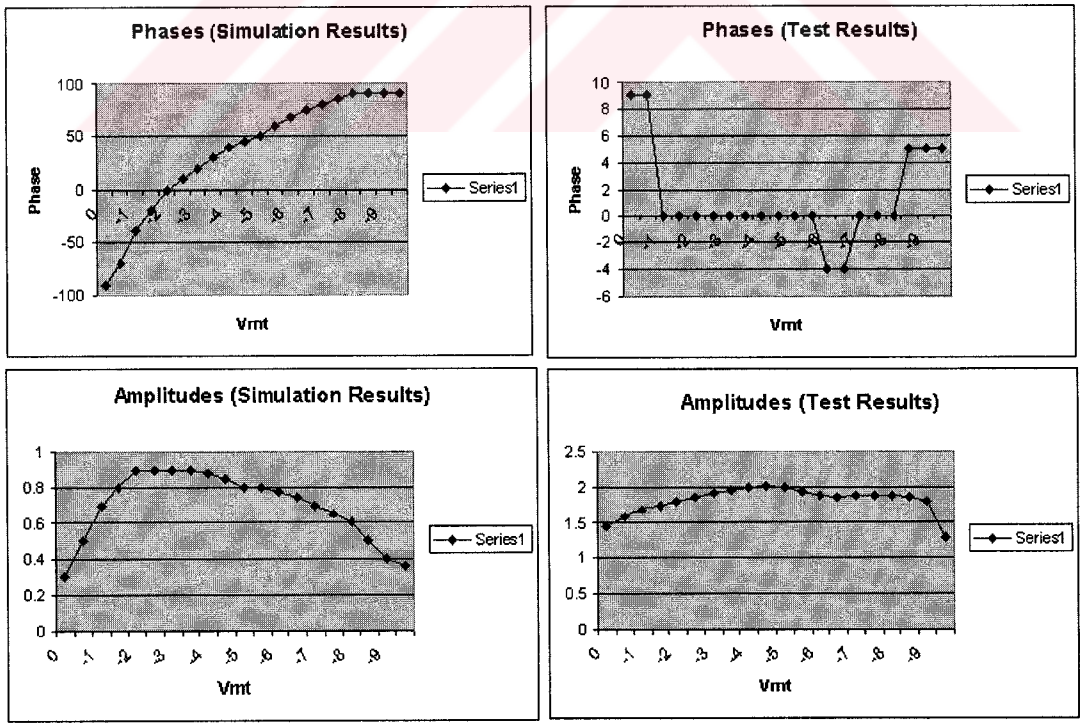


Figure 5.2.11 Phase and Amplitude plots 2-iii.

Table 5.2.12 2nd Set of Measurements iv

Vis=8V		Vms=5.4V		Vmt=6V		R=200Ω			
		Simulation Results				Test Results			
		Phase	Amplitudes			Phase	Amplitudes(V)		
Vit		ΔΦ	Vi	Vo	f(MHz)	ΔΦ	Vi	Vo	f(MHz)
0	V	90	1	0.2	670	4	2.58	1.02	729
-0.5	V	80	1	0.3	680	4	2.47	1.08	740
-1	V	70	1	0.4	695	4	2.41	1.13	753
-1.5	V	60	1	0.45	710	4	2.4	1.16	756
-2	V	50	1	0.5	720	0	2.4	1.17	762
-2.5	V	40	1	0.6	735	0	2.4	1.17	767
-3	V	30	1	0.7	750	-6	2.4	1.18	770
-3.5	V	15	1	0.8	760	-8	2.4	1.19	774
-4	V	0	1.1	0.88	770	-8	2.4	1.21	780
-4.5	V	-20	1.1	0.88	775	-24	2.36	1.23	784
-5	V	-30	1.1	0.88	780	-39	2.24	1.2	797
-5.5	V	-40	1.1	0.88	790	-51	1.93	1.26	815
-6	V	-45	1	0.85	800	-60	1.74	1.34	828
-6.5	V	-50	1	0.85	810	-60	1.67	1.45	831
-7	V	-55	1	0.85	820	-60	1.63	1.56	834
-7.5	V	-60	1	0.85	830	-53	1.64	1.68	835
-8	V	-65	1	0.7	835	-42	1.68	1.77	834
-8.5	V	-75	0.9	0.7	850	-35	1.72	1.84	845
-9	V	-85	0.8	0.7	870	-32	1.69	1.84	850
-11	V	-90	0.8	0.5	895	-11	0.95	1.49	880

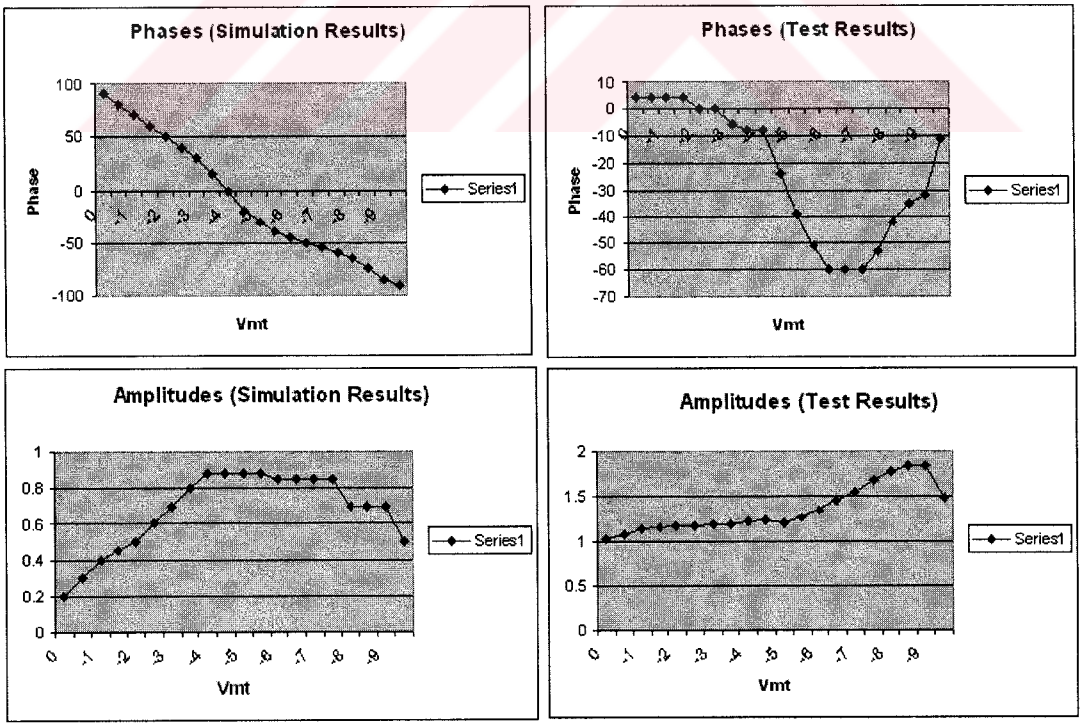


Figure 5.2.12 Phase and Amplitude plots 2-iv.

Table 5.2.13 2nd Set of Measurements v

Vis=8V		Vms=5.4V		Vmt=8V		R=200Ω			
		Simulation Results				Test Results			
		Phase	Amplitudes			Phase	Amplitudes(V)		
Vit		ΔΦ	Vi	Vo	f(MHz)	ΔΦ	Vi	Vo	f(MHz)
0	V	90	1	0.14	665	13	2.61	0.72	640
-0.5	V	80	1	0.15	680	13	2.49	0.78	680
-1	V	70	1	0.18	700	11	2.41	0.8	690
-1.5	V	60	1	0.19	710	12	2.38	0.83	730
-2	V	56	0.9	0.2	720	12	2.37	0.815	717
-2.5	V	60	0.9	0.22	730	11	2.37	0.81	700
-3	V	62	0.9	0.25	745	11	2.37	0.813	700
-3.5	V	60	0.9	0.28	760	0	2.37	0.83	700
-4	V	64	0.9	0.3	775	0	2.37	0.8	700
-4.5	V	45	1	0.4	785	0	2.37	0.8	720
-5	V	30	1	0.6	790	-9	2.26	0.83	720
-5.5	V	15	1	0.8	800	-20	2.1	0.8	750
-6	V	0	1	0.9	815	-39	1.78	0.826	750
-6.5	V	-15	1	0.9	820	-52	1.71	0.8	820
-7	V	-25	1	0.9	830	-72	1.6	0.8	836
-7.5	V	-30	1	0.9	835	-73	1.6	0.915	848
-8	V	-48	1	0.8	840	-80	1.62	0.974	853
-8.5	V	-55	0.9	0.7	860	-87	1.62	1.05	868
-9	V	-75	0.85	0.6	870	-108	1.52	1.26	870
-11	V	-80	0.8	0.6	885	-86	0.938	1.48	880
-12	V	-85	0.76	0.53	905	-83	0.81	1.35	905

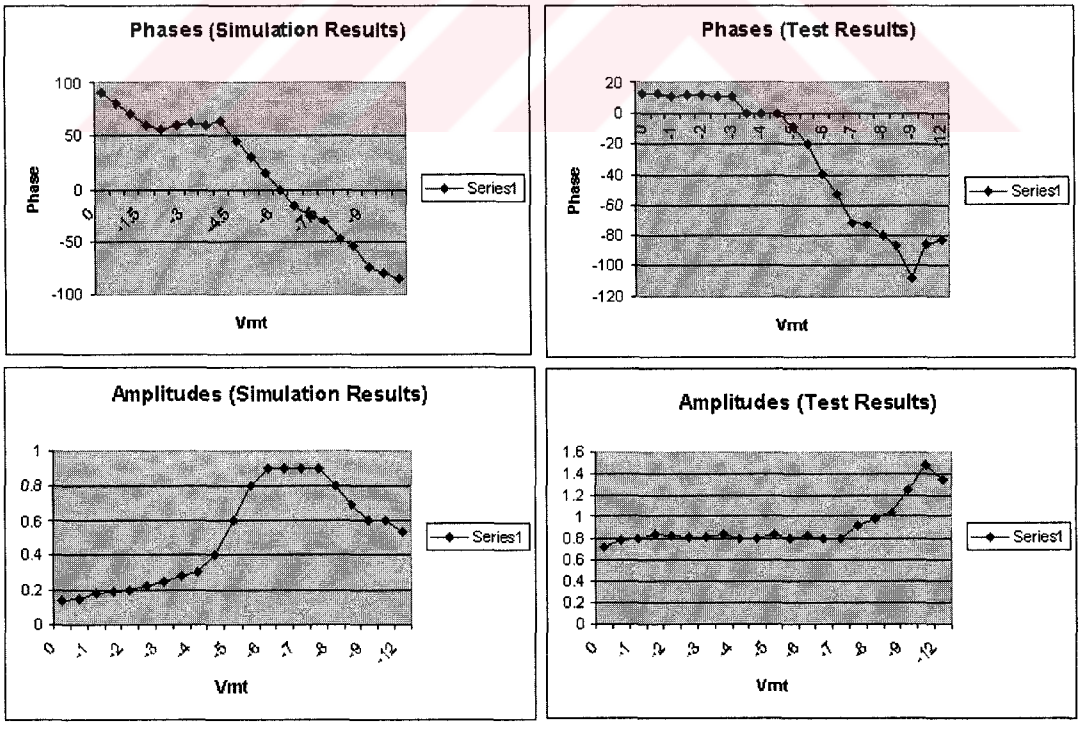


Figure 5.2.13 Phase and Amplitude plots 2-v.

Table 5.2.14 3rd Set of Measurements i (Optimum range)

Vis=8V		Vms=5.4V		Vit=9V					
		Simulation Results				Test Results			
		Phase	Amplitudes			Phase	Amplitudes(V)		
Vmt		ΔΦ	*Vi*	*Vo*	f(MHz)	ΔΦ	*Vi*	*Vo*	f(MHz)
0	V	46	1.61	1.5	855	98	0.8	0.32	860
-0.5	V	42	1.62	1.57	855	94	0.82	0.4	860
-1	V	38	1.63	1.61	855	94	0.82	0.4	860
-1.5	V	35	1.63	1.65	855	94	0.82	0.4	860
-2	V	31	1.64	1.7	857	94	0.82	0.4	860
-2.5	V	26	1.64	1.74	856	90	0.82	0.4	860
-3	V	20	1.65	1.76	858	90	0.82	0.4	860
-3.5	V	14	1.67	1.78	855	90	0.82	0.4	860
-4	V	9	1.66	1.82	857	90	0.85	0.5	855
-4.5	V	0	1.67	1.84	854	90	0.85	0.5	855
-5	V	-5	1.69	1.85	853	85	0.85	0.5	855
-5.5	V	-17	1.7	1.86	851	85	0.85	0.5	855
-6	V	-31	1.7	1.83	850	80	0.9	0.65	855
-6.5	V	-51	1.67	1.78	855	75	0.9	0.68	855
-7	V	-74	1.64	1.66	859	70	0.9	0.7	855
-7.5	V	-95	1.58	1.42	862	65	0.9	0.72	855
-8	V	-108	1.55	1.26	868	62	0.94	0.75	855
-8.5	V	-108	1.56	1	872	40	0.94	0.7	860
-9	V	-109	1.56	0.99	875	20	0.94	0.7	860
-11	V	-109	1.56	0.1	875	0	1	0.5	870
-12						-60	1	0.2	880

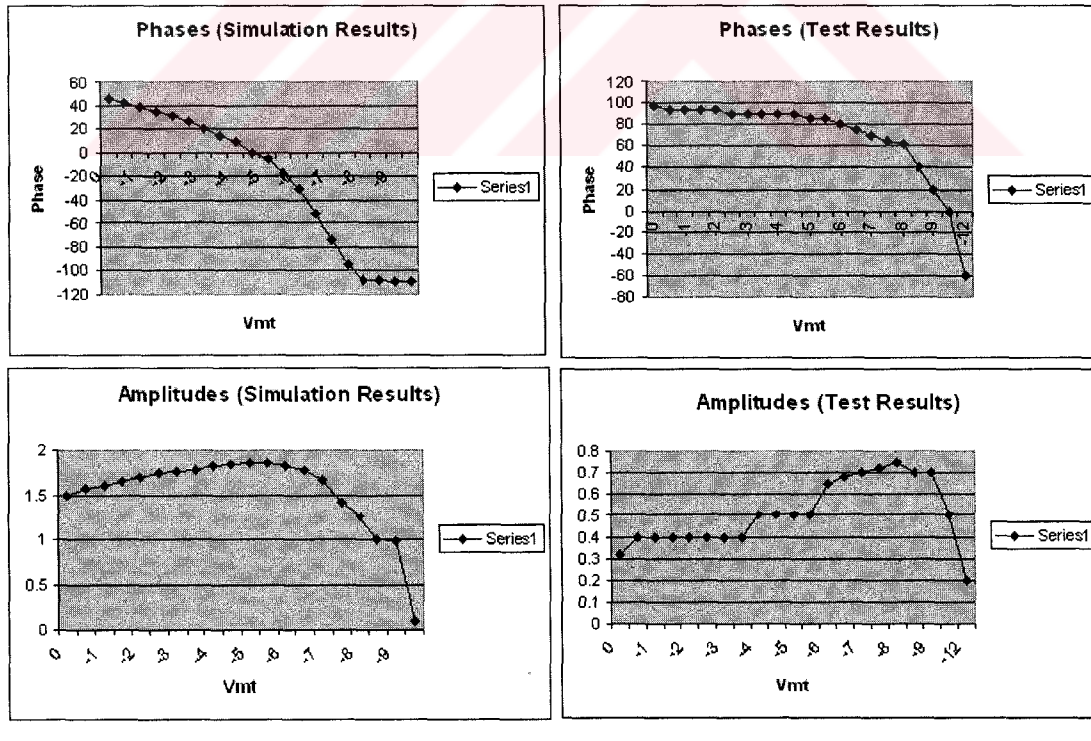
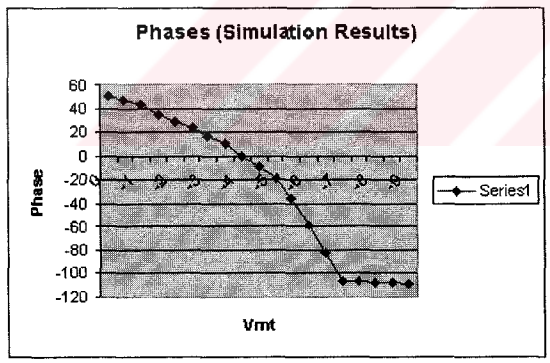
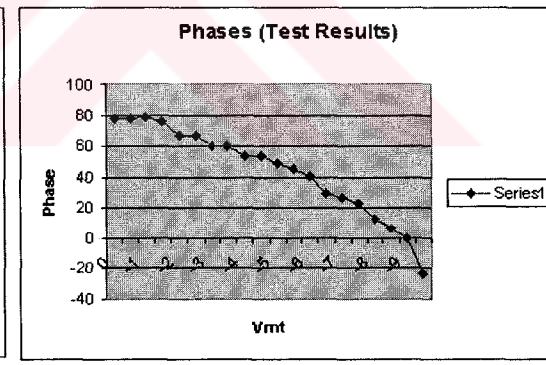


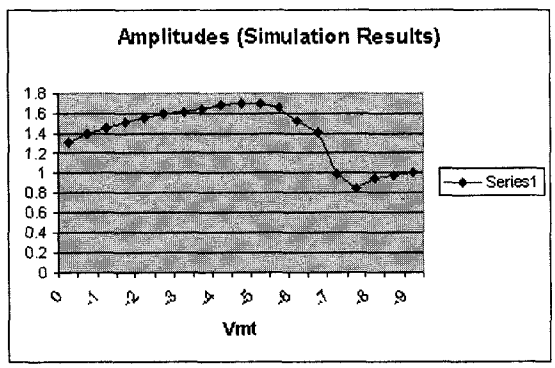
Figure 5.2.14 Phase and Amplitude plots 3-i.

Table 5.2.15 3rd Set of Measurements ii

Vis=6V		Vms=5.4V		Vit=9V					
		Simulation Results				Test Results			
		Phase	Amplitudes			Phase	Amplitudes(V)		
Vmt		ΔΦ	Vi	Vo	f(MHz)	ΔΦ	Vi	Vo	f(MHz)
0	V	50	1.02	1.31	850	78	1.29	0.77	835
-0.5	V	47	1.03	1.4	847	78	1.29	0.77	835
-1	V	43	1.03	1.46	848	79	1.29	0.77	840
-1.5	V	35	1.03	1.51	845	76	1.2	0.6	840
-2	V	29	1.06	1.56	844	67	1.2	0.643	840
-2.5	V	24	1.07	1.6	843	67	1.23	0.704	835
-3	V	17	1.08	1.62	843	60	1.25	0.775	835
-3.5	V	11	1.1	1.65	842	60	1.28	0.86	835
-4	V	0	1.11	1.68	842	54	1.34	0.95	835
-4.5	V	-9	1.13	1.7	840	54	1.34	1	835
-5	V	-18	1.14	1.7	843	49	1.37	1.14	835
-5.5	V	-35	1.15	1.66	845	45	1.4	1.23	840
-6	V	-58	1.12	1.53	854	41	1.43	1.3	840
-6.5	V	-83	1.1	1.41	854	30	1.46	1.37	840
-7	V	-107	1.1	0.99	873	27	1.48	1.42	845
-7.5	V	-107	1.1	0.85	871	23	1.49	1.46	845
-8	V	-108	1.1	0.95	880	13	1.49	1.49	850
-8.5	V	-108	1.1	0.975	885	6	1.5	1.5	850
-9	V	-109	1.1	1	893	0	1.5	1.5	855
-10						-23	1.2	1.34	860







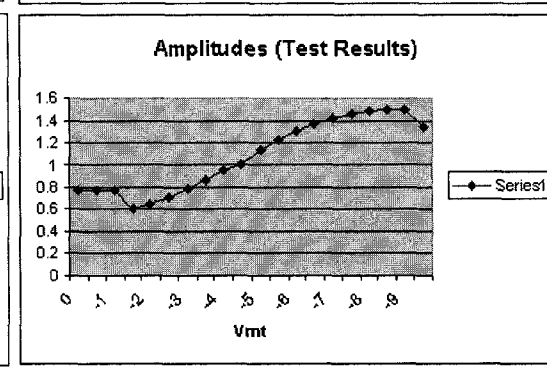


Figure 5.2.15 Phase and Amplitude plots 3-ii.

5.3 Comparison of Simulations and Measurements Under Optimum Conditions:

In this section, computer simulations are compared with the measurements under the optimum locking range conditions. From the measurement results, these conditions are:

V_{is}=Supply voltage of the control signal (injection oscillator)=8V.

V_{ms}=Supply voltage of the master signal (the oscillator being controlled)=5.4V.

V_{it}= Varactor diode tuning voltage of the control signal (injection oscillator)= -9V.

Under the given conditions, V_{mt} is varied from 0V, -4V, -6V, -12V.

In Figure 5.3.1, the simulation results of the phase locking circuit in Figure 4.2.2 (phase locking schematics) are shown. It's seen that the oscillator is locked at 860MHz and it performs phase variations roughly in between -90^0 and 90^0. Following figure 5.3.2 is the measurement results of the circuit in Figure 5.2.1 (phase locking test circuit) by using a high frequency oscilloscope. These screen-shots also display similar phase variations, approximately between -90^0 and 90^0 while being locked at 860MHz.

In terms of the amplitudes, injection signal has an amplitude of 1V for the simulation and 1.5V for the measurements. Similarly, the output signal has an amplitude of 0.8V for the simulation and it is about 1V for the measurements. Another observation is that the output voltage amplitude tends to rise towards the zero phase difference and it falls as the signals move apart. This is a reasonable consequence of the Adler's amplitude differential equation (18) . Also note that, for $|V_{mt}|>12V$, the system runs out of locking, and no oscillations are observed at the output.

Dotted line graph in Figure 5.3.1 (simulation results) is the injection signal and the moving signal is the output voltage waveform. Likewise, in Figure 5.3.2 (measurement results), the darker signal is the output signal and the brighter signal is the injection signal.

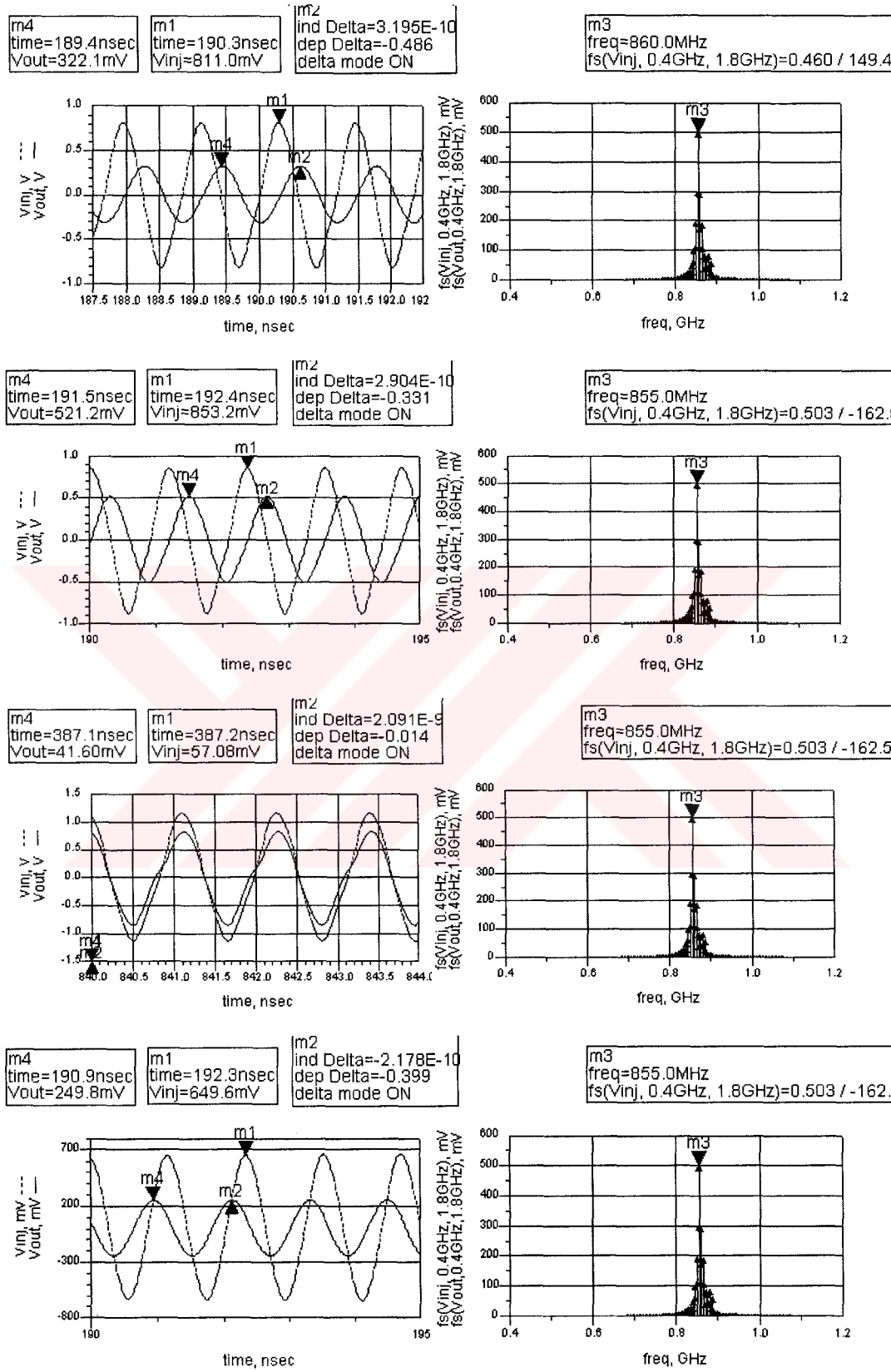


Figure 5.3.1 Simulations for the optimum case.

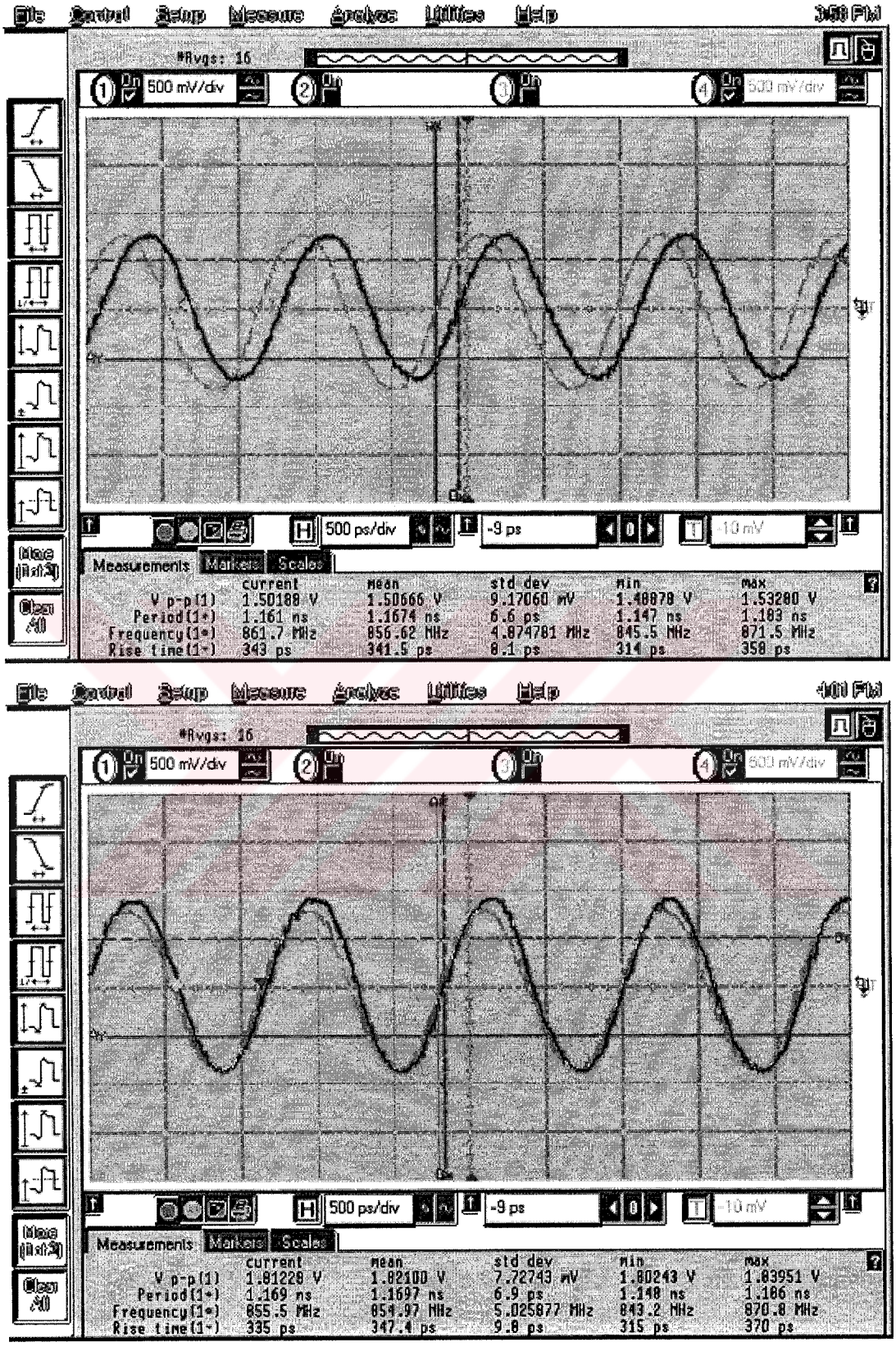


Figure 5.3.2.1 Oscilloscope measurements for the optimum case i.

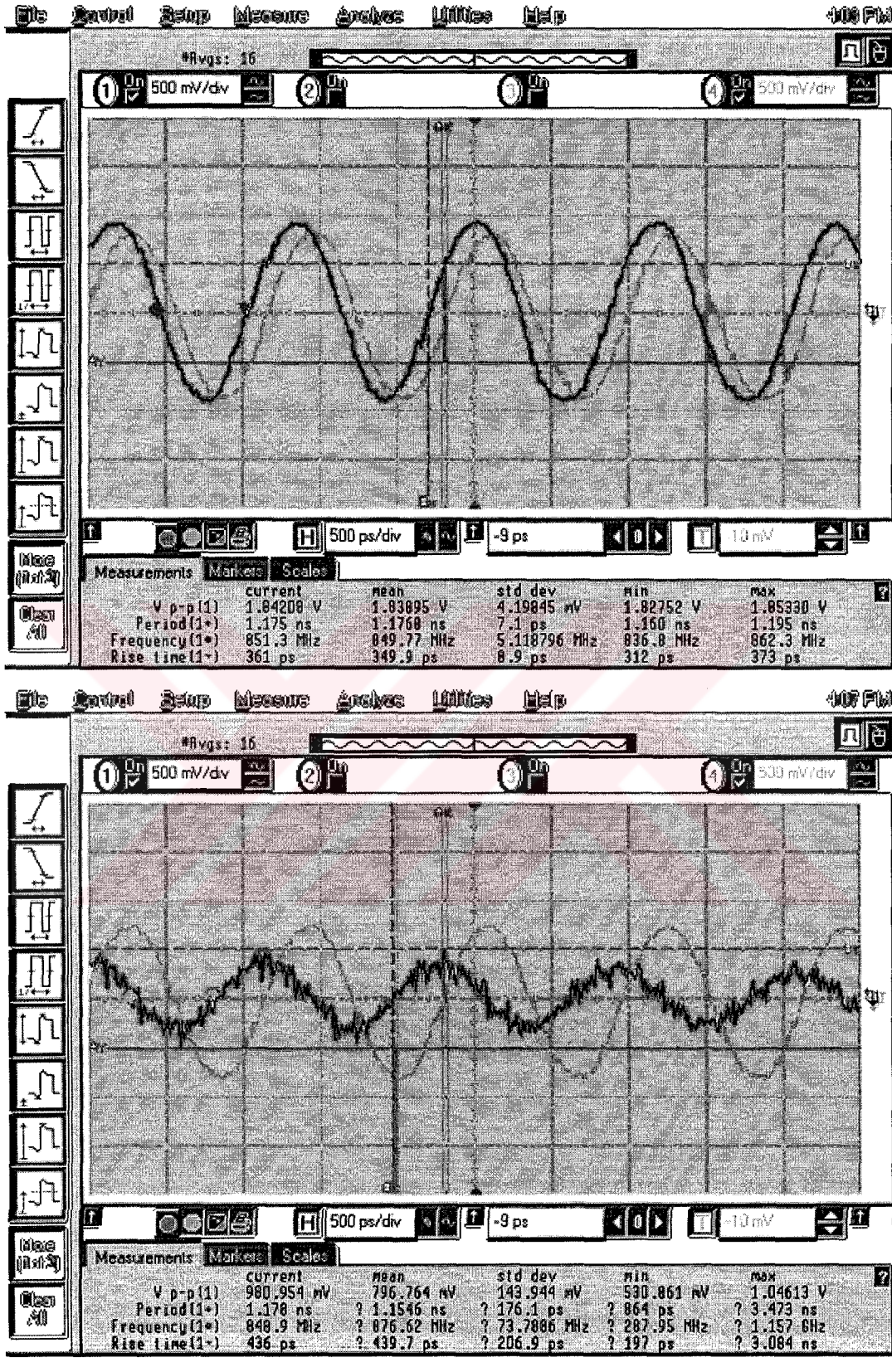


Figure 5.3.2.2 Oscilloscope measurements for the optimum case ii.

CHAPTER 6

CONCLUSION

Phase locking technology is expected to simplify microwave circuits that require phase control and to reduce cost by eliminating phase shifters. This thesis has studied phase locking or injection locking technique in theory and in practice. Two identical oscillators have been used for experimenting this phenomena. One oscillator is used to control the phase of the other under certain conditions. The simulation and measurement results are tabulated in Tables 5.2.3 trough 5.2.15. These results reveal the following conclusions:

i) In the 1st set of tables (Table 5.2.3 trough Table 5.2.8), the widest phase control occurs for V_{it}= Varactor diode tuning voltage of the injected signal = -4V to -10V, while -7V to -9V gives the best results. These conditions are also in agreement with the theoretical values.

ii) In the 1st set of tables, in terms of the amplitudes, the graphs display similarities especially in the rate of change of their values. This amplitude behavior is governed by the amplitude differential equation (18).

iii) In the 1st set of tables, again, the locking frequencies and the locking ranges are quite similar. The widest locking range occurs for V_{mt}=-7V to -9V.

iv) In the 2nd set of tables (Table 5.2.9 trough Table 5.2.13), the widest phase control occurs for V_{mt}= Varactor diode tuning voltage of the master signal = -8V. This is when the range is maximized. In some other cases, the system shows

out of locking behaviors in certain voltage ranges. Typical indications of such cases is that the frequency varies during voltage tunings.

v) In the 3rd set of tables (Table 5.2.14 trough Table 5.2.15), the supply voltage for the injected signal is changed. The results show that the larger amplitude injected signal (9V supply voltage) results in a wider phase variation (90^0 to -60^0 in measurements) whereas smaller amplitudes show smaller phase variations (78^0 to -23^0). This is also expected because of the Adler's range equation

$$w_{inj} = w_0 \pm \Delta w_m \quad \text{where} \quad \Delta w_m = \frac{w_0}{2Q} \frac{A_{inj}}{A}$$

where larger A_{inj} results in a wider range.

In summary, this thesis has explained the phase controlling technique by injection locking. Variations and extensions of this phenomena are still under investigation by several groups. This new technique may be simpler and quite efficient in certain applications. Also, it may replace phase shifter by reducing their cost. Apparently, the straightforward application is the power combining systems in array structures. Advantages are further noticeable at higher frequencies because of the size and simplicity.

REFERENCES

[1] Constantine A. Balanis, "Antenna Theory Analysis and Design," John Wiley & Sons, Inc.pp. 249-337, 1997.

[2] Robert A. York and Tatsuo Itoh, "Injection and Phase –Locking Techniques for Beam Control," *IEEE Transactions on Microwave Theory and Techniques,* vol.46, no.11, November 1998.

[3] Robert A. York, "Nonlinear Analysis of Phase Relationships in Quasi-Optical Oscillator Arrays," *IEEE Transactions on Microwave Theory and Techniques,* vol.41, no.10, October 1993.

[4] J.W. Mink, "Quasi-Optical Power Combining of Solid State Millimeter Wave Sources," *IEEE Trans. Microwave Theory Tech.*, vol. MTT-34, pp. 273-279, Feb. 1986.

[5] D.B. Rutledge Z.B. Popovic, R.M. Weikle, M. Kim, K.A. Potter, R.A. York, and R.C. Compton, "Quasi-Optical Power Combining Arrays," *IEEE MTT-S Int. Microwave Symp. Dig.*, Dallas, May 1990.

[6] R.A. York, and R.C. Compton, "Quasi-Optical Power Combining Using Mutually Synchronized Oscillator Arrays," *IEEE Transactions on Microwave Theory and Techniques,* vol.39, pp.1000-1009, June 1991.

[7] Z. B. Popovic, R. M. Weikle, M. Kim and D. B. Rutledge, "A 100-Mesfet Planar Grid Oscillator," ," *IEEE Transactions on Microwave Theory and Techniques,* vol.39, pp.193-200, Feb 1991.

[8] J. Birkeland and T. Itoh, "A 16-element Quasi Optical FET Oscillator Power Combining Array with External Injection Locking," *IEEE Transactions on Microwave Theory and Techniques,* vol.409, pp.475-481, Mar. 1992.

[9] K. Chang, K.A. Hummer, and J.L. Klein, "Experiments on Injection Locking of Active Antenna Elements for Active Phase Arrays and Spatial Power Combiners," *IEEE Transactions on Microwave Theory and Techniques,* vol.37, pp.1078-1084, July 1989.

[10] T.E. Price, *Analog Electronics*, Prentice Hall, p. 395, 1997.

[11] B. Van der Pol, "The nonlinear theory of electric oscillations," *Proc. IRE*, vol.22, pp. 1051-1085, September 1934.

[12] Canan Toker, "Lecture Notes Microwaves II", *Department of Electrical and Electronics Engineering Middle East Technical University*

[13] Reinhold Ludwig and Paul Bretchko, "RF Circuit Design – Theory and Applications", Prentice Hall, p.467, 2002.

[14] Hamid R. Rategh, "Superharmonic Injection-Locked Frequency Dividers," *IEEE Journal of Solid State Circuits,* vol.34, no.6, June 1999.

[15] David K. Cheng, *Field and Wave Electromagnetics*, Addison Wesley Publishing Company, p. 431, 1989.

[16] P. Liao, R.A. York, "A New Phase-Shifterless Beam-Scanning Technique Using Arrays of Coupled Oscillators," *IEEE Transactions on Microwave Theory and Techniques,* vol.41, no.10, October 1993.

[17] R. Adler, "A Study of Locking Phenomena in oscillators," *Proc. IRE*, vol. 34, pp.351-357, June 1946; also reprinted in *Proc. IEEE*, vol. 61, pp. 1380-1385, Oct. 1973.

[18] K. Kurokawa, "Injection-Locking of Solid State Microwave Oscillators," Proc. IEEE, vol. 61, pp. 1386-1409, Oct. 1973.